Novel Routes for Sintering of Ultra-high Temperature Ceramics and their Properties

Oleg Nikolayevich Grigoriev

SCIENCE AND TECHNOLOGY CENTER IN UKRAINE
METALISTIV 7A, KYIV, UKRAINE

FRANTSEVICH INSTITUTE FOR PROBLEMS IN MATERIALS
SCIENCE OF
NATIONAL ACADEMY OF SCINECES OF UKRAINE
3, KRZHYZHONOVSKY STR, KIEVE 03680 UKRAINE

EOARD STCU P-511/STCU 11-8002

Report Date: October 2014

Final Report from 1 November 2011 to 31 October 2014

Air Force Research Laboratory
Air Force Office of Scientific Research
European Office of Aerospace Research and Development
Unit 4515, APO AE 09421-4515

REPORT DOCUMENTATION PAGE

Form Approved OMB No. 0704-0188

Public reporting burden for this collection of information is estimated to average 1 hour per response, including the time for reviewing instructions, searching existing data sources, gathering and maintaining the data needed, and completing and reviewing the collection of information. Send comments regarding this burden estimate or any other aspect of this collection of information, including suggestions for reducing the burden, to Department of Defense, Washington Headquarters Services, Directorate for Information Operations and Reports (0704-0188), 1215 Jefferson Davis Highway, Suite 1204, Arlington, VA 22202-4302. Respondents should be aware that notwithstanding any other provision of law, no person shall be subject to any penalty for failing to comply with a collection of information if it does not display a currently valid OMB control number.
PLEASE DO NOT RETURN YOUR FORM TO THE ABOVE ADDRESS.

1. REPORT DATE *(DD-MM-YYYY)*	2. REPORT TYPE	3. DATES COVERED *(From – To)*
31 October 2014	Final Report	1 November 2011 – 31 October 2014

4. TITLE AND SUBTITLE

Novel Routes for Sintering of Ultra-high Temperature Ceramics and their Properties

5a. CONTRACT NUMBER

STCU P-511

5b. GRANT NUMBER

STCU 11-8002

5c. PROGRAM ELEMENT NUMBER

61102F

6. AUTHOR(S)

Oleg Nikolayevich Grigoriev

5d. PROJECT NUMBER

5d. TASK NUMBER

5e. WORK UNIT NUMBER

7. PERFORMING ORGANIZATION NAME(S) AND ADDRESS(ES)
SCIENCE AND TECHNOLOGY CENTER IN UKRAINE
METALISTIV 7A, KYIV, UKRAINE

FRANTSEVICH INSTITUTE FOR PROBLEMS IN MATERIALS SCIENCE OF NATIONAL ACADEMY OF SCINECES OF UKRAINE
3, KRZHYZHONOVSKY STR, KIEVE 03680 UKRAINE

8. PERFORMING ORGANIZATION REPORT NUMBER

N/A

9. SPONSORING/MONITORING AGENCY NAME(S) AND ADDRESS(ES)

EOARD
Unit 4515
APO AE 09421-4515

10. SPONSOR/MONITOR'S ACRONYM(S)

AFRL/AFOSR/IOE (EOARD)

11. SPONSOR/MONITOR'S REPORT NUMBER(S)

AFRL-AFOSR-UK-TR-2015-0017

12. DISTRIBUTION/AVAILABILITY STATEMENT

Distribution A: Approved for public release; distribution is unlimited.

13. SUPPLEMENTARY NOTES

14. ABSTRACT
The objective is to obtain new knowledge about mechanism of activated sintering of eutectic systems based on refractory compounds as well as regularities of structure formation of UHTCs.
The suggested approach is to find out methods of elevation of diffusion mobility of surface atoms of grains being sintered. The effective way to increase this mobility is introducing additives in charge that together with the main phases form eutectic systems. The primary results obtained: 1. Mechanisms of eutectic interactions and processes ongoing in eutectic systems at high temperatures were investigated, namely: -A) at the boundary of grains of eutectic alloys, diffusion zones are formed where the processes of eutectic melting develop as well as processes responsible for sintering; -B) it is showed that Debay temperature of Al in composite is 288 K that is about by 25% lower than that in monophase sample. Thus, at high temperatures the thermal vibration amplitude of aluminum atoms in grains of eutectic alloys is by 25% higher than in monophase condition and it defines the elevated diffusion activity at sintering. 2. In the ZrB_2-SiC-5% Cr_3C_2 system, hot pressing allows to obtain porous free ceramics at temperatures 1500-1600° C, and in the mode of free sintering at temperatures 1800-1900 °C, meanwhile the ceramic ZrB_2-SiC has a porosity about 0-5% at hot pressing at temperatures 2100-2200 °C. Sintering of ZrB_2-SiC-5% Cr_3C_2 ceramic occurs in conditions of eutectic interactions with disappearing liquid phase and formation of secondary high temperature phases (on the base of ZrC and CrB) in diffusion zones. 3. A result of eutectic interaction of sintered compositions ZrB_2-SiC-5% Cr_3C_2 is also the elevated creep rate of those that is one of the factors of intensification of their sintering. 4. As a result of investigations performed, being based on the proposed approach, new compositions of perspective UHTCs were developed.

15. SUBJECT TERMS

EOARD, Materials, mictrostructural characterization, high temperature

16. SECURITY CLASSIFICATION OF:			17. LIMITATION OF ABSTRACT	18, NUMBER OF PAGES	19a. NAME OF RESPONSIBLE PERSON
a. REPORT UNCLAS	b. ABSTRACT UNCLAS	c. THIS PAGE UNCLAS	SAR	83	Matthew Snyder
					19b. TELEPHONE NUMBER *(Include area code)* +44 (0)1895 616420

Standard Form 298 (Rev. 8/98)
Prescribed by ANSI Std. Z39-18

A THREE-YEAR PROJECT REPORT – STCU PROJECT

Project Title: <u>Novel Routes for Sintering of Ultra-high Temperature Ceramics and their Properties</u>

Reporting Period: 01.11.2011-31.10.2014

Principal Investigator: <u>Grigoriev Oleg Nikolayevich</u>

Institution: <u>Frantsevich Institute for Problems of Materials Science of National Academy of Sciences of Ukraine</u>

EOARD Project Number: P511

STCU Project Number: P511

Summary

Project's objective – 1) to investigate mechanisms of activation of sintering of ultrahigh temperature ceramics with the use of sintering activators forming eutectic systems with main components; -2) being based on these investigations, to search the effective sintering activators, to develop a technology of UHTCs production at lowered temperatures and to investigate structure and properties of this ceramic.

It is shown that the thermal characteristics of crystals (Debay temperature and value of dynamic thermal displacement of atoms) significantly depend on a structural state of a material. At high temperatures in eutectic systems, at least in diffusion zones near to interfaces, the above-stated thermal characteristics of components appear essentially distinct from those in a monophase condition and there essential weakening of interatomic bonds and increase of amplitude of thermal oscillations of atoms occur. This phenomenon can be a principal reason for elevation of diffusion activity in grain boundary volumes of phases in eutectic systems and to stimulate the elevation of rate of some high-temperature processes (sintering of powders, creep, etc.).

The investigation of contact interactions of components of UHTCs charge (zirconium and hafnium borides, SiC) with additives (chromium carbide, nickel, chromium, etc.), which activate sintering process, is carried out. It is found out that for the above said systems eutectic interactions resulting in activation of sintering are typical, namely when sintering proceeds in a mode with disappearing liquid phase which can be formed at temperatures about 1300° C, and with formation of secondary high temperature phases in a form of carboborides of zirconium and bi borides of zirconium or chromium. Elevation of densification rate of sintered borides is escorted by elevation of re-crystallization rate as well.

This project was to investigate regularities of ceramics densification depending on composition and grains size of components. On the base of investigations of contact and phase interactions with formation of diffusion zones at sintering the technologies of vacuum sintering and hot pressing which allow to obtain dense ceramic materials at temperatures 1600-1900° C, that is by 300-600° lower than at sintering of basic UHTC materials, were developed. Structure and some mechanical properties of the obtained ceramic (hardness, characteristics of contact strength, bending strength) were investigated. Low temperatures of ceramics production at a level of properties not yielding those of traditional UHTCs govern perspectives of application of new materials in

machine building, power industries, etc.

Creep processes of ultrahigh temperature ceramic at temperatures up to 1900° C in conditions of measurement indentation creep and in experiments on material's creep at uniaxial compression are investigated. For both methods the curves deformation-time at chosen levels of loading were recorded. It is shown that the ceramic ZrB_2-SiC-Cr_3C_2 at temperature about $1700^{\circ}C$ can be deformed by 50 % and higher without essential degradation of mechanical properties. The obtained data allow supposing that creep process is developed almost in the mode of superplasticity under the slip mechanism of zirconium boride and silica carbide grains on grain boundary interlayers with nanocrystalline grains of carbon-boride of zirconium and diborides (carbon-boride) of zirconium –chromium.

Some peculiarities of high temperature deformation and diffusion behavior of eutectic systems were investigated by the methods of MD modeling. Computer programs for MD modeling and testing of the developed potentials including calculations of thermodynamic state of nanocrystals of carbides and relaxation changes in their structure associated with surface influence were developed. The potentials and programs are convenient for their use as virtual "trying stand" at various mechanical tests of nanocrystals (tension, compression, bending, nanoindentation, etc). It is found out that as temperature increases Young's modulus of the considered objects decreases under a linear law. Fracture stress and deformation increase at elevation of relative strain rate and fall when temperature increases. MD modeling of contact melting in eutectic system Cu-Si qualitatively confirmed the formation of diffusion zone at heating in the area of contact Cu-Si and showed that melting process starts namely in diffusion zone.

ACCOMPLISHMENTS OF PROJECT

1. **Experimental investigation of activated sintering mechanisms of eutectic systems on the base of refractory compounds, and regularities of formation of ceramics structure and its physical-mechanical properties.**

Introduction

The methods of activation of sintering of zirconium and hafnium borides by means of introduction in charge of carbides (boron and tungsten carbides), silicides (tungsten, zirconium and molybdenum), borides and nitrides are well known. To obtain porous free ultrahigh-temperature ceramics on the basis of ZrB_2 a number of technological methods allowing to carry out sintering at temperatures below the temperature of collective re-crystallization which for zirconium diboride makes about $1900-2000^{\circ}C$, is used. It is attained, first of all, by removal of oxygen from the surface of powder particles and use of activating additives. Now a wide spectrum of activators of sintering /1/, including those which form eutectic systems with sintered substance is known. Use of such activators allows obtaining dense materials not only in a liquid phase sintering mode, but also at temperatures below a point of eutectic melting at the expense of raised diffusion in contact zones of phases.

The main objective of this work was to investigate mechanisms and regularities of solid phase sintering (or sintering in the presence of liquid disappearing at isothermal holding) of refractory compounds based eutectic systems. Investigations were based on the supposition that in eutectic systems a material near grain boundaries has the elevated amplitude of thermal oscillations, namely this phenomena is responsible for the elevated grain boundary diffusion and sintering of the investigated ceramics. This supposition was directly proved as a result of measurement of Debay temperature of one of the eutectic phases and a value of dynamic thermal displacements of atoms while X-ray investigation of nanolayered model eutectic system Al-Si. The elevated grain boundary activity of atoms of eutectic systems brings to formation of powerful diffusion zones on contact interfaces and to elevation of ceramics sintering rate (and to elevation of high temperature creep rate.

This effort was to investigate an influence of refractory compounds of chromium (carbides and borides) and metal additives Ni, Cr, NiCr-alloy on sintering of zirconium boride and compositions ZrB_2-SiC, ZrB_2-$MoSi_2$. A possibility of manufacturing of dense zirconium boride based ceramics at temperatures $1400 - 1600^o$ C i.e. at temperatures on $500 - 600^o$ C lower if compared with those temperatures used in sintering technology of ultra-high temperature ceramics is being considered. Обнаружено, что поставленная задача решается, в частности, при использовании в качестве активатора спекания небольших добавок карбида хрома. We found out, that in a process of sintering of ceramic composite materials which include chromium carbide Cr_3C_2, chromium carbide losses a part of carbon with its transformation into lower carbides. According to the equilibrium diagram Cr – C it means a transition of chromium carbide in much fusible states even up to eutectics Cr – $Cr_{26}C_7$ and Cr-ZrB_2, which melting temperature is close to 1500° C.

A presence of liquid phase in a form of carbon solution in chromium in the above said system may bring to interaction of eutectic type of liquid chromium based solution with zirconium diboride and is escorted by a formation of new liquid phase even at temperature near 1300° C. At sintering the highlighted eutectic interaction is followed by a formation of lower chromium borides (Cr_2B, Cr_5B_3), and the process itself goes in presence of liquid phase that disappears with the lapse of time.

Thus, carbon allocated in a process of transformation of initial chromium carbide should reduce zirconium oxide presented on the surface of zirconium diboride particles and facilitate its sintering.

As to vacuum hot pressing, material's behavior at sintering was investigated at the amount of second phase (chromium carbide) in a broad interval from 0 to 50%. As to hot pressing of ceramics on the base of zirconium and hafnium borides without special protective medium, chromium carbide amount was varied in terms of 2-15%. It's found out that even small amounts of chromium carbide (up to 5%) provide sintering of ceramic up to almost porous free states at temperatures 1400-1600° C. Investigation of structure and phase composition of ceramic highlights the active interaction of charge's components. The final ceramic's structure includes zirconium boride, new phase in a form of solid solution Zr (B, C) on the base of cubic crystal lattice of NaCl type and chromium borides (CrB, CrB_2). Zirconium and hafnium borides based ceramic samples with the amount of

chromium carbide in charge up to 5% possess grain size of 5 mkm and strength 560-640 MPa at room temperature.

1.1. Interaction of zirconium and hafnium borides with chromium, nickel, nichrome

To analyze the effective sintering of UHTCs is reasonable to start with investigation of processes of interaction of borides with some metals. The obtained results are directly related to activation of sintering of simple borides for example zirconium boride, which is a rather promising material for creation of ultra high temperature constructional ceramic [2]. However, its use as such application is rather hard, mainly, according to two reasons: pure zirconium boride oxidizes already at $900–950^0C$ [3]; due to a big share of covalent bonds and their strength it has a low diffusion mobility of atoms in crystal lattice and, respectively, difficulties associated with it at production of articles by sintering.

Recently the elevation of heat resistance has been successfully resolved by introduction of additives with formation of composite ceramic materials, at which oxidation defects free protective films are formed on surface. The most effective in this respect are the additives of SiC and $MoSi_2$ [4-6]. While looking into the activation of sintering process, mechanical, chemical, electro-physical methods of grinding and purification of surface were used. The most efficient was an introduction of 1-5% of various additives (carbon, boron carbide and other refractory compounds) in charge, which interact with surfaces of sintering particles and weak a strength of interatomic bonds and thus to elevate diffusion mobility of atoms in their pre-surface layers [7-9]. Not less effective in this respect one may consider the additives of metals especially those which form eutectics at interaction with borides. This way of activation of sintering was approbated in work [10], where it was shown that introduction of metallic chromium up to 5% in boride charge allows decreasing sintering temperature on $250–300^0C$, porosity – up to 2–5% and t elevate strength characteristics in 1,2–2 times. Thus, the introduction of metallic additive interacting with boron under eutectic mechanism turns the system in sintering mode in the presence of disappearing liquid phase. The appearance of this phase, its interaction with the matrix material, phase and structural transformations occurring both in liquid and the matrix material starting with a moment of its formation up to complete degradation, for now are insufficiently studied and has some certain scientific and practical interest. That is why they are the objective of this section of report.

1.1.1. Wetting processes and phase formation in system $ZrB_2(HfB_2)$ – Cr (Ni, NiCr)

A liquid phase, which amount grows with a time, appears at interaction of zirconium boride with nickel in a contact area. The interfacial angle from the moment of appearance of liquid phase at $1150^o C$ with elevation of temperature up to $1350^o C$ decreases from 40° to $3-5^o$. Products of interaction go inside samples volume in a full amount.

Interaction of zirconium boride with chromium begins at much higher temperatures. Thus, the first signs of appearance of liquid phase in the contact area were detected at temperature near 1800°C. Change of sample's surface interfacial angle by the products of interaction is illustrated on fig. 1.1.

A character feature of interaction of the investigated systems is that a liquid phase is formed in the contact area at temperatures lower than melting temperature of interacting components i.e. a contact melting, which exists only in systems with eutectics, takes place. According to the equilibrium diagrams the systems Cr – TiB_2, Cr – ZrB_2, and TiB_2 – (Fe, Ni, Co) possess eutectics. If to proceed from a character of interaction of ZrB_2 with nickel and chromium, these eutectics are present in these systems as well.

Contact melting occurs under the mechanism, which is defined by peculiarities of interfaces. The main issue in this process is an interaction of atoms of two neighboring lattices, which form a layer where an interphase area with atomic bonds distinguishable from those realized in separate phases, is formed. In this layer there is always a volume composition made from different atoms that has the eutectic composition. Namely this area at eutectic temperature turns into a liquid state forming nucleus of liquid phase of eutectic composition, as a free energy of liquid phase at T ~ $T_{eutectic}$ becomes lower than a free energy of solid interface layer.

A process of initiation occurs immediately after heating of alloy up to eutectic temperature. The last is governed by a relationship of a number of factors: energy of interaction between contacting components at interface, dimension correspondence in location of atoms on this surface, characteristics of elastic properties of phases and an appropriate elastic energy on interfaces, a ratio of free energies of liquid and solid state. Eutectic character of interaction zone is confirmed by the data of metallographic analysis.
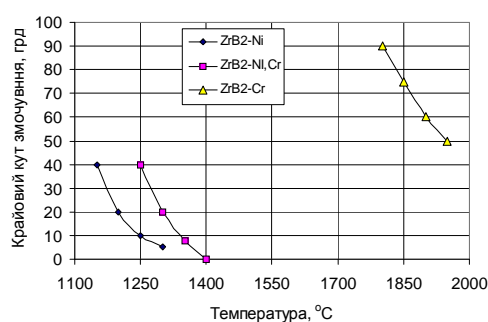

Fig.1.1. Temperature dependence of interfacial angle of zirconium boride by products of its interaction with chromium and nickel and Ni-Cr alloy for comparison

For investigation of both structure and phase composition of reaction products a set of model samples with different ratio of components in charge were prepared and investigated. For a correct comparison of samples' structures with equal amount of ZrB_2 a calculation of charges was carried out in a way that a ratio of number of

atoms of metal component to boron atoms was equal for all three metals – nickel, chromium and Ni-Cr alloy. The calculations were carried out through Avogadro's number.

For all samples of system ZrB_2 –Ni at heating the first signs of formation of liquid phase appear at temperature about 1150°C, and total melting occurs at 1500° C and *visa versa* a crystallization begins at 1250°C and stops at 1100 – 1040°C depending on components ratio in samples. This hysteresis of temperature of transformation *solid body – melt* and *melt – solid body* is probably associated with a re-arrangement of crystal lattice and certain energy consumption.

Analogously the interaction of ZrB_2 with nichrome occurs. A difference is only that the first signs of formation of liquid phase appear at 1250°C. More than that, apart from hysteresis in temperature of melting and crystallization, which made more than 100°C, in temperature interval 950–1000°C as a result of solid phase reaction there is a short temperature fall on 100–150°C at heating and temperature elevation at cooling. Especially this effect appears for samples with components ratio close to eutectic one. It should be also noted, that the samples, where the ratio Me/B made 3,54–2,35 even at temperature 1750°C were not completely melt.

In general, in quasibinary system ZrB_2–Ni two eutectics are found. One crystallizes at temperature 1150±30 °C, which component is pure nickel and intermetallide Ni_5Zr doped by boron, another – ternary eutectic, which crystallizes at temperature 1080±30 °C, and includes nickel and two intermetallides Ni_5Zr and Ni_7Zr_2. As ratio ZrB_2/Ni increases up to 0,3 and bigger metal component of reaction products disappears completely,and along with intermetallides Ni_5Zr and Ni_7Zr_2 doped with boron, the lower borides of nickel Ni_2B and NiB appear. Analogously the interaction of zirconium boride with chromium occurs. A difference is that the process occurs at rather higher temperatures –1700–2000 °C.

In quasibinary system ZrB_2–Cr the alloy is in a zone of hypoeutectic concentrations and at cooling at temperature 1880–1900 °C crystallites of pure chromium are formed, which shape's roundness is governed by a high level of symmetry of its bcc lattice. In intergrain space at temperature 1700–1750 °C eutectic crystallizes. The last represents regularly crystallized mixture of pure chromium and one of its lower borides. A peculiarity of the last is that because of low symmetry of crystal lattice it has one at maximum two planes energetically favorable for conjugation. Crystal nucleus in this case grows mainly in one or two directions, forming needle- or leaf-like form and this, in its turn, governs a typical eutectic structure. In chromium part of quasibinary system ZrB_2–Cr the interaction of zirconium boride with chromium goes on eutectic mechanism with formation of chromium borides, and lower boride are partially doped with zirconium.

At interaction of ZrB_2 with alloy Ni–20 Cr a structure of reaction products even in hypoeutectic alloys with ratio ZrB_2/(Ni,Cr) from 0 to 0,15 differs significantly. Apart from classic components, such as initial metal crystallites and eutectic, there appears a net of needle-like crystallites, which number and size increase as concentration of ZrB_2 in charge grows. Separate eutectic colonies are similar to those formed at interaction of ZrB_2 with nickel, and are cutoff by regularly located parallel planes of another phase. Structure of eutectic

colonies more and more becomes similar to structure of "brooms". Especially clear it is manifested for hypoeutectic and hypereutectic alloys close to eutectic. Probably it is one of ternary eutectics.

Needle-like initial crystals of one of boride phase are formed in hypereutectic alloys. The structures of this alloy point out that the main mass of chromium is concentrated in eutectic in the form of lower borides, that was confirmed by measurements of their microhardness. Thus, a microhardness of initial crystals at loading 50g makes 2040 ± 80 kgf/mm^2, that is in an agreement with data for CrB_2. In its turn nickel is concentrated from one hand in eutectic component of structure, and from the other – together with zirconium in a ratio 50/50 in the second boride phase, which has a microhardness 1900 ± 80 kgf/mm^2.

As ratio $ZrB_2/(Ni,Cr)$ increases in charge composition up to 0,3 and higher the eutectic component disappears. The alloy crystallizes in a form of mixture of elongated variously headed crystallites – boride phases with a low level of symmetry of crystal lattices. At given ratio of components in charge as a result of annealing at temperature 1850^0C metal component – nichrome disappears and a number of compounds are formed: residual unreacted ZrB_2, nickel borides – Ni_2B, NiB, Ni_4B_3, chromium borides Cr_5B_3 and CrB_2, intermetallides – Zr_2Ni_7 and Ni_2Cr_3, as well as ternary boride $Cr_2Ni_3B_6$. A lot of phases each of those has its own coefficient of thermal expansion, bring to significant inner stresses which often are close to ultimate strength. Thus after crystallization the alloy becomes brittle and even at negligible loading easily fractures.

Thus, the investigation of interaction of zirconium diboride with nickel and chromium and their alloy Ni–20Cr in metal angle of quasibinary equilibrium diagram Me – ZrB_2 has been carried out. It is shown that the process goes under the mechanism of contact melting typical for eutectic systems. A phase composition of products of interaction depends on components ratio in charge. For nickel and nichrome in hypo- and eutectic alloys the main components which form eutectic are nickel itself and its intermetallides $ZrNi_5$, Zr_2Ni_7. Boron does not form thus independent structural elements and dissolves mainly in intermetallides as its solubility in nickel is negligible. In case of interaction with nichrome even in hypoeutectic alloys together with eutectic nickel – intermetallide a net from boride Cr_3B_4 is formed.

In hypereutectic alloys where the amount of boron in alloys strongly increases, along with intermetallides Zr_2Ni_7 and Cr_3Ni_2 doped by boron, a number of borides – Cr_5B_3, CrB_2, Ni_2B, NiB, Ni_4B_3 and even ternary boride $Cr_2Ni_3B_6$ are formed. At interaction of zirconium diboride with chromium the process goes under the mechanism of contact melting with formation of eutectic alloys. As ratio ZrB_2/Cr increases with correspondent elevation of boron amount in alloy, along with Cr_2B the phase Cr_5B_3 appears in structure.

Contact interaction of hafnium diboride with chromium is investigated. It is found out, that the first signs of liquid phase in a contact zone appear at temperature near 1750^0C. Interfacial angle of boride makes 10^0. As temperature reaches 1900^0C it decreases up to 0^0.

Investigations of depending of melting temperature and phase composition of products of interaction vs. components ratio in alloy showed that quasi-binary system HfB$_2$–Cr is eutectic equilibrium diagram. Eutectic

point with melting temperature near 1750^0C is found at 20 mass% HfB_2. By metallographic, x-ray phase and x-ray micro spectrum analyses it is found out that phase composition of reaction products depends on components ratio in alloy. In chromium part of quasi-binary state diagram there is approx. up to 28–30% HfB_2 and lower chromium boride Cr_2B with rhombic crystal lattice is the main product of reaction. Low symmetry of the last defines both a way and a form of boride crystallization and a character and appearance of eutectic which it forms with chromium. In boride hafnium angle of the diagram a phase composition of reaction products is rather variegated. Along with Cr_2B, Cr_5B_3, HfB and intermetallide Cr_2Hf are crystallized here, which together with excess HfB_2 form ceramic composite material. X-Ray phase and MRS analyses of HfB_2-Ni and HfB_2-(Ni,Cr) hypoeutectic alloys have been carried out. The main peculiarity of the alloys is the formation of $Hf_3Ni_{20}B_6$ and $Cr_2Ni_3B_6$ triple compounds.

1.1.2.   Peculiarities of interaction of ZrB_2 with chromium

In this section a systematic investigation of processes of phase interactions is demonstrated by the example of rather simple system of interaction ZrB_2 – Cr.

Materials and methodology

As initial materials the powders which compositions presented in Table 1.1 were used.

Initial sizes of chromium and zirconium boride powders made not more than 56 mkm. Preparation of charges and a production of samples were made under the common methodology of production of articles by powder metallurgy techniques [11]. Mixing and grinding of initial powders were performed in hard alloy ball mills in ethanol medium. Billets were pressed at 1000MPa. Sintering and melting were carried out in alundum crucibles in vacuum furnace СШВЛ–06/25 at temperatures $1700-1900^0$C, residual pressure 0,1Pa and holding up to 0,5 hour. Contact interaction of ZrB_2 and chromium– temperature of appearance of liquid phase and dependence of boride wetting angle vs. temperature, temperature of the beginning and final stage of melting, the beginning and accomplishment of crystallization, as well as phase composition of alloys depending on components ratio in charge were investigated.

Structural investigation was carried out on metallographic microscope MIM–10, x-ray phase analysis– x-ray device DRON–2. Microhardness was measured by MPT–3 device. Investigation of material surface was carried out at scanning electron microscope ZEISS EVO 50XVP with the use of detectors of secondary electrons CZBSD (phase contrast). All investigations were carried out at accelerating voltage 20 kV and probe current 50pA.

Table 1. Chemical composition of used powders

Material	Amount of elements,%						Notes
	Me	B	C	Fe	N	O	
ZrB_2	78,5–80,8	17–19	1,2	0,1	–	0,1	TU88.USSR. 147.0.06–77
Cr(Пx-1)	99,3	–	0,1	0,2	0,15	0,1	TU14–1–1474–75

X-ray spectrum investigation of composition of sample area and in local parts the probes were made on energy dispersive analyzer of x-ray spectrums INCA 450. Sensitivity of analysis – from 0,1 to 1 % mass.

Results and discussion

Investigation of interaction of pair of compact ZrB_2–Cr showed, that the first signs of appearance of liquid phase in contact zone are observed at temperature close to 1800^0C. These data essentially differ from temperature of eutectic melting, obtained in [12]. It is governed by, most of all, that at contact melting the process occurs in inhomogeneous conditions with a big drop of components concentration in zone of melting. As temperature increases from 1800 to 1950^0C, wetting angle of boride by products of melting decreases from 90 to 40^0. All chromium turns in liquid, which with a time, flowing on surface and crystallizes. It should be noted that a characteristic feature of interaction in this system is that the liquid phase in a contact zone is formed at temperatures lower than those of melting of contacting components, i.e. there is a contact melting typical only for the systems with eutectic in their alloys equilibrium diagrams [13]. The second peculiarity is that the formed liquid as the result of contact melting with the substrate ZrB_2 turns in more refractory product which crystallizes at holding.

For more detailed investigation of structure, phase composition and its subsequent change depending on ratio of components in contact zone a set of molten samples with various ratio of zirconium boride and chromium in those samples (see table 1.2) is prepared and investigated.

Typical structure of formed alloys is represented on fig. 1.2.

Structure analysis shows that at ratio ZrB_2/Cr from 0 to 0,15 in quasi-binary system ZrB_2–Cr the alloy is found in the zone of hypoeutectic concentrations. At its' cooling at temperatures $1900–1880^0$C crystallites of pure chromium are the first to be born and their round shape are governed by high rate of symmetry of its bcc lattice.

At temperature $1760–1750^0$C eutectic crystallizes in inter-crystallite space. The last represents a mixture of crystallites of solid solution on the base of chromium and lower borides, carbo-borides and other binary and ternary compounds of chromium and zirconium built on the base of their lattices. A feature of the last is that due to a low symmetry of crystal lattice they have one and/or maximum two planes energetically favorable for

construction at crystallization. In this case, the popped up embryo of crystal grows mainly in one or two directions, forming thereby needle- and/or petal like form that is stipulate eutectic typical structure (see fig. 1.2 a, b).

Table 1.2. Ratio of components in melted samples

Materials	Components ratio, g							
	Samples, №							
	1	2	3	4	5	6	7	8
ZrB_2	3,4	6,8	10,2	13,6	20,3	27,1	40,7	47,5
Cr	83,3	77,9	72,6	67,3	56,7	47,8	27,8	14,2

a

b

c

d
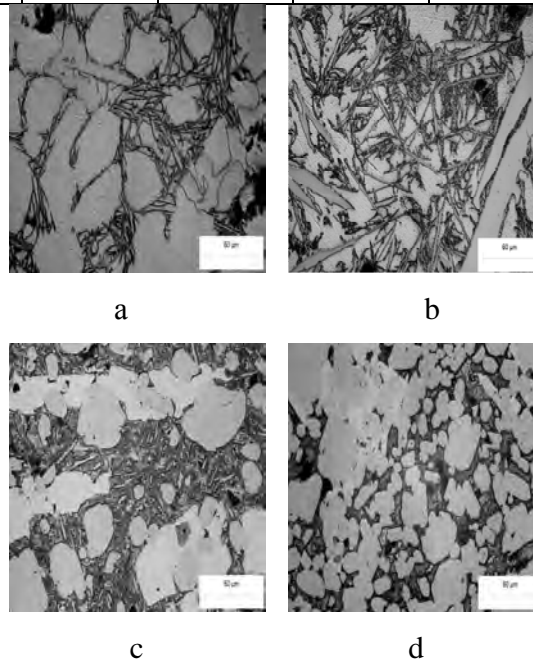
Fig.1.2. Structure of products of interaction of zirconium boride and chromium depending on ratio of interacting components: a–6,8ZrB$_2$–77,9Cr;   b–13,6ZrB$_2$–67,3Cr; c–27,1ZrB$_2$–47,8Cr; d– 40,7ZrB$_2$–27,8Cr.

X-ray micro spectrum analysis of eutectic area is presented on fig. 1.3., where a distribution of concentration of the main elements of system participating in a reaction is illustrated. Obviously, that eutectic represents a mixture of solid solution of boron and zirconium in chromium from the one hand and from the other hand zirconium borides doped with chromium and ternary compounds of zirconium, chromium and boron.

a)   b)
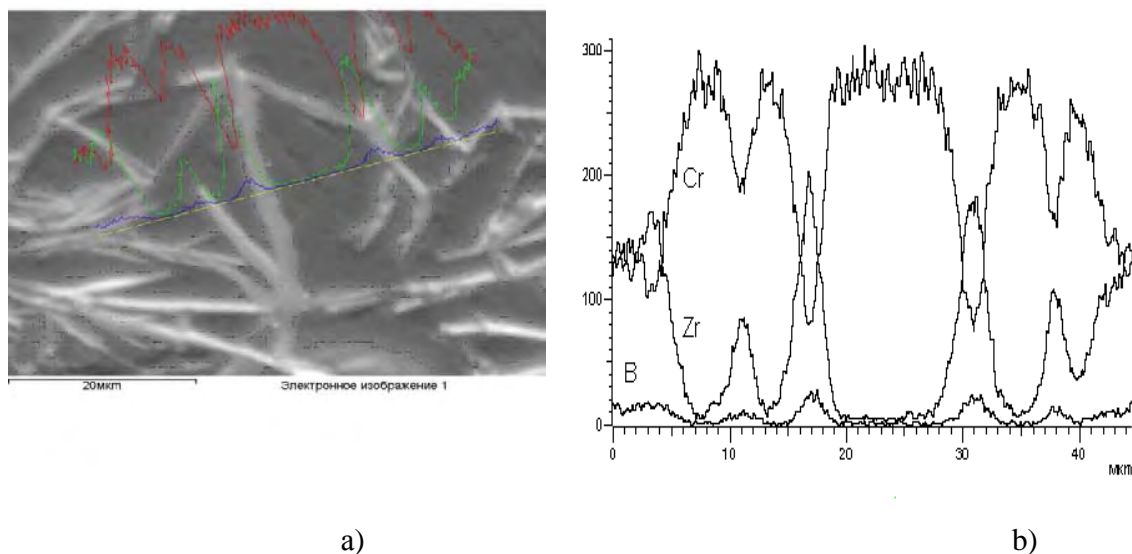
Fig.1.3. Micro X-ray spectrum analysis of eutectic in system ZrB$_2$–Cr: a - microscopic image and scanning line, along which elements distribution is defined (b).

As ratio ZrB$_2$/Cr increases up to 0,3 and bigger the alloy turns into eutectic and hypereutectic with allocation of initial hypereutectic crystals (see fig. 1.2c,d). Metallographic and X-ray micro spectrum analyses of structure both before and close to eutectic hypereutectic alloys showed that zirconium and boron in crystallized crystallites of metal and metallic component of eutectic are within the limits of their solubility in chromium. Moreover, Al and oxygen entering the alloy due to its interaction with alundum crucible are also present (see fig. 1.4).

Zirconium and born together with chromium and carbon available in charge as a technological impurity form initial hypereutectic crystals and the second after solid solution chromium based eutectic component. It should be noted that, these crystals have a rather complicated chemical composition and represent ternary compounds on the base of chromium, boron, zirconium and carbon in different variations (see fig. 1.5). Moreover, initial hypereutectic crystals are at least bi-phase (see fig.1.5 a). Obviously, at a time of crystallization, a single phase compound chemically complicated and stable only in the field of high temperatures is formed. At cooling it disintegrates onto two components. Thus, both in initial and compounds formed at disintegration the basement of metal sub-lattice is made by zirconium, non-metallic lattice - for one boron for another - more likely carbon (see figs. 1.5 b, c). Each of those is partially doped with chromium (see fig. 1.6).

Analysis of elements, % wt.

Spectr.	B	C	O	Al	Cr	Zr	in total
1					100,0		100,00
2	10,18		2,03		87,79		100,00
3				0,62	99,38		100,00
4				0,42	99,58		100,00
5	22,91	8,81			1,03	67,25	100,00
6	24,21	8,83			0,87	66,09	100,00
7	23,24	8,06			1,16	67,54	100,00
8	16,80	12,3			18,13	52,80	100,00
9	21,77	10,4			5,72	62,10	100,00
10	22,75	9,31			0,87	67,08	100,00
11	14,96	5,87	2,65	0,24	17,31	17,31	100,00

Fig.1.4. Structure and chemical composition of phases close to eutectic of hypereutectic alloy $16,6ZrB_2$–$67,3Cr$: numbers mean points of executed analysis which results are presented in table.

At temperature 1760–1750^0C eutectic crystallizes in inter-crystallite space. The last represents a mixture of crystallites of solid solution on the base of chromium and lower borides, carbo-borides and other binary and ternary compounds of chromium and zirconium built on the base of their lattices. A feature of the last is that due to a low symmetry of crystal lattice they have one and/or maximum two planes energetically favorable for construction at crystallization. In this case, the popped up embryo of crystal grows mainly in one or two directions, forming thereby needle- and/or petal like form that is stipulate eutectic typical structure (see fig. 1.2 a, b).

X-ray phase analysis of these alloys showed that their structures apart from chromium based solid solution possess phases with parameters of crystal lattices close to those typical for borides ZrB_2, Cr_2B, Cr_2B_3, ZrB. That is why one may assert that namely on the base of lattices of these compounds ternary and more complex phases were formed by means of partial substitution of atoms of their metallic and non-metallic sub-lattices by atoms of other metal and carbon. Thus a micro-hardness of the main phases at loading 50g made $2\pm0,3$ and $21,6\pm0,8$ GPa, that is close to values of micro-hardness of pure chromium and chromium and zirconium diboride respectively.

This is proved by X-ray micro spectrum analysis of eutectic area. The lastly solidified eutectic represents a mixture of chromium based solid solution, its carbide $Cr_{23}C_6$ and the above described carbo-borides of zirconium and chromium (see fig. 1.6).

| a | b | c |
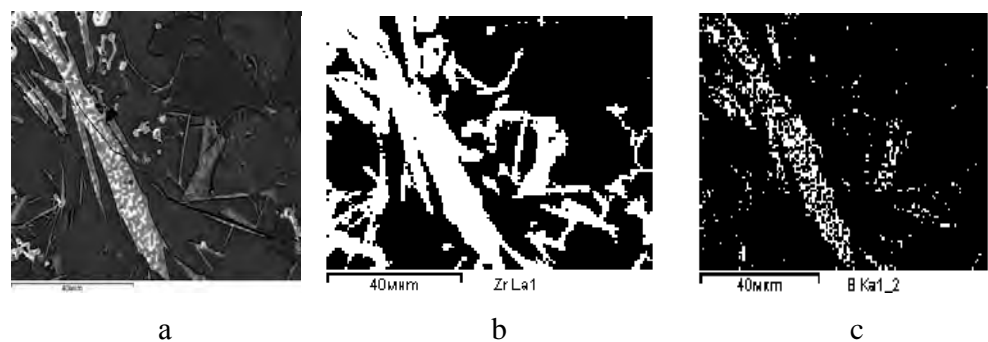
Fig.1.5. Typical appearance of hypereutectic initial crystals and distribution of zirconium and boron in it

Further elevation of ratio of zirconium boride to chromium up to 0,5 and even higher the ratio of structural components of alloy changes: decreases up to disappearance of eutectic which space is occupied by the above said products of interaction (see fig.1.2d). In boride angle of quasi-binary state diagram ZrB_2–Cr alloy structure represents a carcass from zirconium boride, which intergrain space is filled with one of the most complex zirconium boride-chromium, thus, the bigger is ZrB_2 content in alloy the bigger is boron content in this boride. So in alloy with 77%ZrB_2 this filler is zirconium carbo-boride– chromium, built on the base of lattice Cr_2B_5. As it was shown above, being in the intergrain space, some of these complex borides are stable only in the field of high temperatures and at cooling disintegrate (see fig. 1.6). This phase transformation greatly stimulates diffusion processes on boundaries of adjoining grains facilitating their consolidation.
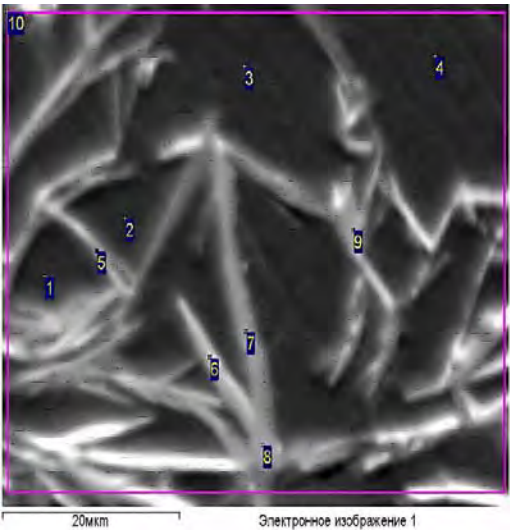
Spectrum	B	C	O	Cr	Zr	In total
1		7,62		92,38		100,00
2		6,50		93,50		100,00
3		6,38		93,62		100,00
4		5,49		94,51		100,00
5		7,53		92,47		100,00
6	9,27	10,81		74,69	5,22	100,00
7	17,13	15,02		63,03	4,82	100,00
8	32,93	16,40	2,47	23,27	24,93	100,00
9	12,90	21,85		53,81	11,44	100,00
	20,62	12,95	4,28	50,28	11,86	100,00

Fig.1.6. Structure and chemical composition of elements of eutectic colony

Thus, the process of interaction of zirconium boride with chromium occurs under the mechanism of contact melting. The liquid of eutectic composition formed in contact zone wets zirconium boride with wetting angle about 40^0. The next interaction of this liquid with a substrate with formation of much higher multi-component refractory compounds brings to its disappearance. Chemical composition of these compounds is governed by components ratio in a liquid phase which in its turn is defined by initial composition of alloy and temperature of process. Realization of this mechanism in conditions of pressed powder compositions brings the whole system to sintering in the presence of disappearing liquid phase. The above said phase transitions in newly formed compounds on grain boundaries make it easier. Moreover, chromium has a rather high vapor elasticity, which at temperature 1800^0C makes about $8 \cdot 10^2$ n/m^2 [14]. Thus even in the process of heating up to the temperatures of contact melting chromium present in powder composition in a solid state partially vapors out uniformly distributing on surface of zirconium boride particles surrounding chromium. In other words there is a contact of two eutectic phases (chromium and zirconium boride) with high specific surface and low eutectic temperature of melting ($T_{Melting}$ ~1530^oC). At temperatures below the eutectic one it brings to formation of diffusion zones with high energies of deformation (see the previous quartile report) and to higher diffusion activity of atoms of chromium, zirconium and boron in diffusion zone to its landmark that accelerates sintering process. Falling from this chromium may be a promising element as the agent which activates sintering of boride systems including ZrB_2.

1.1.3. Sintering and some properties of ceramics

Being based on the results obtained at previous stages devoted to the investigation of hafnium and zirconium borides with nickel and chromium and their alloys, for sintering of the above said borides and ceramics ZrB_2-20 mass. % SiC as sintering activator the alloy Cr-20 mass. % Ni was taken. Approbation of sintering activator was carried out at sintering of the above said ceramic with addition of 5 vol. % of chosen alloy. As a result it was found out that optimum sintering mode for this composition is temperature 1800-1850°C at isothermal holding 1 hour. Thus the porosity is found within up to 5 % and ceramic bending strength -400MPa.

Temperature dependence of shrinkage and bending strength of ceramic composite material obtained as a result of interaction of mixed and grinded powders of zirconium boride and NiCr-alloy in a ratio (% vol.) ZrB_2– 81 (Ni–20Cr)–19 is investigated. Sintering was carried out in vacuum at pressure 10^{-2} mmHg during 30min in temperature interval 1100–1700^{0}C. The obtained results are presented on figs. 1.7, 1.8.

X-ray phase analysis of composite showed that at the above said sintering mode a metallic component of charge-nichrome in the process of formation of composite disappears completely. As a result of its interaction with zirconium boride a number of borides such as Ni_2B, NiB, Cr_5B_3, CrB_2, as well as ternary compound $Cr_2Ni_3B_6$ are formed. Thus a background of composite is still the phase ZrB_2.
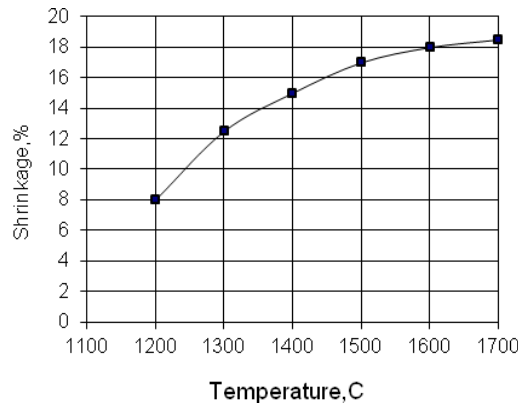
Fig.1.7. Dependence of shrinkage vs. sintering temperature of composite 81ZrB$_2$–19(Ni–20Cr).
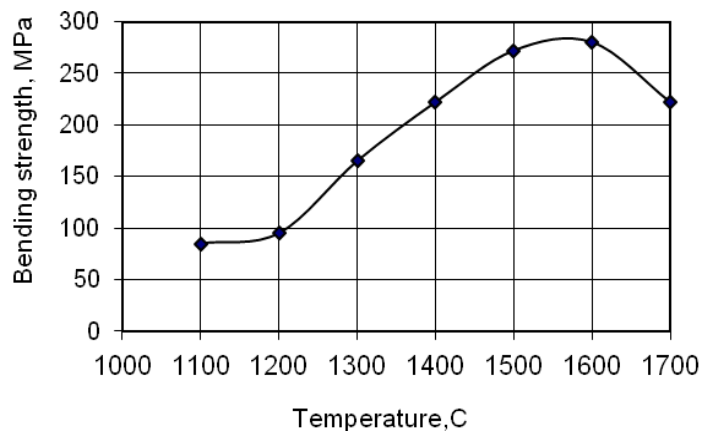

Fig 1.8. Dependence of bending strength vs. temperature of composite 81ZrB$_2$–19(Ni–20Cr).

Maximum bending strength (about 300MPa) at given ratio of components and conditions of formation is achieved at sintering temperature 1600^{0}C. Comparatively small level of strength, first of al, is governed by a fact that composite's structure has a small amount a number of various boride phases, each of those has own different thermal expansion coefficient that brings to inner stresses. This at rather big size of grain influences on a level of composite's strength as a whole. Composite hardness makes about 88–89HRA.

A character of structure of sintered samples is illustrated on fig. 1.9.
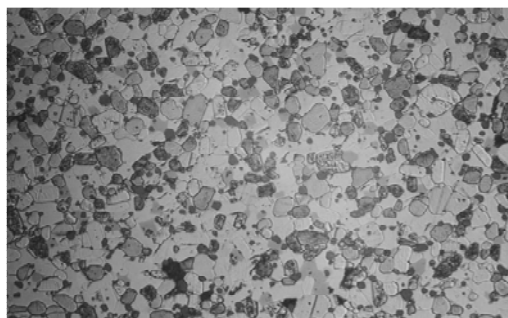
Fig. 1.9. Microstructure of ceramic composite material of system (%vol.) $81ZrB_2$–$19Cr$, obtained at temperature 1600^0C

Analogously temperature dependence of formation of composite of system ZrB_2–SiC was investigated. Calculation of charge was thus carried out in a way that volume ratio ZrB_2/SiC in it met 3÷4, that corresponds to optimum one. To decrease the influence of inner stresses the amount of active agents was reduced to minimum. As a result the following composition of charge was calculated (% vol.): ZrB_2–72, SiC–22, Cr–5, Ni–1.

After 15 hours grinding in ball mill the samples were formed according to standard methods of powder metallurgy. Sintering was carried out in temperature interval 1600–1900^0C.

The results are presented on figs. 1.10,1.11. Unlike the above considered variant at x-ray analysis of the investigated system, it was found out that phase composition of samples after sintering is rather modest. Dominating phases are still ZrB_2 and SiC. New phases are Cr_5B_3 and CrB_2. New Ni based formations are absent at all. Obviously its' amount in the alloy is in proportion to its solubility in the main phases of composite. Less amount of new formed phases an respectively low level of inner stresses may explain higher bending strength of composite (see fig. 1.11). Composite hardness makes 89–90 HRA.

Character of structure of these composites are illustrated on fig. 1.12. Thus the process of formation of ceramic composite material on the base of ZrB_2 by activated sintering in vacuum was investigated. It is shown that to provide the higher physico-mechanical properties at activated sintering the amount of active agents introduced in charge should be enough to stimulate sintering processes (intensification of pre-surface diffusion of boride particles) and minimum to develop reactions of formation of new phases being based on elements entering in active agent.
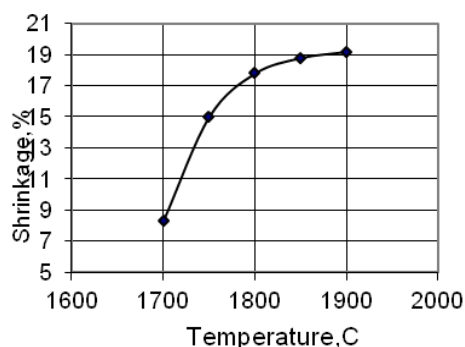
Fig.1.10.Dependence of shrinkage vs. sintering temperature of composite material $72ZrB_2$–$22SiC$–$5Cr$–$1Ni$ (vol.%).
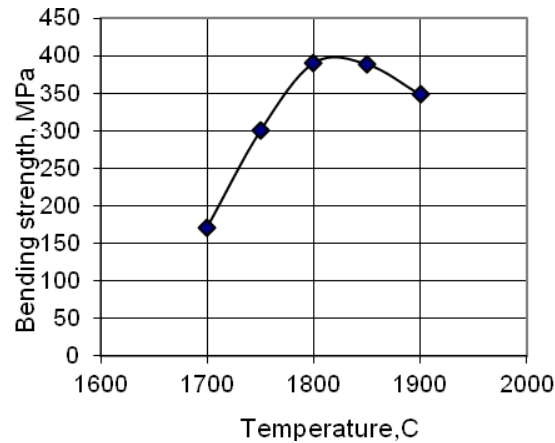
Fig.1.11. Dependence of bending strength vs. sintering temperature of composite material (vol.%):

$72ZrB_2–22SiC–5Cr–1Ni$.
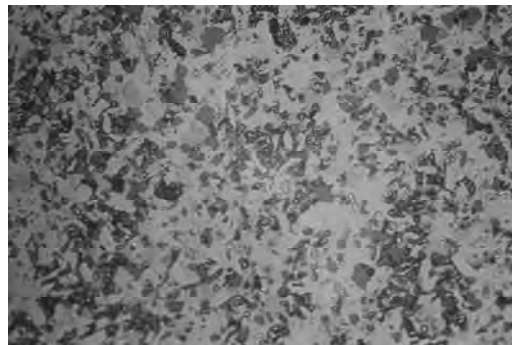
Fig.1.12. Microstructure of ceramic composite material of system

$72ZrB_2–22SiC–5Cr–1Ni$ (% vol.)

1.1.4.   Conclusions

• The interaction of zirconium boride with chromium within quasi-binary state diagram $Cr–ZrB_2$ with variation of concentration of zirconium boride from 4 to 77% was investigated. It's shown that the process goes under the mechanism of contact melting that is typical for eutectic systems. Eutectic melting temperature is near 1800^0C at concentration of ZrB_2 in alloy is near 16% by mass.

• Eutectic wets boride surface with wetting angle close to 40^0 and, while interacting with a formation of more refractory compounds disappears.

• Phase composition of products of interaction depends on components ratio in alloy and temperature, representing bi- and ternary compounds built mainly on the base of crystal lattices of zirconium and chromium borides.

• Eutectic character of quasi-binary diagram $Cr–ZrB_2$, small wetting angle between eutectic and boride surface, phase interactions in products of interaction, located in intergrain layers, and an opportunity of uniform

distribution through the whole volume of charge via steam phase make chromium rather promising material for its use as activating agent for sintering.

- Being based on the results obtained at previous stages devoted to the investigation of hafnium and zirconium borides with nickel and chromium and their alloys, for sintering of the above said borides and ceramics ZrB_2-20 mass. % SiC as sintering activator the alloy Cr-20 mass. % Ni was taken. Approbation of sintering activator was carried out at sintering of the above said ceramic with addition of 5 vol. % of chosen alloy. As a result it was found out that optimum sintering mode for this composition is temperature 1600 - 1850^oC at isothermal holding 1 hour. Thus the porosity is found within up to 5% , ceramics grains size is 10-15mkm, ceramic bending strength up to 400MPa and hardness level is 88-89 HRA. Interaction of ceramics components brings to a presence of chromium boride based secondary phases apart from the main phases ZrB_2 and SiC.

1.2. Investigation of kinetics of densification of ZrB_2 based materials at hot pressing in vacuum

1.2.1. Influence of chromium carbide (Cr_3C_2) on consolidation process of zirconium diboride

Introduction

This section studies the additives of chromium carbide which activates sintering of UHTCs /15/. Perspectives of use of higher chromium carbide Cr_3C_2 are presumably associated with that Cr_3C_2 in the presence of other refractory compounds, as nitrides /16/ and borides, loses carbon with formation of lower carbides up to the eutectic $Cr-Cr_{23}C_6$ (melting temperature 1530^oC). Free carbon thus promotes system refining, eliminating oxygen from it and enters as a part of new formed phases. With appearance of free chromium a formation of other eutectic $Cr-ZrB_2$ with melting point about 1500^oC /12/ is also possible. One may assume that irrespective of presence of liquid phase, activation of sintering in the investigated system will be possible as result of phase interactions with formation of new refractory compounds.

In this section of work the objective is to investigate the mechanism of influence of Cr_3C_2 on the process of consolidation ZrB_2, and structure - and phase formation in the system [ZrB_2-Cr_3C_2].

Materials and methodology

Investigations of shrinkage kinetics of HfB_2 with sintering activators and system $ZrB_2 + Cr_3C_2$ were carried out by static hot pressing method at lab vacuum press with the aim to accumulate the experimental data about parameters of manufacturing process of compact materials.

Powders of ZrB_2 and Cr_3C_2 of type "Ч" manufactured by Donetsk plant of chemicals (Donetsk) were used. The composition of powders is presented in table 1.3. The average size of grain ZrB_2 and Cr_3C_2 in an initial state was 7,7 and 9,1 mkm accordingly. The charges containing 5, 20 and 50 wt. % of chromium carbide obtained in a ball mill lined by Kaprolon according to the standard technique in powder metallurgy. The average size of particles was 3,5 mkm.

Table 1.3. Impurities, %mass

Powder	O2	C_{total}	C_{free}	Fe	B	B_2O_3
ZrB_2	1,25	0,10	–	0,10	18,6	0,20
Cr_3C_2	1,10	12,7	0,10	0,11	–	–

The structure and phase composition of samples were investigated by the methods of X-ray analysis (XRD), raster electronic microscopy (REM), transmission electronic microscopy (TEM) and optical microscopy (OM). The kinetics of consolidation of a number of compositions [ZrB_2-Cr_3C_2], in temperature interval 1520 … 1740 C under pressure 48 MPa was investigated. Temperature elevation rate varied from 30 to 1000 C/min.

Results and discussion

For ZrB_2 without additives the density was 0,820 and 0,912 respectively at temperatures 1600 ^{0}C and 1915 ^{0}C samples. The obtained kinetic curves are characterized by a presence of two stages of densification of ZrB_2: initial, terminated over 1,5...2 min, and a long-term diffusion ones where a kinetic curve is linear.

The peculiarities of densification of four compounds of $ZrB_2 + Cr_3C_2$ system with the amount of Cr_3C_2 from 5 to 80 mass. % are investigated. It's found out that densification up to a compact state of compounds with additives of Cr_3C_2, could proceed at temperatures on 300…700°C lower than a densification of pure ZrB_2. Thus, a mixture with 50 mass. % Cr_3C_2 is densified up to a compact state at 1600°C, and with 80 mass. % Cr_3C_2 – at 1250 ^{o}C. Kinetic curves of densification of the above said compounds are recorded; optimum parameters of densification process are defined. Decreasing of the amount of chromium carbide in charge up to 5 % as previously provides a high density of ceramic at rather low temperatures of hot pressing. Due to the differences of phase compositions in the same conditions of pressing (T = 1425°C; P = 45 MPa) a mixture with 5 mass. % Cr_3C_2 is densified much faster then mixture with 20 mass. % Cr_3C_2.

Shrinkage kinetic curves of composites with the above said compositions are recorded; optimum technological parameters of the process are defined. Fig. 1.13 provides a general idea about possible modes of pressure sintering of ceramics of system $ZrB_2 – Cr_3C_2$ and an effectiveness of activation of sintering of zirconium diboride in presence of chromium carbide. This figure illustrates kinetic curves of consolidation of composition [50mass% ZrB_2 + 50mass. % Cr_3C_2] at temperature 1740°C: the curve T1 matches to the elevation of temperature - 30°C/min, $\square_1 = 0,958$; the curve T2 - 1000°C/min, $\square_2 = 0,970$. Analogous dependences of speed and density were obtained for other compositions as well. Densification rate and final density essentially depend on a temperature mode at sintering. Heating with a low speed allows to track in details behind the processes of sintering acceleration and deceleration, associated with phase and chemical interactions in charge

whereas the high speed of temperature elevation with maximization of a stage of isothermal holding provides a reception of max dense sintered ceramic.
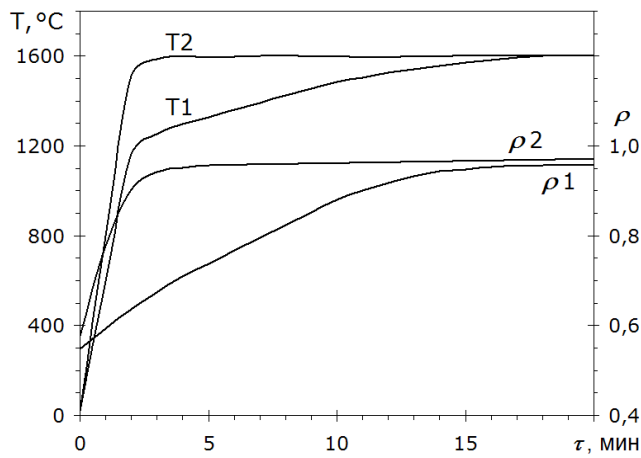

Fig. 1.13. Influence of speed of temperature elevation on densification at hot pressing [50mass. % ZrB2 + 50mass. % Cr3C2]. Final density $\square_1 = 0,958$; $\square_2 = 0,970$ at T = 1740°C.

Fig. 1.14 illustrates the kinetic curves of shrinkage of compositions on the basis of ZrB_2 with additives from 5 to 50 mass. % Cr3C2, and also initial ZrB_2.
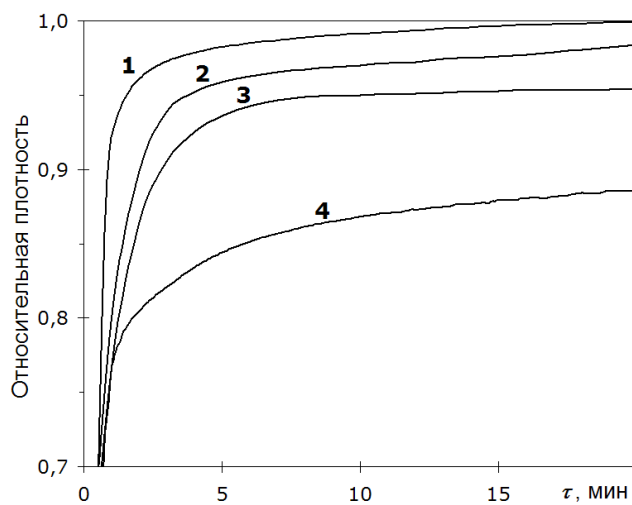
Fig. 1.14. Kinetics of densification ZrB_2 with Cr_3C_2 (curves 1 … 4):

1. 5 mass. % Cr3C2;   T=1520 C; $\square$ =1,000;

2. 20 mass. % Cr3C2;   T=1520°C; $\square$ =0,987;

3. 50 mass. % Cr3C2;   T=1740°C; $\square$ =0,954;

4. ZrB_2 initial; T=2170°C; $\square$=0,885

From comparison of kinetic curves of shrinkage ZrB_2 with Cr_3C_2 and without a conclusion comes about considerable activation of densification of ZrB_2 by chromium carbide. Densification of [50 mass. % ZrB_2

+50 mass. % Cr_3C_2] to almost compact condition is attained at temperature 1740°C. The compositions with Cr_3C_2 in the amount of 5 … 20 mass. % are already dense at temperature 1520°C.

The X-ray phase analysis (see Fig. 1.15) of samples of studied system with various quantities of additives of chromium carbide shows that at hot pressing in ceramics there is an interaction of components accompanied by carbon loss of from initial Cr3C2 and its consecutive transformation into the lower carbides (Cr7C3, Cr23C6) up to their disappearance, even at the high amount of chromium carbide in the initial charge. Thus depositing carbon is spent for a formation of a new high-temperature phase - zirconium carbide ZrC (with lattice NaCl) and solid solutions on its basis (the phase 2 in fig. 1.15). Formation of new solid solutions is witnessed by a displacement of diffraction lines regarding their position for ZrC. For the investigated system it is associated with boron dissolution in the specified carbide, in quantity comparable with a total amount of carbon, with formation of ZrBC. A formation of this phase at interaction of zirconium boride with carbides is well known, for example, in system ZrB2-SiC /17/. Elevation of the amount of chromium carbide is accompanied by drastic decrease of the amount of initial zirconium diboride (the phase 1 in fig. 1.15) and increase of the amount of phase on the basis of ZrC and formation of chromium boride (the phases 2 and 3 in fig. 1.15). Hence, chromium and boron from disintegrating chromium carbide and zirconium boride is spent for formation of chromium borides of type CrB (as shows the detailed analysis of samples of given system, other lowest chromium borides up to CrB_2 and appropriate solid solutions Cr (Zr) B (C)). The roentgenogram A (fig. 1.15) has also weak lines which are identified as the lines of tungsten carbide, but with essential loss of carbon to the amount matching W_3C.
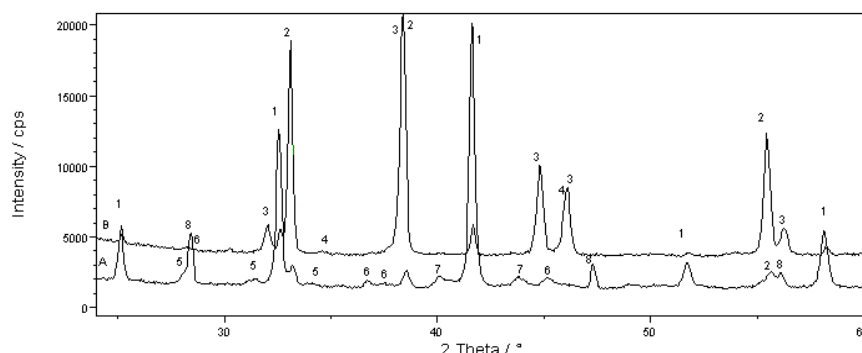
Fig. 1.15 Fragments of roentgenograms of hot pressed samples of system ZrB_2-Sr_3C_2.
 A - 95%ZrB2+5%Cr3C2, T=1520°C; **B** - 50%ZrB2+50%Cr3C2, T=1740°C; lines of the identified phases: 1-ZrB2; 2-ZrC; 3 CrB; 4-CrB2 (traces); 5-ZrO2; 6-Cr5B3; 7-W3C; 8-Si (the internal standard)

Formally a final composition of ceramic as a result of interaction of zirconium boride and chromium carbide is reduced to carbon and boron exchange in initial phases under the scheme

$$ZrB2+Cr3C2 \rightarrow ZrB2_{(Residual)} +ZrC_{(ss)} +CrBx_{(ss)},$$

where ZrC $_{(ss)}$ and CrBx $_{(ss)}$ – solid solutions (ZrBC) and (CrBC) accordingly.

Thus, at high amount of chromium carbide (50 mass. %) phase interactions completely modify material composition. After hot pressing a dominating phase is the solid solution on the basis of zirconium carbide. Also the residual (~ 20 %) zirconium boride and new phases on the basis of chromium boride are present. Sintering of actually new ceramic system on the basis of refractory ZrC occurs at temperature 1740°C (fig 1.14). At the same time the charges on the basis of zirconium boride with small amount of chromium carbide (5 … 20 mass. %) and, accordingly, with small amount of formed zirconium carbide, are condensed to almost compact condition at lower temperature 1520°C (fig. 1.14).

The presented results allow assuming that in the system [ZrB2-Cr3C2] the observed activation of sintering is associated with eutectic interactions in system Cr-Cr$_{23}$C$_6$ specified above and in similar system Cr-ZrB$_2$. In that case the activation of ceramics sintering is caused by a formation of liquid phase disappearing at further phase interactions with formation of new high-temperature phases. Consolidation process proceeds, mainly, on the mechanism of contact melting [13], passing at the final stage (linear parts of kinetic curves) in diffusion stage.

Investigation of the nature of fixed acceleration of shrinkage at introduction of additives Cr$_3$C$_2$ was carried out in the experiments on investigation of contact interaction ZrB$_2$ and Cr$_3$C$_2$ in temperature interval 1310 - 1740°C with subsequent studying of the processes of structure - and phase formation in a contact zone. The experiments were carried out in graphitic moulds in a vacuum chamber of hot pressing press. Compact and porous billets of ZrB2 and Cr3C2 were used. To provide a contact between billets in an initial stage of the process of interaction the applied pressure was 48MPa. Samples were studied by REM and DFA methods. It was found out that a formation of diffusion zones at contact interaction of these materials begins at temperature near 1310°C.

Fig. 1.16 presents the example of contact interaction of samples ZrB2 and Cr3C2. Light stains of a break of a contact zone of samples ZrB$_2$ and Cr$_3$C$_2$ match to the parts of changed phase composition. By the method of the X-ray phase analysis it is found out that both surfaces of a contact stain except the main phase have solid solutions on the basis of ZrC, borides and chromium carboborides. The carried out X-ray microanalysis of the zone of contact interaction between ZrB$_2$ and Cr$_3$C$_2$ confirmed and specified the XRD results. It is revealed that the zone of contact interaction is structurally and chemically non-uniform, and is characterized by high dispersion of formed phases (grain size - of about 100 nm) with intensive diffusion re-arrangement of the main chemical components (Zr, B, Cr, C).

Cr$_3$C$_2$, ZrB$_2$

Fig. 1.16. Contact interaction and melting of pair ZrB$_2$/Cr$_3$C$_2$, temperature 1400°C, holding - 15 min. A fracture on a zone of contact interaction

Typical structure of a fracture surface through the diffusion zone and the results of X-ray microanalysis of a contact surface of ZrB$_2$ sample after interaction with Cr3C$_2$ are available in fig. 1.17. Diffusion zone has light grey grains which correspond to carbide and zirconium carboboride grains (points S9-S11), dark grey grains of chromium borides with carbon dissolved in it (points S5-S6), inclusions of carbon (points S2-S4, S13). Not numerous grains of tungsten carbide (point S1) are also observed which presence is associated with pollution of charge by a material of grinding bodies.

Points	B	C	O	Cr	Zr	W	In total
S1		52,7		2,3		45,0	100,0
S2		95,7	3,9	0,2	0,2		100,1
S3		95,3	3,3	0,1	0,7		99,9
S4		95,6	3,0	0,1	0,9		100,0
S5	57,4	6,4		35,7	0,5		100,0
S6	51,1	4,7		43,6	0,5		99,9
S9	15,1	47,7	4,8	0,9	23,0		100,1
S10	21,3	31,2		1,3	33,6		100,1
S11	17,6	31,0		1,4	36,2		100,0
S12	18,1	37,0		1,3	30,7		100,1
S13		95,7	3,7	0,1	0,4		100,1
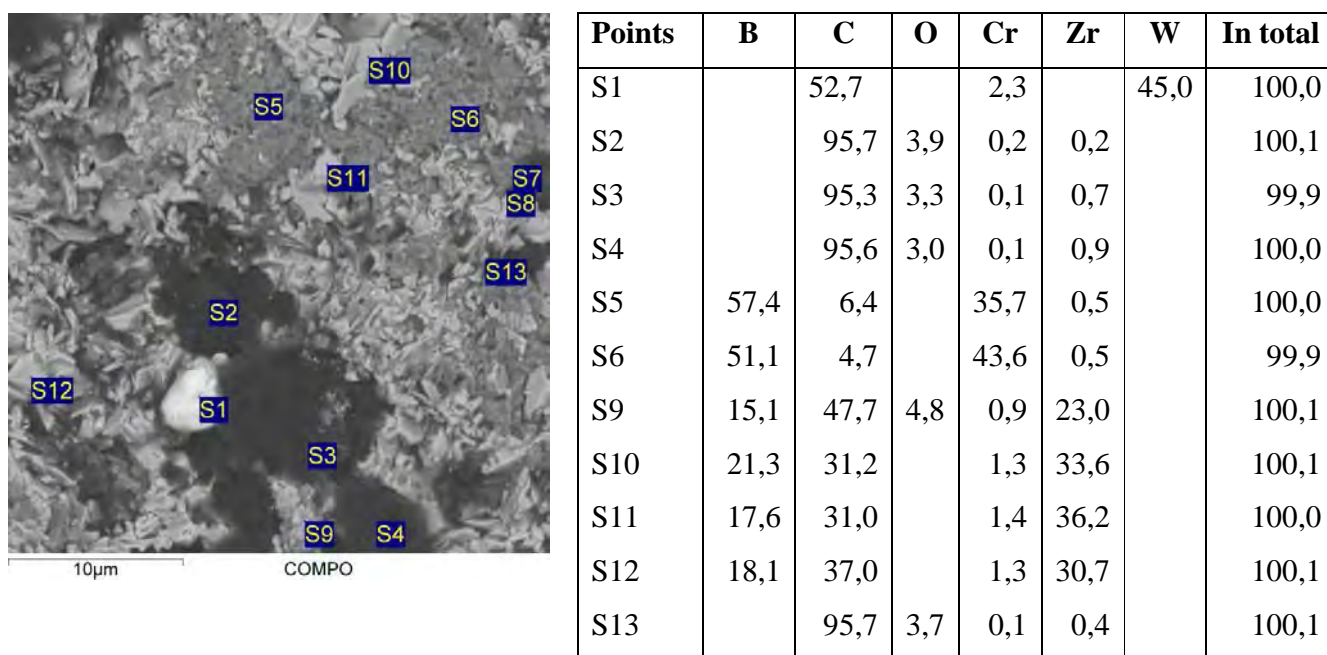
Fig. 1.17 Contact surface of ZrB$_2$ after interaction with Cr3C2; T = 1400 °C, holding - 15 min. Structure of break and results of local microanalysis in points S1-S13 (% at.)

As temperature elevates the interaction of components in the contact zone occurs more intensively, increase a depth of diffusion zone and sizes of crystals. Fig.1.18 presents a fracture on contact zone after interaction of ZrB_2 and Cr_3C_2 at temperature 1740°C with a holding of 15 min. X-ray investigation of break surface showed that in ZrB_2 sample in pre-surface contact zone a quantity of the main phase decreases, solid solutions on the basis of ZrC and chromium borides appear. In diffusion zone of sample Cr_3C_2 the amount of the main phase decreases and, besides Cr7C4, and ZrC based phase borides and carboborides $Cr_3B_{0,44}C_{1,41}$, Cr_3 $(B_{0,44}C_{0,56})$ $C_{0,85}$, CrB, Cr_7BC_4 are identified by the X-ray. Structure of the contact zone becomes coarse-grained and re-crystallized. The phase composition of samples out of diffusion zone remains almost monophase.

Cr_3C_2 ZrB_2

Fig. 1.18. Fracture on a zone of diffusion interaction between ZrB_2 and Cr_3C_2 at 1740°C.

Figs. 1.19-1.20 illustrate the results of analysis of the zone of contact interaction at temperatures 1360^0C and 1430°C and holding of 30 min. Almost porous free diffusion zones in the width of 5 … 10 mkm are observed on the transverse sections. Thus the relative density of samples makes 0,8 … 0,9. The big difference of TEK of contacting materials leads to formation of cracks on samples at cooling, approximately perpendicular to the contact zone on Cr_3C_2 (tensile stresses along the contact surface) and bow-shaped ones, approximately along the contact zone on ZrB_2 (tensile stresses are perpendicular to diffusion zone).

Results of X-ray microanalysis of elements near the diffusion zone are presented in fig. 1.19. It is found out that element and, hence, the phase composition of samples out of a contact zone practically did not change. However, in zirconium boride near the diffusion zone (points SS4-S6, S10-S12), carbon is present.
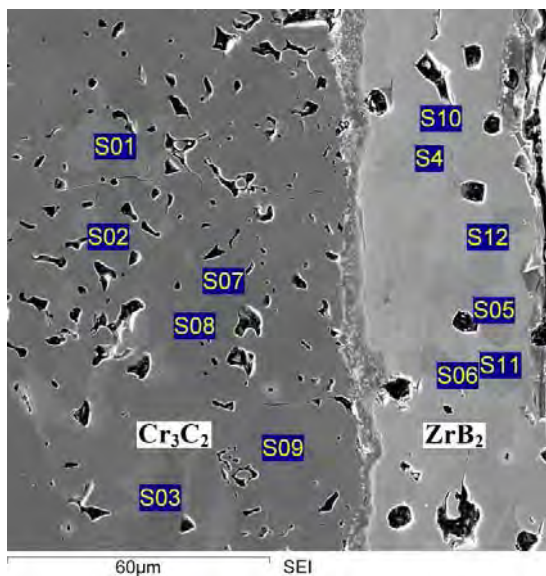
Analysis points	B	C	Cr	Fe	Zr	In total
S01		33,6	64,2	2,2		100,0
S02		34,0	66,0			100,0
S03		33,1	66,9			100,0
S4	69,0	6,3			24,6	99,9
S05	70,1	4,6			25,2	99,9
S06	69,4	6,0			24,6	100,0
S07		42,8	57,2			100,0
S08		42,7	57,3			100,0
S09		42,4	57,6			100,0
S10	68,9	7,1			24,0	100,0
S11	70,0	5,0			24,9	99,9
S12	70,6	4,3			25,1	100,0

Fig. 1.19 Contact interaction of ZrB_2 and Cr_3C_2, T=1360 ^{0}C, holding of 30 min; structure and distribution of elements in points S01-S12 near to the contact zone, % at.

The structure of the diffusion zone formed during 30 min at temperatures 1360°C and 1430°C is presented in figs. 1.20a and 1.20b accordingly. The carried out X-ray microanalysis along given directions (pointed by a dot line) and the built maps of distribution of elements for diffusion zone matching T=1430°C (see Fig. 1.20c and 1.20d) showed that if temperature increases, a diffusion and re-arrangement of elements go more intensively. Along both boundaries of diffusion zone there are almost continuous layers (white in figs) of carbide and zirconium carboboride, more coarse ones from the side of chromium carbide. From the side of ZrB_2 in a continuous layer of small white color crystals there is also a chromium (chromium zirconium carboboride). The same grains are present in volume of diffusion zones along with areas of borides and chromium carboborides (sections of dark color).

a)   b)

c)   d)
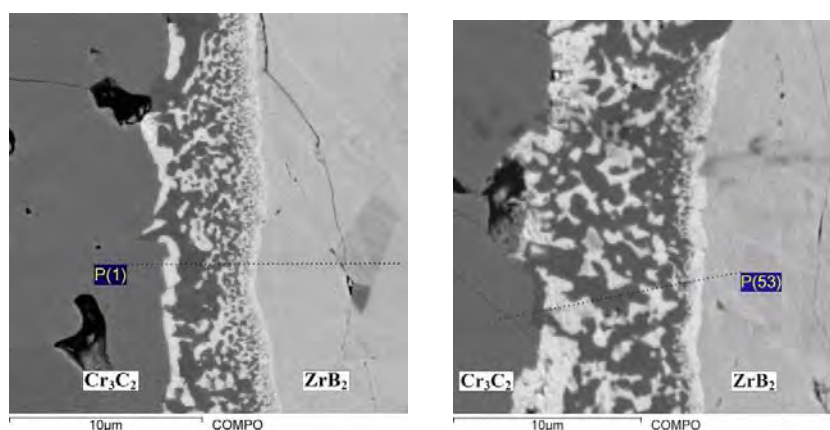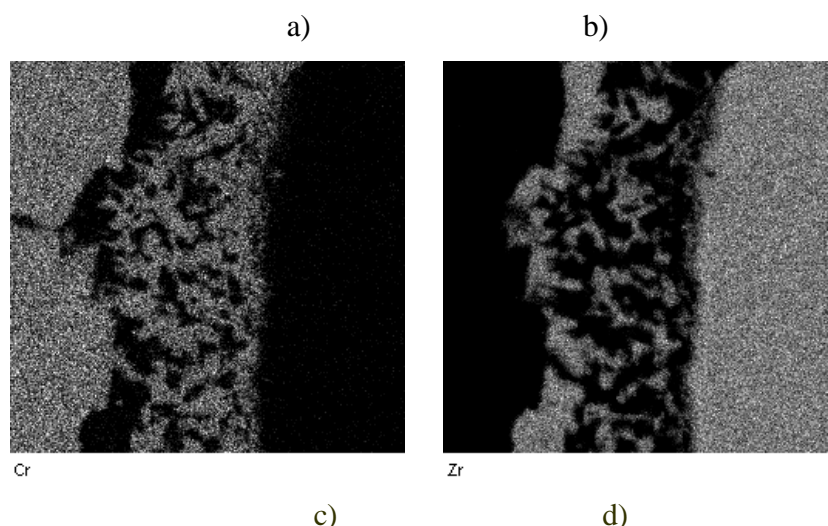
Fig. 1.20. Structures and chemical inhomogeneity of diffusion zones: a) T=1360°C, b) T=1430°C; c) and d) – distributions of Cr and Zr (to fig. 1.20b).

Migration of elements out of the diffusion zone is also observed: in Cr_3C_2 – zirconium (0,9 … 6,2 at. %) on depth to 1 mkm; in ZrB_2 – chromium (0,3 … 0,4 at. %) on depth to 4 mkm and carbon (22 … 32 at. %) on depth of the order of 10 mkm. As temperature of hot pressing increases the width of diffusion zone increases from 5 to 7 mkm, the number of crystallites of borides and chromium carboborides grows, as well as a layer of small crystals of zirconium-chromium carboboride along the boundary with ZrB_2. The general for all samples regularity –the amount of chromium in diffusion zone decreases towards ZrB_2.

Hence, one may to assert that densification of layer ZrB_2 close to the contact zone (fig. 1.21) up to porous free condition is explained by a diffusion of atoms of chromium and carbon in ZrB_2 through a zone of contact interaction.
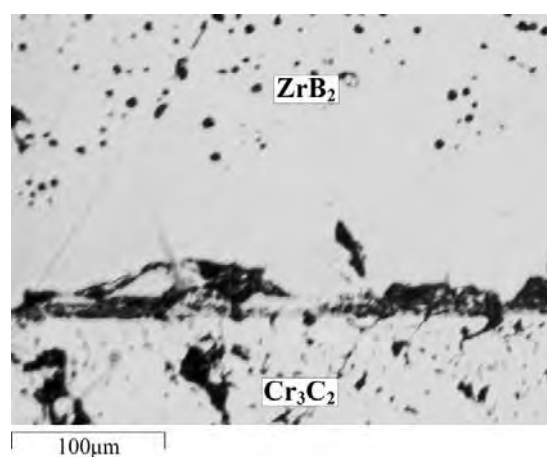
Fig. 1.21. Contact interaction of ZrB_2 and Cr_3C_2. At temperature 1370°C and holding of 30 min; densification of boundary layer ZrB_2

As it's seen from fig. 1.21, this diffusion interaction is accompanied by intensive activation of densification of a material in a neighborhood of diffusion zone as a result of which in zirconium boride a porous free layer is formed on the depth to 50-100 mkm at a thickness of diffusion zones - 5mkm.

For investigation of structural and chemical micro-inhomogeneity the thin foil was cut off the contact zone on which separate fragments of structure of diffusion zone were investigated with use of methods of analytical electronic microscopy. Fig. 1.22 presents the general layout of diffusion zone with considerable structural inhomogeneity. From the side of chromium carbide grains size makes about 1 mkm. Towards the boundary of zirconium boride a dispersity of grains increases and, attains 0,1 mkm. Formed grains of new phases, in view of their chemical inhomogeneity, are defective and have a high level of micro-deformation. This factor can promote diffusion activity at sintering.
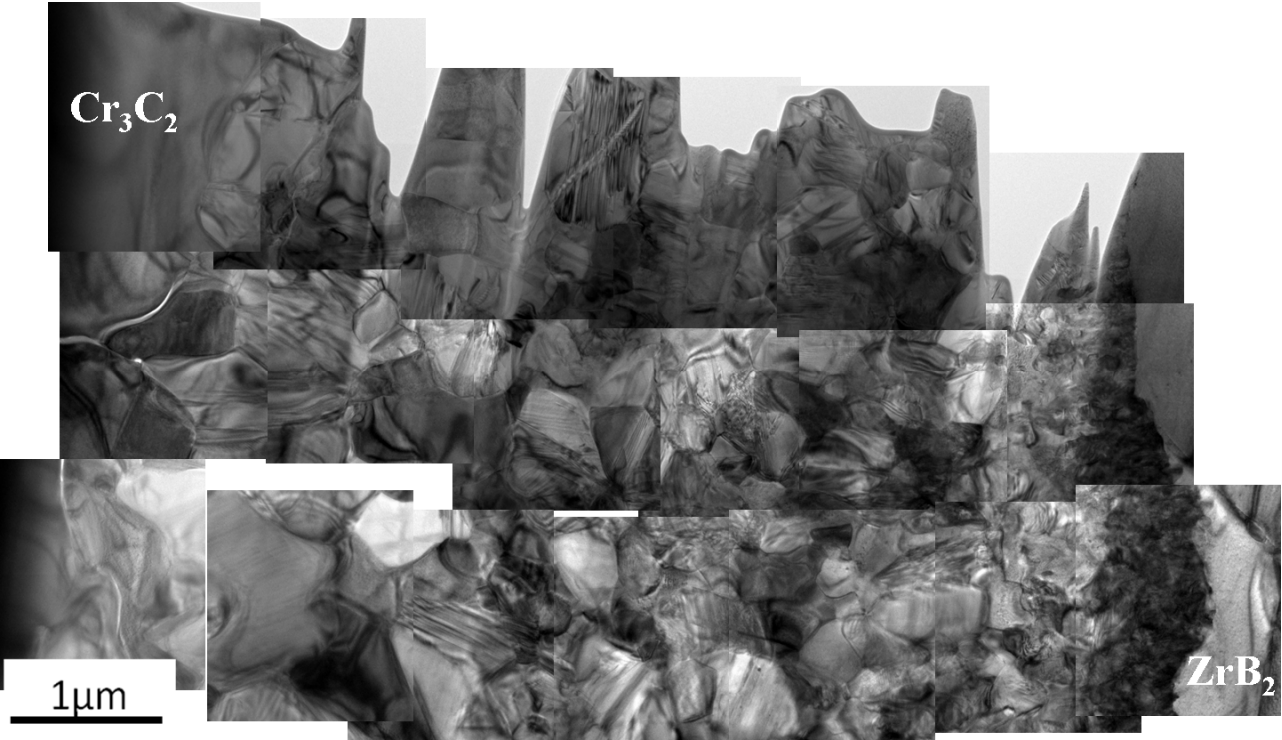
Fig. 1.22. Structural micro-inhomogeneity of diffusion zone (temperature 1360°C, holding - 30 min).

Analysis sections	B	C	Cr	Zr
Spectrum 1	35,52	34,95	0,86	28,63
Spectrum 2	24,04	53,49	0,69	21,75
Spectrum 3	51,3	17,65	30,67	0,08
Spectrum 4	45,4	29,07	25,3	0
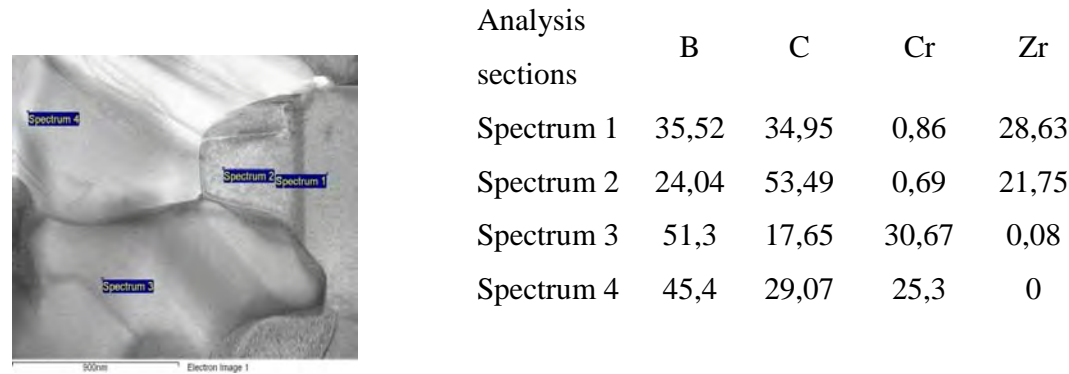
Fig. 1.23. Chemical micro-inhomogeneity of grains of diffusion zone close with the boundary with Cr_3C_2

The fragment of diffusion zone near to chromium carbide, illustrating structure and chemical micro-inhomogeneity of contact zone of interaction ZrB_2 and Cr_3C_2 at temperature 1360°C and holding 30 min is shown on fig. 1.23. Large crystals (0.5-1 mkm) –chromium carboboride, small (less than 0.5 mkm) –zirconium carboboride.

Analogously, structural and chemical inhomogeneity of diffusion zone between ZrB_2 and Cr_3C_2 near to zirconium boride at temperature 1360°C and holding of 30 min is shown on fig. 1.24. Zirconium bearing phase in the form of light coarse grains of size of about 1 mkm has almost close amount of carbon and boron. Transition in high dispersive area (dark in fig.) with sizes of structural elements up to 50 nm is not accompanied by change of the amount of zirconium, but in this area a ratio boron/carbon strongly increases and small amounts (up to 5 %) of chromium are observed. As a whole, grains in the above specified areas can be presented as zirconium carboborides and zirconium-chromium carboborides.
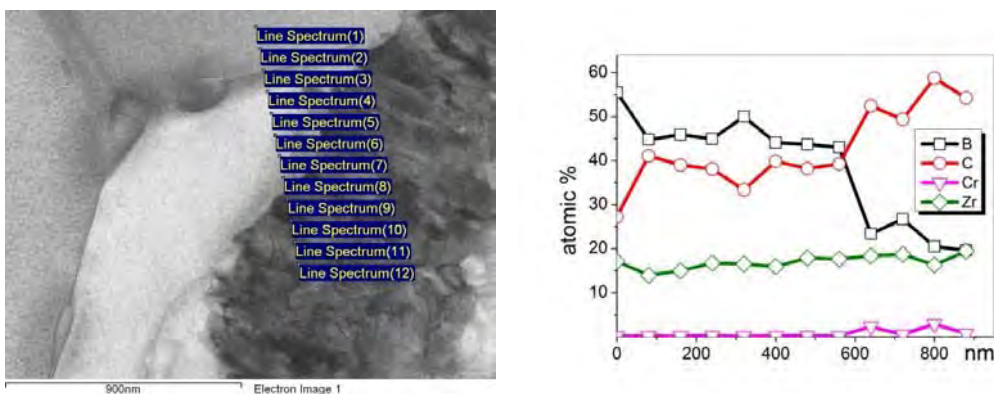
Fig. 1.24. Structure and characteristics of its chemical micro-inhomogeneity in diffusion zone near ZrB_2

In this way it was found out that grain boundary contact interactions of grains of initial refractory compounds even at rather low temperatures bring to formation of powerful diffusion zones. In terms of these zones there are the processes of local eutectic melting with formation of secondary refractory phases (solid solutions on the base of zirconium carbides and chromium borides). In these conditions sintering mode with disappearing liquid phase allows forming almost porous free ceramic at temperatures about 1500°C at hot pressing and in the mode of free sintering at 1850°C. Schematically the phase transformations in system are showed in terms of pseudo-forth tetrahedral scheme available on fig. 1.25.

The results obtained up today point out that in "chromium angle" of the presented tetrahedron there are fusible quadruple eutectics, apart from highlighted ternary eutectics. Thorough analysis of phase interactions is not that easy and accounting for real quinary system (including silicon), may be carried out as further another effort.
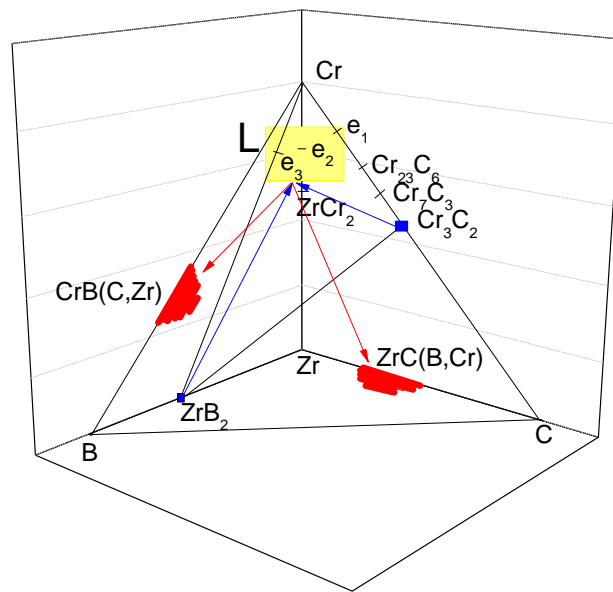
Fig. 1.25. Phase interactions in diffusion zone ZrB_2-Cr_3C_2

e_1 – eutectic $Cr_{23}C_6$- Cr, T_m= 1530° C; e_2 – eutectic $ZrCr_2$- Cr, T_m= 1590° C;

e_3 – eutectic ZrB_2 - Cr, T_m= 1550° C; ZrB_2, Cr_3C_2 – initial phases

$ZrC(B,Cr)_{ss}$, $CrB(C,Zr)_{ss}$ – final phases, $T_m \geq 3000^o$ C and 2000^oC respectively

1.2.2. Investigation of interaction of ZrB₂-SiC ceramics with chromium carbide

This section of report witnessed the investigation of phase and elementary composition of ceramic ZrB_2-SiC-Cr_3C_2 in terms of zones of diffusion interaction of initial components. The investigations were done by TEM and the methods of energy-dissipative micro-analysis. A special attention was paid to investigation of composition of grain boundary interlayers between grains of forming new phases (solid solutions on the base of zirconium and chromium carbo-borides). Typical results of investigation of structure and composition of diffusion zones are available on figs. 1.26-1.31.

Analysis of the obtained results allows us to make the following conclusions:

- Formed solid solutions on the base of zirconium and chromium carbo-borides possess a variety of compositions and near interfaces plane changes of elements concentration take place;

- Foreign impurities (Fe, W, Co, which presence is associated with pollution of initial powders at the stages of synthesis and preparation of mixtures) are localized in grain boundary interlayers.

- Grain boundary interlayers are also presented by solid solutions on the base of zirconium-chromium borides, Cr-Fe borides and zirconium carbo-borides;

- In diffusion zone of interaction of initial grains silicon from silica carbide dissolves in the lattice of secondary phases with its concentration 1-2% and, obviously, forms interlayers of chromium silicide near the boundary of initial chromium carbide;

- Eutectic nature of components interaction brings to appearance of nanosized grains of new phases with laminar morphology and with alternating compositions on the base of zirconium and chromium carbo-borides.
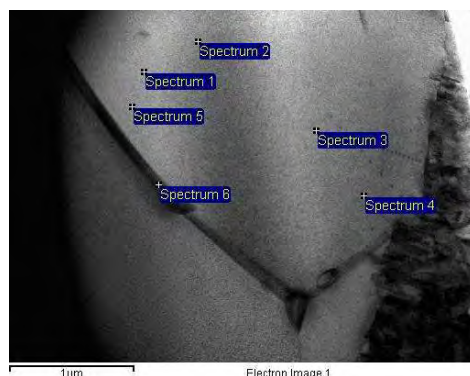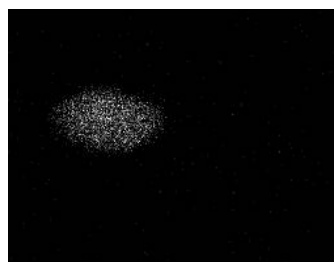

	B	C	Cr	Fe	Co	Zr	W
Spectrum 1	66,02	4,76	0,31			28,91	
Spectrum 2	64,09	4,09	0,65			31,17	
Spectrum 3	62,25	2,06	0,42			35,27	
Spectrum 4	56,95	4,23	0,64			38,19	
Spectrum 5	64,64	2,98	0,56			31,83	
Spectrum 6	47,49	1,53	13,23	14,06	0,92	21,81	0,97

Fig.1.26. Compositions of solid solutions in grain boundary interlayers and in grains of initial ZrB_2
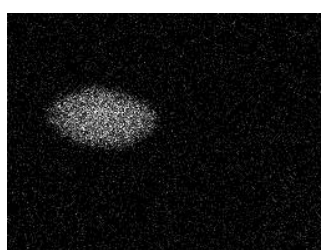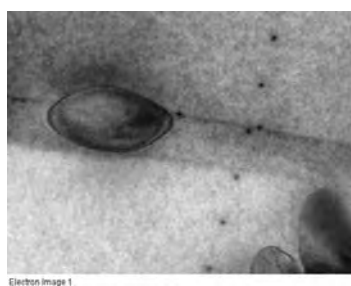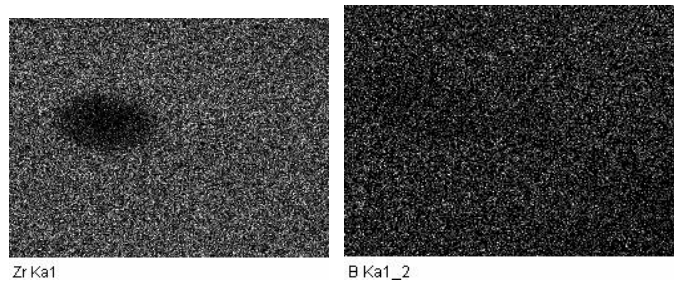
Fig.1.27. Grain boundary egesta on the base of chromium-iron borides in the vicinity of initial grains ZrB_2
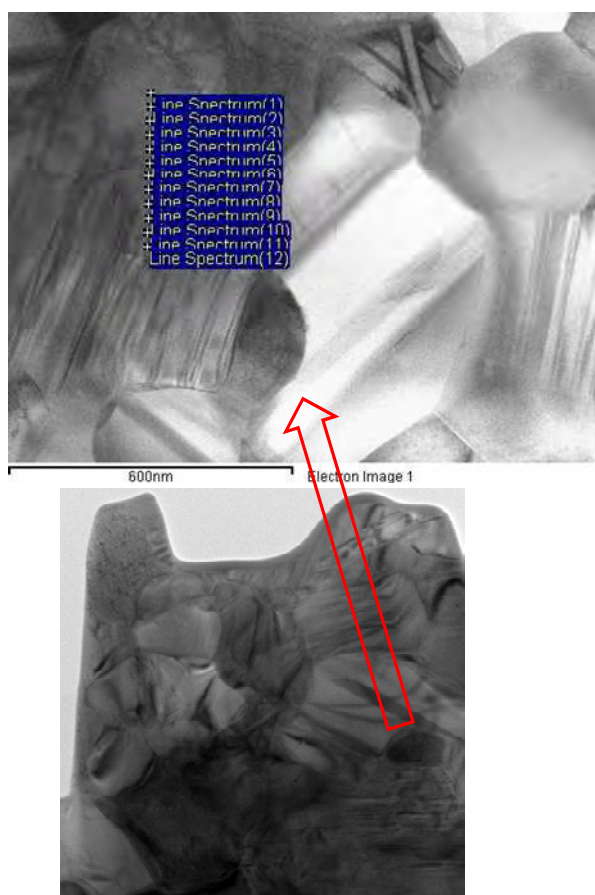
1 line 10
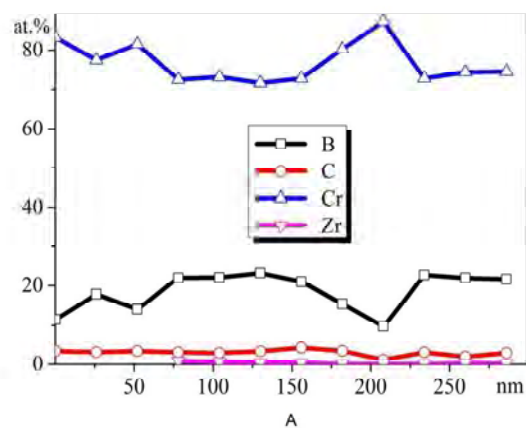
	B	C	Si	Cr	Zr	Fe
Line Spectrum(1)	11,5	3,35	0,82	83,27		1,06
Line Spectrum(2)	17,85	3,07	0,74	77,47		0,87
Line Spectrum(3)	14,12	3,32	0,75	81,53		1,03
Line Spectrum(4)	21,9	3,01	0,77	72,47	0,84	1,01
Line Spectrum(5)	22,01	2,85	0,73	73,15	0,58	0,68
Line Spectrum(6)	23,14	3,29	0,89	71,61	0,29	0,78
Line Spectrum(7)	20,96	4,22	0,77	72,78	0,29	0,98
Line Spectrum(8)	15,47	3,41	0,8	80,27	0	0,85
Line Spectrum(9)	9,73	1,16	0,89	87,25	0	0,98
Line Spectrum(10)	22,63	3	0,69	72,79	0	0,88
Line Spectrum(11)	21,89	1,94	0,75	74,38	0,19	0,86
Line Spectrum(12)	21,59	2,86		74,5	0,1	0,95

a)
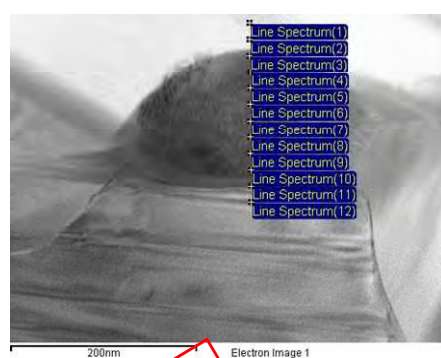
1 line 11
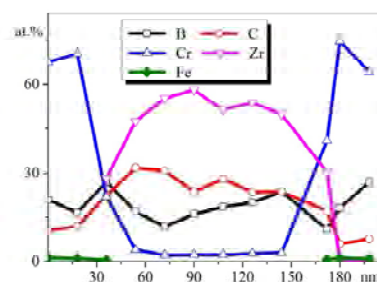
	B	C	Cr	Zr	Fe
Line Spectrum(1)	20,77	10,36	67,6		1,27
Line Spectrum(2)	16,52	11,97	70,49		1,02
Line Spectrum(3)	26,96	22,34	21,96	28,25	0,49
Line Spectrum(4)	16,85	31,8	3,85	47,5	
Line Spectrum(5)	11,84	30,71	2,05	55,4	
Line Spectrum(6)	16,11	23,6	2,14	58,15	
Line Spectrum(7)	18,44	27,9	2,16	51,5	
Line Spectrum(8)	19,97	23,51	2,59	53,92	
Line Spectrum(9)	23,65	23,66	2,81	49,87	
Line Spectrum(10)	10,91	17,08	41,02	30,36	0,63
Line Spectrum(11)	18,11	5,96	74,72		1,21
Line Spectrum(12)	26,89	7,65	64,36	0,16	0,94

b)

Fig.1.29 a, b - Chemical composition and elements distribution in grains of zirconium and chromium based refractory compounds
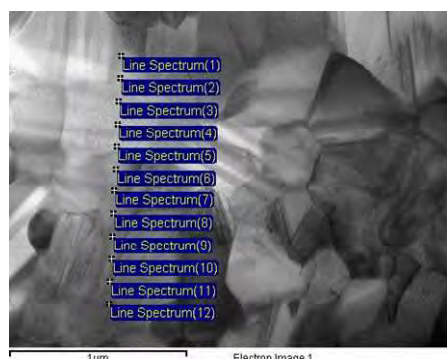
3 line 5
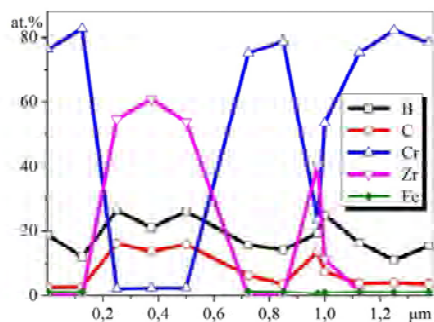
	B	C	Cr	Zr	Fe	Si
Line Spectrum(1)	18,91	2,69	76,37		1,14	0,89
Line Spectrum(2)	12,03	2,77	82,77		1,06	1,37
Line Spectrum(3)	26,45	16,19	2,25	54,74		0,37
Line Spectrum(4)	20,99	13,76	2,45	60,85		1,96
Line Spectrum(5)	26,06	15,87	2,53	53,98		1,55
Line Spectrum(6)	15,7	6,28	75,19		1,25	1,58
Line Spectrum(7)	14,2	3,64	78,83		1,15	2,19
Line Spectrum(8)	19,5	13,73	23,4	40,36	0,69	2,31
Line Spectrum(9)	24,94	7,44	53,64	11,37	0,92	1,69
Line Spectrum(10)	16,44	3,85	75,34	1,39	1,15	1,84
Line Spectrum(11)	11,07	4,06	82,26		1	1,61
Line Spectrum(12)	15,42	3,67	78,39		1,1	1,43

Fig.1.30. Submicron lamellar grain structure and composition of zirconium and chromium carbo-borides formed in diffusion zone

Fig.1.31. Inhomogeneity of chemical composition near the boundary between grains of zirconium carboboride and chromium boride
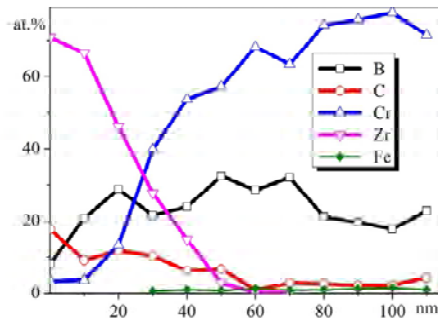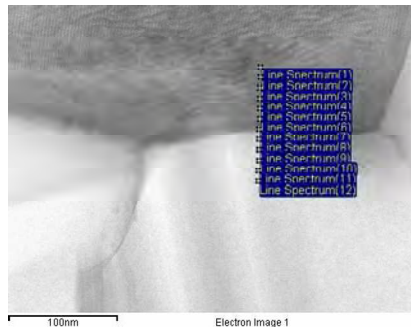
	B	C	Cr	Zr	Fe	Si
Line Spectrum(1)	8,18	17,7	3,28	70,83		
Line Spectrum(2)	20,75	9,15	3,59	66,51		
Line Spectrum(3)	28,77	11,68	13,35	46,2		
Line Spectrum(4)	21,53	10,24	39,88	27,7	0,65	
Line Spectrum(5)	23,93	6,3	53,82	14,89	1,05	
Line Spectrum(6)	32,41	6,68	57,24	2,84	0,83	
Line Spectrum(7)	28,53	0,92	68,23	0,26	1,27	0,79
Line Spectrum(8)	32,01	2,82	63,44	0,14	0,95	0,64
Line Spectrum(9)	21,18	2,59	74,23		1,02	0,97
Line Spectrum(10)	19,63	2,16	75,76		1,28	1,16
Line Spectrum(11)	17,74	2,24	77,69		1,44	0,89
Line Spectrum(12)	22,83	4,21	71,48		1,04	0,44

In general the above described results which concern a formation of structure of ceramic of system ZrB_2-SiC-Cr_3C_2 and kinetics of its densification at hot pressing bring to a possibility of development of a technology of production of UHTC with accounting of the following factors:

1. It is found out that the use of Cr_3C_2 as the activator of ZrB_2 reduces temperature of hot pressing from 2170°C to 1520 … 1740°C depending on Cr_3C_2 content.

2. It is found out that in the system [ZrB_2+Cr_3C_2] an intensive contact interaction with formation of diffusion zones which begins at temperature 1310°C, takes place.

3. Within the diffusion zone, the processes of phase formation with formation of new high-temperature refractory compounds in a form of zirconium carboborides, borides and chromium carboborides, zirconium – chromium carboborides intensively develop. Intensive diffusion of chromium and carbon in zirconium diboride, accompanied by formation of porous free states in zirconium diboride (on depth up to 50-100 mkm at temperature 1360°C) near diffusion zone is observed.

4. As a whole, the observed activation of sintering of zirconium diboride up to porous free state in the investigated system containing eutectic components, is explained by an intensive diffusion of atoms of chromium and carbon in ZrB_2 through a zone of contact interaction and development of phase transformations in diffusion zone itself. The results of investigation do not contradict the assumption that the process of sintering in the conditions of contact interaction and formation of diffusion zone occurs with a formation of

disappearing eutectic liquid phase spent on formation of new high-temperature refractory compounds (the phases on the basis of zirconium carbide and chromium borides).

5. The obtained data confirm a general scheme of phase and chemical interactions at sintering of ceramic ZrB_2-SiC-Cr_3C_2 (see Fig.1.25).

1.3. Vacuum pressureless sintering of ceramics ZrB_2-SiC-Cr_3C_2

The results of previous section which show sintering up to dense porous free condition of UHTC of system ZrB_2-SiC-Cr_3C_2 in condition of hot pressing at temperatures about 1600^oC open the perspectives of its production at relatively low temperatures and in the mode of sintering without pressure. That is why experiments on vacuum pressureless sintering of ceramics ZrB_2-SiC-Cr_3C_2 have been carried out. For ceramics with 10 mass. % SiC and 10-15 mass. % Cr_3C_2 at temperatures of sintering 1850-1900^oC the shrinkage arrived 19%. The obtained samples possess density of 5.54-5.65 g/cm^3, which corresponds to 98-100% of theoretical one. This section of the report presents the results of investigation of structure and mechanical properties of ceramic ZrB_2-SiC with additives (0-20 %) Cr_3C_2 sintered in temperature interval 1800-2200^oC.

The powders ZrB_2 and Cr_3C_2 produced at Donetsk plant of Chemical Reagents and powders SiC (UF10 grade) manufactured by Shtarck were used. Grinding of powders was made in planetary mill with Kaprolon drum in acetone medium with the use of grinding zirconium diboride balls. Grains size of powders in prepared charges was $D_{50} = 2$ mkm and $D_{95}=5$ mkm. Samples with a diameter of 15 mm and height 8 mm were formed by one axis pressing. Sintering of samples was carried out in vacuum furnace. Density of sintered samples was defined by hydrostatic method. Etching of sections aiming to uncover a grain structure was carried out in the solution HCl-HF-HNO_3 in glycerin.

It is shown that for the used powders and methods of charges preparation sintering of ceramic of composition ZrB_2 –10 % SiC at 2000 and 2200° C is accompanied by intensive re-crystallization with elevation of zirconium boride grains size up to 15 and 40 mkm respectively (Fig. 1.32). At temperature of sintering 2200° C a change of morphology of silica carbide grains located in a form of interlayers on grain boundaries of zirconium boride is observed. Zirconium diboride grains are mainly equiaxed. Porosity at sintering temperature is up to 10-15 % with pores size up to 30-40 mkm.

Additional introduction of only 5% of chromium in charge ZrB_2 –10 % SiC is accompanied by drastic acceleration of shrinkage with manufacturing of structures with low porosity (less than 5 %) even at sintering temperature 1900° C (fig.1.33). In this ceramic boride grains remain iso-symmetrical, but SiC grains as in ceramic ZrB_2 –10 % SiC loose their initial morphology and also are located as interlayers on boride grain boundaries. As it's seen from fig. 1.33 the elevation of ceramics sintering behavior at introduction of chromium carbide additives is also followed by acceleration of crystallization rate and boride grains size (up to 60 mkm) at 2100° C become higher than for ceramic ZrB_2 –10 % SiC at temperature 2200° C.

a   b
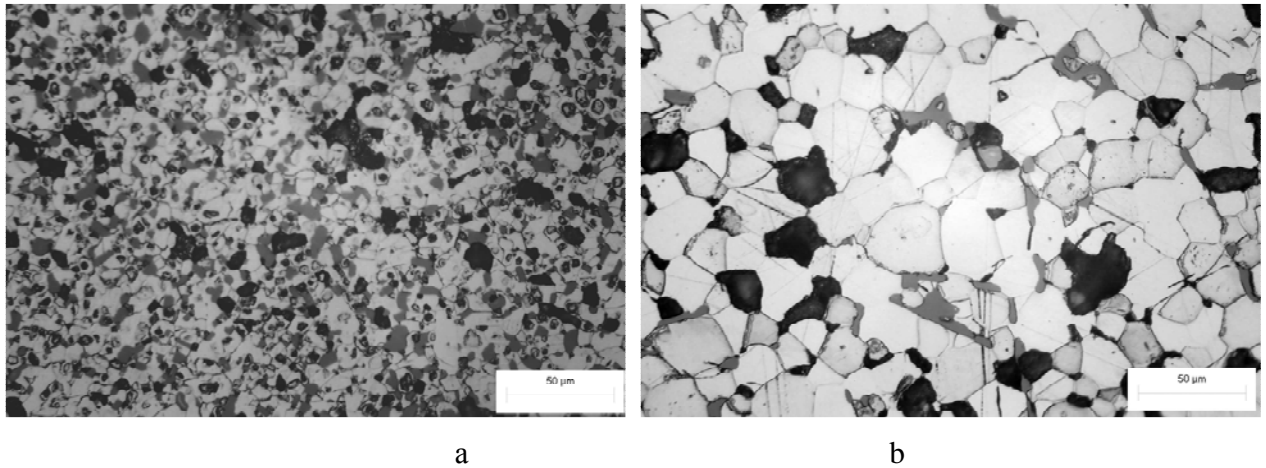
Fig. 1.32. Structure of ceramic ZrB_2 –10 % SiC sintered at 2000 (a) and

2200° C (b)
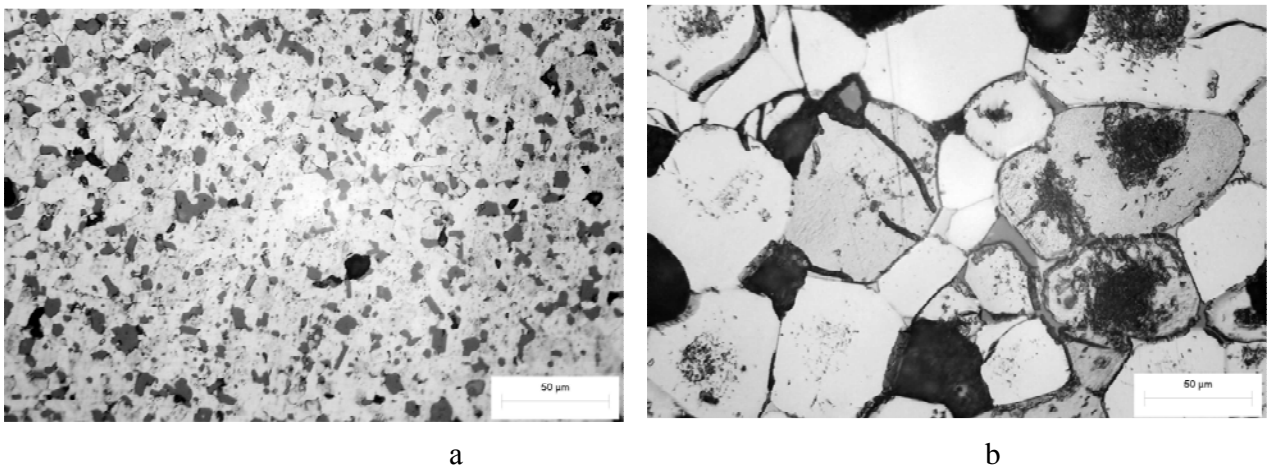

a   b

Fig. 1.33. Structure of ceramic ZrB_2 –10 % SiC -5% Cr_3C_2, sintered at 1900 (a) and 2100° C (b)

Qualitatively a structure of ceramic ZrB_2 –10 % SiC -10% Cr_3C_2, sintered at 1900° C turns closer to that one of ceramic ZrB_2 –10 % SiC -5% Cr_3C_2, with an exception that its' porosity falls up to 1 % with grains size up to 10-15 mkm. However further increase of chromium carbide amount up to 15 % is escorted by abrupt change of morphology of boride grains, which from isometric become elongated with elevation of aspect ratio up to the value more than 2 (fig.1.34a). At the amount of chromium carbide 20 % even at 1850° C dendrite-like, dense and almost porous free structure is formed (fig. 1.34b).

<center>a   b</center>
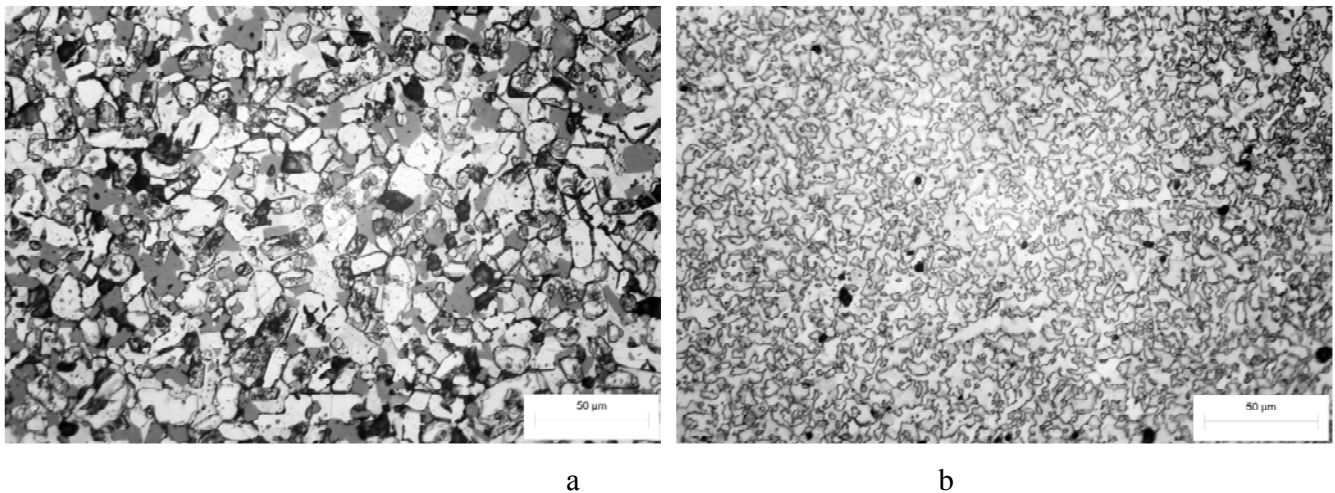
Fig. 1.34. Structure of ceramic ZrB_2 –10 % SiC -15% Cr_3C_2, T_{sint}=1900°C (a) and ZrB_2 –20% Cr_3C_2, T_{sint}=1850°C (b)

In all cases chromium carbide initially introduced which as a result of interaction with zirconium boride, according to x-ray analysis forms heterophase system with high temperature phases of zirconium diboride, diboride zirconium chromium and zirconium carbide, is absent. Material's densification occurs in the process of liquid-phase eutectic re-crystallization with disappearing liquid phase.

Thus introduction of active agent in a form of chromium carbide in ceramic ZrB_2-SiC allows in the mode of vacuum sintering to obtain dense ceramic at sintering temperatures 1850-1900° C. Sintering occurs in condition of eutectic interactions with disappearing liquid phase and formation of secondary borides of chromium-zirconium and zirconium carbide. mechanical properties of ceramic increases with increase of the amount of chromium carbide up to 10-15 mass.%.

1.4. Investigation of processes of manufacturing of ultra high temperature ceramics by the methods of hot pressing without any protective environment

With the use of hot pressing equipment (SPD120) for pilot-scale production (induction heating without specially created protective atmosphere, graphite molds (operating temperatures up to 2300$^°$C), the articles of up to 100x50 mm (diameter and height, respectively)) the experiments to obtain samples of model ceramics of ZrB_2-Cr_3C_2 and HfB_2-Cr_3C_2 systems containing chromium carbide in the range of 2-15 vol.% were carried out. Phase and chemical interactions (including eutectic) of components at approximately low hot pressure temperatures (about 1700° C) cause the formation of ceramics with the following composition: zirconium (hafnium) boride – new phase Zr(Hf)BC with NaCl lattice – chromium boride. Depending on chromium boride content the bending strength of ceramic varies 300-620 MPa.

1.5. Mechanical properties of ceramics

The carried out contact tests of sintered ceramic materials of system ZrB_2 –SiC-Cr_3C_2 showed that in a rather wide range of loadings (10 - 200H) the above said composites keep high values of hardness (fig. 18). Analysis of the obtained results shows that an introduction of Cr_3C_2 in composites elevates their hardness (fig.1.35) – max hardness (~13-17GPa), in the indicated interval of loadings, is for sintered composites with 10-15 mss.% chromium carbide. From the fig. it's clearly seen that if loading decreases up to 10 N hardness increases for all samples, and in the interval of loadings 100 – 200 N hardness does not change. Minimum hardness is observed in ceramic ZrB_2 –10%SiC.
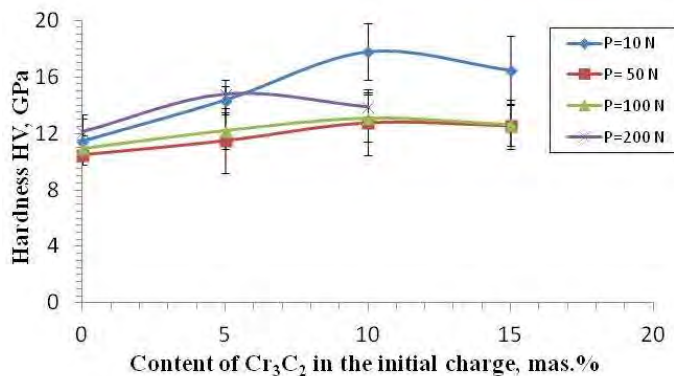
Fig.1.35. – Dependence of hardness of sintered ceramic materials of system ZrB_2 – SiC vs. the amount of Cr_3C_2 and loading on indenter

Being based on carried out hardness measurements and measurements of cracks length, which formed near the print we built statistic Weibull's distributions for contact strength of composites ZrB_2 –SiC-Cr_3C_2 (fig.1.36). In the majority of cases, the obtained distributions are bimodal, i.e. as a rule, have two direct parts which are responsible to two populations of cracks – „long" and „short". Thus Weibull's module m defined for „long" cracks varies in interval 14-16. As loading increases the number of „long" cracks grows, and the distribution itself shifts left. It witnesses that characteristics of contact strength falls. Another Weibull's analysis of population of „long" cracks reveals a scale dependence of contact strength of composites more realistically (fig.1.37).

From fig. 1.37 it's seen that as loading increases the contact strength drastically falls and arrives minimum value at maximum loading 200 N. Introduction of Cr_3C_2 in composites a bit elevate their contact strength in interval of loadings 10-100 N. However at loading 200H the contact strength of sintered composites almost does not depend on the amount of Cr_3C_2 in final charge and is found at a level of 210-270 MPa. It should be noted that average values of contact

strength are calculated for „long" cracks of composite at maximum loading and allow to evaluate their bending strength only approximately.

Measurements of fracture toughness are carried out by size of radial cracks near hardness prints by the methodology described early/see the first year report/. The obtained values of fracture toughness of composites of system **ZrB$_2$ – SiC – Cr$_3$C$_2$** are presented on fig. 1.38.
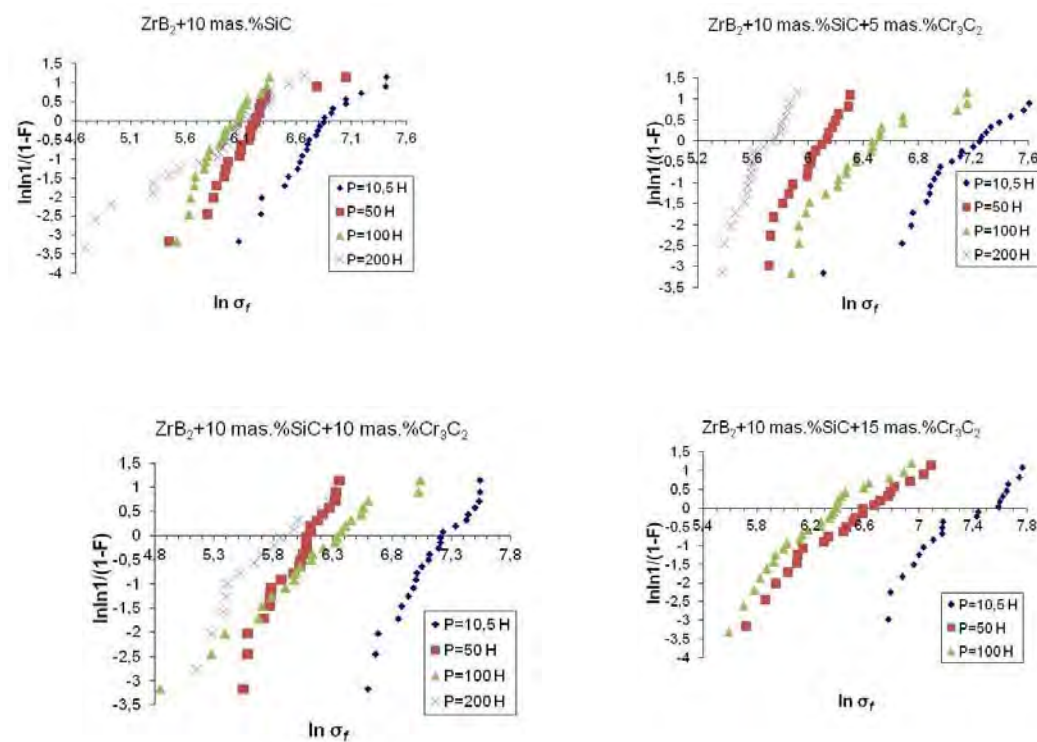

Fig. 1.36. – Weibull's Statistic distribution for contact strength of sintered composites **ZrB$_2$ –SiC-Cr$_3$C$_2$** vs. loading
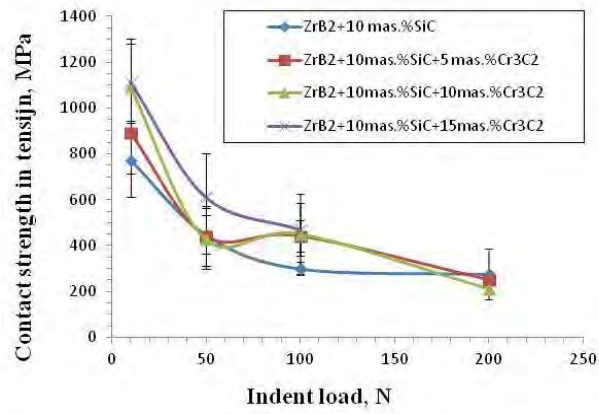
Fig. 1.37. – Dependence of contact strength of ceramic materials $ZrB_2 – SiC$ vs. the amount of Cr_3C_2 and loading on indenter .
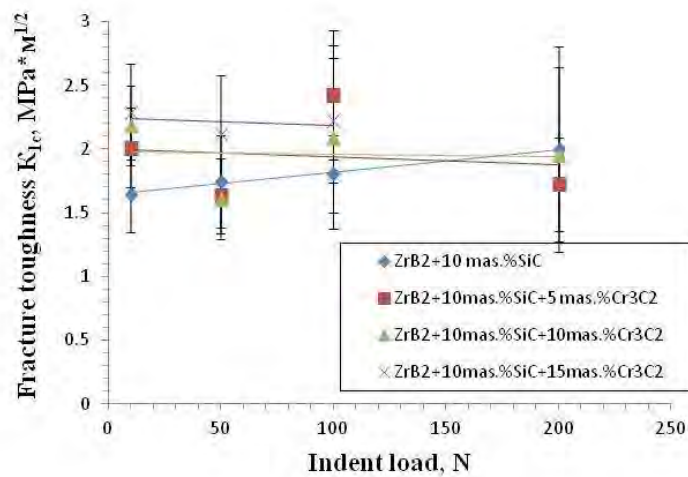
Fig. 1.38. – Dependence of fracture toughness of ceramic materials $ZrB_2 –SiC$ vs. the amount of Cr_3C_2 and loading on indenter.

From the presented results it is clear that the values of fracture toughness only weakly depend on loading on indenter. Fig. 1.38 illustrates that elevation of content Cr_3C_2 in the composites $ZrB_2 - SiC$ brings to increase of their fracture toughness (2,0–2,4 MPa*m$^{1/2}$).

Investigation of creep of ceramics at uniaxial compression

Apart from the experiments on ceramics creep at indentation a complex of experimental works on definition of technical possibility of using of available hot pressing device to evaluate creep in temperature interval up to 2000 ºC at loading up to 50MPa was carried out, including: high temperature rigging was developed; elastic and plastic deformation of graphite rigging were defined (see fig. 1.39); deformation of device units under loading was defined (see fig. 1.40); high temperature densification of graphite was carried out; thermo-expansion of a number of materials with various electro-resistance was defined as well.
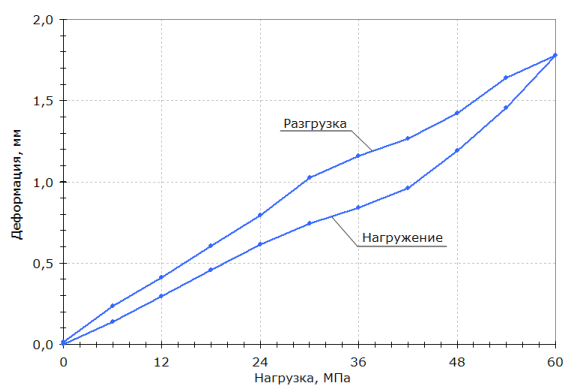
Fig. 1.39. Deformation of graphite rigging under loading
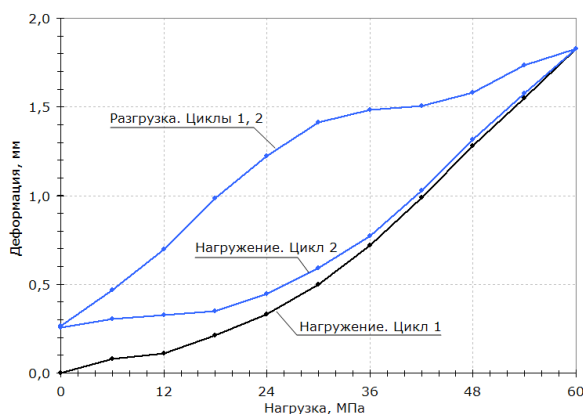
Fig. 1.40 Deformation of device units under loading

Accounting for the works performed, the methodology of investigation of high temperature creep was developed. Trial investigations of creep for the samples [80%vol. ZrB$_2$ + 20%vol. SiC] (see fig.1.41) and [95%mass.(80%vol.ZrB$_2$ + 20%vol.SiC)+5%mass.Cr$_3$C$_2$] (see fig.1.42) were carried out. Being based on the first carried out experiments on creep evaluation one may draw a conclusion that creep of binary system begins at T=1820°C, and ternary system – at T=1670°C. It is found out that creep and deformation are in proportion to relative density of the investigated samples. Thus to obtain accurate results for example, to estimate energy of activation required using samples with similar relative density. Images of the investigated samples are presented on fig. 1.43. Curves of creep L1 and temperature T1 (1620°C) are illustrated on fig. 1.42. The results of samples investigation for creep are presented in Table 1.4.
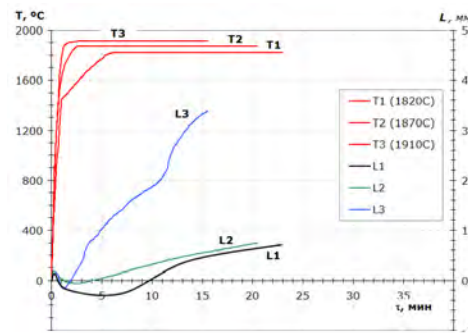
Fig. 1.41 Creep kinetics of samples [80%vol. ZrB$_2$ + 20%vol. SiC]

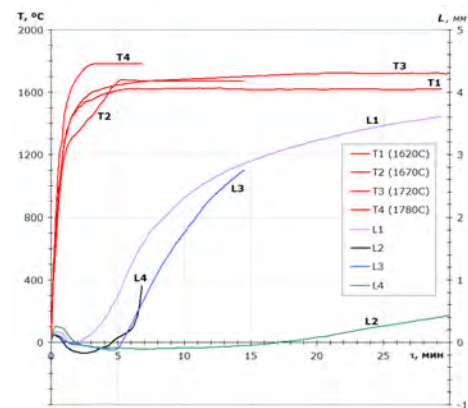Fig.1.42 Creep kinetics of samples [95%mass.(80%vol.ZrB$_2$ + 20%vol.SiC)+5%mass.Cr$_3$C$_2$]

Fig. 1.43. Samples after testing

Composition [80% vol. ZrB_2 + 20% vol. SiC] – 1, 2, 3;

Composition [95% mass.(80% vol.ZrB_2 + 20% vol.SiC)+5% mass.Cr_3C_2] – 4, 5, 6.

Table 1.4. Evaluation of high temperature creep at P=48MPa

№ sample	T, °C	$\square_{initial}$	Deformation, %
	80% vol. ZrB_2 + 20% vol. SiC		
1	1820	1,000	16,8
2	1870	1,000	13,2
3	1910	0,960	54,6
	95% mass.(80% vol.ZrB_2 + 20% vol.SiC)+5% mass.Cr_3C_2		
4	1720	0,990	33,3
5	1670	0,988	6,85
6	1780	1,000	31,0

Some mechanical properties of the investigated ceramic samples after creep test up to rather high deformations are available in table 1.5.

As it is seen from the table ceramic as a whole preserves rather high mechanical properties, which rather are turned to be not that small than it were before testing. It points out its' relatively small damage at a creep up to a strain 30-50%, though a porosity increases in ceramic (figs. 1.44, 1.45), and at high strain rates pores size increases and their agglomeration is observed. Pores thus are localized on grain boundaries and if united may achieve 15-20 mkm.

Table 1.5. Samples properties after creep

Samples	P, N	HV, GPa	St.dev, GPa	K_{1c}, MPa $м^{1/2}$	St.dev, MPa $м^{1/2}$	$\sigma_{f\,avr}$, MPa	St.dev., MPa
ZrB_2-SiC 1820°C	50	19,6	1,26				
ZrB_2-SiC 1870°C	50	20,1	2,01				
ZrB_2SiC 1910°C	50	18,3	1,53	3,3	0,3	1081,1	110,8
ZrB_2-Cr_3C_2-SiC 1720°C	50	22,8	1,77	2,6	0,4	660,0	89,8
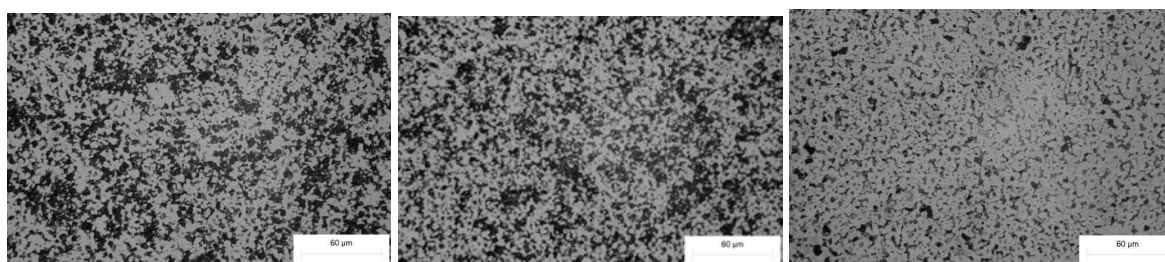
a   b   c

Fig. 1.44. Structure of ZrB_2+20 vol.% SiC after creep testing: a) - 1820°C, b) 1870°C; c) 1910°C
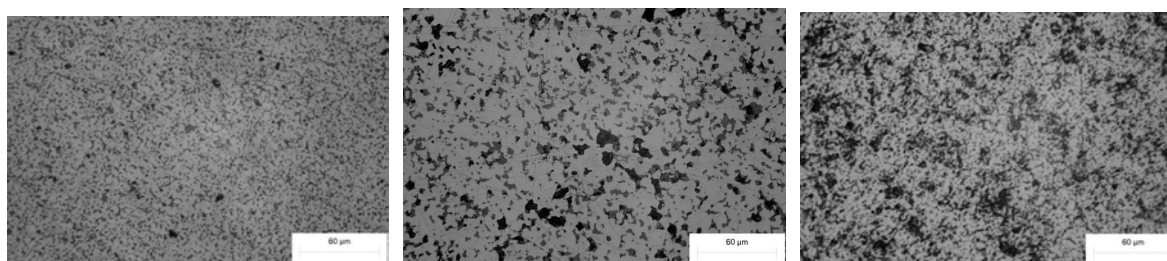
a   b   c

Fig. 1.45. Structure of ZrB_2+20 vol.% SiC+ Cr_3C_2 5vol.% after creep testing: a) - 1670°C, b) - 1720°C, c)

- 1780°C

a   b
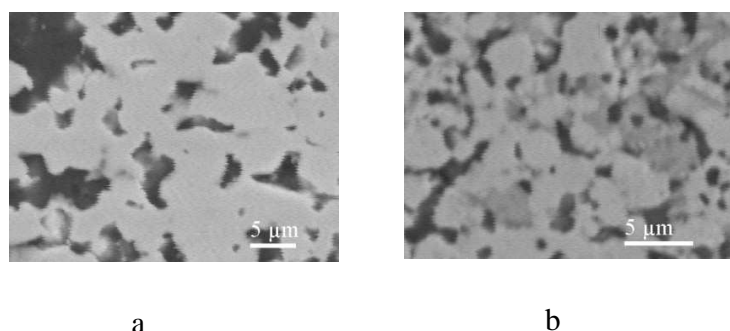
Fig. 34. REM images of ZrB$_2$+20 об.% SiC – Cr$_3$C$_2$ ceramics after creep testing:a) 1670°C, b) - 1720°C,

As a whole it is shown that the ceramic ZrB2-SiC-Cr3C2 at temperature about 1700°C can be deformed by 50 % and higher without essential degradation of mechanical properties. Creep process is developed almost in the mode of superplasticity under the slip mechanism of zirconium boride and silica carbide grains on grain boundary interlayers with nanocrystalline grains of carbon-boride of zirconium and di-borides of zirconium – chromium.

2. High temperature X-ray investigations for definition Debay-Velar factor and further analysis of amplitude of thermal oscillations of lattice of monophase powders and their eutectic mixtures - X-ray determination of dynamic displacements of Al atoms in monophase condition and in eutectic alloy Al-Si

2.1. Introduction

Investigation of sintering of ultrahigh temperature ceramics in terms of the project P511 was mainly based on the assumption that activation of sintering in eutectic systems may cause a specific interest for a development of the observed materials. It is known that for activation of sintering of refractory compounds the effective are additives forming eutectic systems and providing consolidation in a mode of liquid phase sintering. Our investigations of sintering of borides which are a basis of the new class of materials – ultrahigh-temperature ceramics, showed the efficiency of such additives even at modes of solid-phase sintering [18]. Activation of sintering assumes the raised diffusive mobility of atoms in grain boundary areas of components of eutectic systems. Consideration of the nature of such activation can be executed with use of various approaches and solution of this question is interfaced with understanding of the nature (the microscopic mechanism) of eutectic or contact melting that has been discussed in scientific literature for more than 60 years [13,19]. Recently a formation of diffusion zones on boundaries of contacting eutectic components has been found out even in those

cases when there are no areas of solubility on state diagrams [20, 21]. It is shown also that material's behavior of diffusion zone defines many features of eutectic systems. In particular, melting of a material at eutectic temperature begins and develops namely within a diffusion zone [20-22]. The analysis of the nature of the raised diffusive mobility and activation of sintering can be observed on the basis of the assumption of higher amplitudes of atoms oscillation in a neighborhood of eutectic grains boundary. This work is to analyze dynamic thermal displacement of atoms by the methods of X-ray diffraction in one of phases (Al) of eutectic system Al-Si in comparison with those in pure monophase polycrystal. For the purpose of increase in square of interfaces the samples of layered structure with a thickness of consecutive layers of eutectic components of an order of tens nm were prepared. Formation of diffusion zones on components boundaries means that aluminium layers in contact with silicon will be modified and thus the effective thermal characteristics of aluminium of diffusion zone of eutectic alloy are studied in comparison with those for pure monophase aluminium.

2.2. Materials and techniques

The work is executed by XRD methods for the samples of monophase powdered aluminum and aluminum which is a part of model eutectic system Al-Si. State diagram Al-Si is characterized by a solubility of silicon in aluminum in a range of 2 at. % at temperature of eutectic melting 850K and absence of solubility of aluminum in silicon. Layered samples of Al-Si composition close to eutectic were produced by vacuum evaporation by a technique described in [23]. For implementation of this method a vacuum chamber with two evaporators was divided by impermeable shield so that it prevented mixing of steam flows from evaporators (fig. 2.1). The substrate fixed on a vertical shaft, in the process of rotation alternately gets to steam flows of pure elements. By variation of rotation speed and evaporation rate of components from separate targets one may vary both a ratio of elements in a foil, and the period of alternation of layers. For investigation multilayered foils of Al/Si eutectic composition with the period of alternation of layers of 45 nm (thickness of Al and Si layers - 35 and 10 nm respectively) and with the period of alternation of 640 nm (thickness of Al and Si layers - 440 and 200 nm, respectively) were produced. As the monophase aluminum a powder with average size of particles of 30 mkm was used.
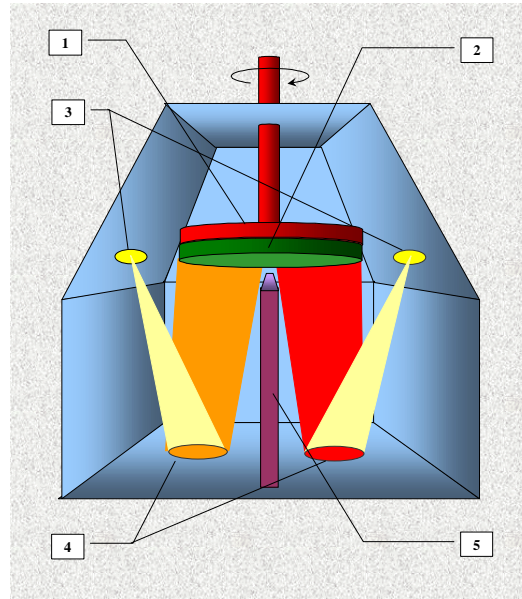
Fig. 2.1 Scheme of production of multilayered foils by the method of electron-beam vacuum evaporation of elements: 1 - substrate; 3 - electron beam guns; 4 - evaporators; 5- dividing shield; 6 -shaft;

Amplitude of atoms oscillation was studied using a temperature dependence of thermal multiplier in intensity of X-ray diffraction reflexes. The investigation is carried out in helium atmosphere using high-temperature X-ray diffractometer DRON-UM1 with high-temperature device UVD- 2000 (temperature interval 290-830K) and monochromatic Cu-K_α radiations (graphitic monochromator on diffracted beam).

The influence of temperature on value of thermal multiplier 2M of intensity of reflexes, depending on atoms thermal oscillations was investigated

$$I_T/I_{0K} = \exp(-2M)$$

Value M is defined by expressions [24]:

$$M = \left(\frac{8\pi^2}{3}\right)\overline{U^2}\left(\frac{\sin\vartheta}{\lambda}\right)^2, \qquad (1)$$

for independent from each other isotropic oscillations of atoms which possess equal energy, or

$$M = \frac{6h^2}{mk\theta}\left[\frac{\Phi(x)}{x} + \frac{1}{4}\right]\left(\frac{\sin\vartheta}{\lambda}\right)^2, \qquad (2)$$

for scattering on superposition of elastic waves propagating through a crystal with primitive lattice. In ratios (1) and (2) the following designations are used:

$\overline{U^2}$ - root mean square (rms) dynamic displacement of atoms, ϑ – угол дифракции, λ – длина волны рентгеновского излучения, $\Phi(x)/x$ - Debay's function, $x = \theta/T$, θ-Debay's characteristic temperature, h- Plank's constant, k- Boltzmann's constant, m- atoms mass.

Debay's characteristic temperature, defined as

$$\theta = \frac{h\nu_0}{k},$$

(where ν_0 - ultimate frequency of atoms thermal fluctuations) occurs to be sensitive to changes in oscillations spectrum and depending on temperature as well as from measurement methods (by definition of x-ray characteristics, thermal and mechanical properties). In this work for Al we accept the value $\theta = 385\,K = const$ at T>300K [25].

In the whole, the value M increases with temperature, but depends on it in a rather complicated way. Equating (1) and (2) and transforming (2) as

$$M = \frac{6h^2}{mk\theta^2} T \left[\Phi(x) + \frac{x}{4} \right] \left(\frac{sin\vartheta}{\lambda} \right)^2$$

one may show that for the interval of high temperatures (T>θ), for which the value in square brackets approx. equals to one, the value of rms dynamic displacements of atoms depends only linearly on temperature

$$\overline{U^2} = \frac{9\pi^2 h^2}{4mk\theta^2} T \qquad (3)$$

In this work to define temperature dependence $\overline{U^2}$ we used the ratio of intensities of typical reflexes of Al at various diffraction angles. It allows partially minimizing or excluding experimental errors or errors associated with sample's physical condition. In particular, texture effects are excluded at use of aliquot reflexes, for example (111) and (222) [26].

Then to define the characteristics of thermal oscillations at given temperature T, we obtain:

$$\gamma_T = \frac{I_T^{111}}{I_T^{222}} = \frac{I_0^{111} e^{-2M_T^{111}}}{I_0^{222} e^{-2M_T^{222}}} = A \frac{e^{-2M_T^{111}}}{e^{-2M_T^{222}}},$$

$$\gamma_T = \frac{I_T^{111}}{I_T^{222}} = \frac{I_0^{111} e^{-2M_T^{111}}}{I_0^{222} e^{-2M_T^{222}}} = A \frac{e^{-2M_T^{111}}}{e^{-2M_T^{222}}},$$

$$(4)$$

where value A unites multipliers of used reflexes, not depending on temperature and calculated, for example, with the ratio

$$A = \frac{I_0^{111}}{I_0^{222}} = \frac{|F_{111}|^2 \left(1 + \frac{cos^2 2\vartheta}{sin 2\vartheta cos\vartheta}\right)_{111}}{|F_{222}|^2 \left(1 + \frac{cos^2 2\vartheta}{sin 2\vartheta cos\vartheta}\right)_{222}},$$

(5)

Structural factor of considered fcc lattice is similar for both reflexes ($F_{111}=F_{222}=4f$, where f – atomic factor of scattering).

After substitution of values M from (1) in (4), making logarithm and simple transformations we obtain a value of dynamic displacements normalized on lattice period of Al (a)

$$\frac{\overline{U_T}}{a} = \sqrt{\frac{ln\gamma_T - lnA}{6\pi^2}}.$$

(6)

This expression was used to define oscillations amplitude however it requires a calculation of the value A, which can be associated with considerable errors.

Accounting for (3), valid for the interval of high temperatures T> θ, the ratio (6) can be re-written as

$$ln\gamma_T = lnA + \frac{B}{\theta^2}T,$$

(7)

which by slope of graph $ln\gamma_T(T)$ enables to define θ and then using (3) to find out values of thermal displacements U_T. Thus it is supposed that definition of θ is carried out for temperature interval in which the value A can be accepted as a constant.

2.3.   Results and discussion

Experimentally measured integrated intensity of reflexes (111) and (222) of aluminum obtained in the investigated temperature interval from the layered sample with the period of 45 nm and the monophase standard, are available in tabl. 2.1. It is found out that in the course of actual annealing at high-temperature X-ray measurements the texture brining to deviations from monotonous falling of intensity of reflexes with formation of a maximum of intensity at temperature of 630K was developed in the layered sample. For monophase aluminum monotonous falling of intensity of reflexes with temperature was observed. Aiming to exclude the influence of texture on intensity of reflexes according with textural model of Marshall - Dallas [27] the corrections with reception of corrected values of intensities of Al reflexes from layered sample (tab. 1) were computed. As it's seen from the table, introduction of textural corrections left almost invariable ratios of

intensities of reflexes (111) and (222) that witness about a reasonableness of Marshall - Dallas method in the discussed case.

Temperature dependences of intensities of reflexes of standard and layered sample (taking into account textural corrections for the last one) are given on fig. 2.2.

As it is seen from fig. for composite sample Al-Si there is a sharper falling of Al intensity for both reflexes (111) and (222). It directly specifies big values of thermal multiplier of aluminium being found in eutectic composition. However, decrease of intensity of reflexes of investigated layered sample can be also defined by change of value A in ratios (5) and (7) owing to actual decrease of reflecting volume because of formation of diffusion zones and formation of new metastable phases in those [20,21].

Tabl. 2.1. Integrated intensity of reflexes (111) and (222) and their ratios for aluminum as a part of a layered composite and monophase sample

T, K	Etalon Al			Layered sample Al-Si (As-06)		
	I_{111}	I_{222}	γ (I_{111}/I_{222})	I_{111}	I_{222}	Γ (I_{111}/I_{222})
290	39063	2955	13.21	45630 (33012)	3630 (2631)*	12.57 (12.54)
470	35012	2485	14.089	40036 (24867)	3067 (1905)	13.05 (13.05)
630	31700	2085	15.2	53570 (18037)	3688 (1241)	14.52 (14.53)
730	29133	1784	16.33	37223 (14025)	2255 (851)	16.5 (16.48)
830	26736	1528	17.49	31281 (9394)	1674 (503)	18.69 (18.67)

*- Intensities of reflexes and their ratio after introduction of textural corrections are given in brackets.

a)

b)
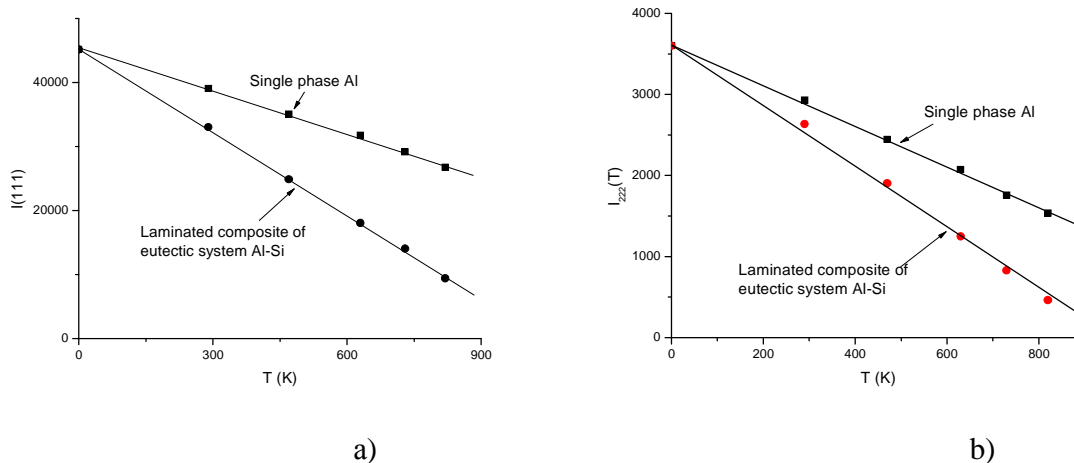
Fig. 2.2. Temperature dependencies of reflexes intensity (111) and (222) Al in one phase and composite samples

To define such possibility the microstructure of multilayered samples was investigated by TEM methods. Fig. 2.3 illustrates the microstructure of multilayered foil with the period of alternating layers of 640 nm in initial state (a, b) and after heating up to temperature 518K (c, d). It is seen that in the initial state a microscopic structure of foil represents an alternation of Al and Si layers for which a split of elements on interface is characteristic.

After heating of foil up to 518K its microstructure has the same typical features – a consecutive alternation of layers. However of attention is that near to interfaces between elements "diffusion zone" is observed at transition from one element to another (fig. 2.3 c, d) thickness up to 100 nm. It means that in X-ray studied sample with the period of 45 nm the diffraction pattern from aluminium layers is formed minimum by a solid solution and other possible phases. This is proved by additional peaks observed on diffractograms of samples after high temperature annealing along with reflexes of Al and Si, these additional peaks could be associated with a structure of diffusion zone (fig. 2.4). These additional lines were identified as lines of approximated cubic phase like α-(AlMnSi) with a period a=1,2614 nm [28] and referred by us to metastable phase of diffusion zone. Revealing of approximated phase witnesses the existence of appropriate quasi-crystal component in the investigated sample in certain temperature interval. Lattice periods of Al in layered sample are 0.4043 nm and 0.4118 nm for room temperature and 830K respectively. The observed relative change $\Delta a/a=1.85*10^{-2}$ insignificantly exceeds a change of lattice period due to thermal expansion ($\sim 1.5*10^{-2}$ at $\Delta T \sim 500^{o}$ and coefficient of thermal expansion of Al $\alpha \sim 30*10^{-6}$). Thus, at high temperatures thin layers of Al represent heterophase system: Al based solid solution (for which measurements of thermal multiplier is carried out) with a low concentration of silicon and quasi-crystal phase.
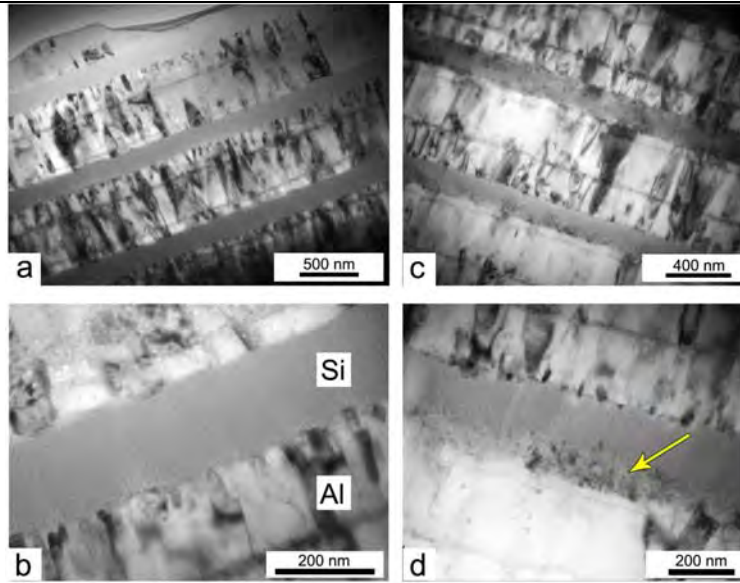
Fig.2.3. Bright field images of microstructure of cross section of multi-layered foil Al/Si in initial condition (a, b) and after its heating up to 518K (c, d). A row shows «diffusion» zone, which is formed between the layers of Al and Si after foil heating up to 528K.
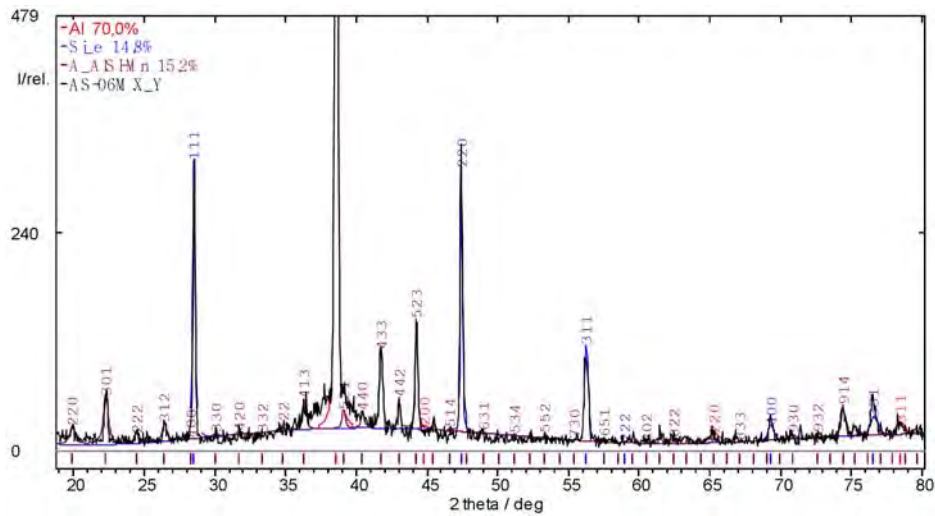

Fig. 2.4 Complete profile analysis of a diffraction pattern of sample AS-06 after high-temperature X-ray measurement in temperature interval 290 - 830K

As in further analysis of thermal multiplier, not measured intensities of Al reflexes but ratios of intensities of reflexes are used then it appreciably expels the effects associated with the above-stated features of a structural state of Al layers. Dependences $ln\gamma_T (T)$ for Al reflexes as a part of investigated layered eutectic composites and in monophase reference sample for high temperature interval $T>\theta$ are presented on fig. 2.5a.

For the high-temperature interval 630-830 K inclinations of curves ln γ(T) for the sample and the etalon appear $1.25*10^{-3}$ and $7.015*10^{-4}$ respectively. Using known value of Debay temperature for monophase Al (385 K) on the basis of (7) we obtain Debay temperature for Al in eutectic nanolayered composite 288 K, i.e. by 25% lower, than for etalon monophase Al. Owing to the ratio (3) it means that in the specified temperature interval the average thermal dynamic displacements of Al atoms in layered eutectic sample (actually in diffusion zone on Al basis) appear by 25% higher in comparison with those for monophase Al. Calculation results of dynamic displacement U for the area of high temperatures (up to the pre-melting ones for the layered sample) by means of (3) and with use of the obtained value Θ are resulted on fig. 2.5b.

a)   b)
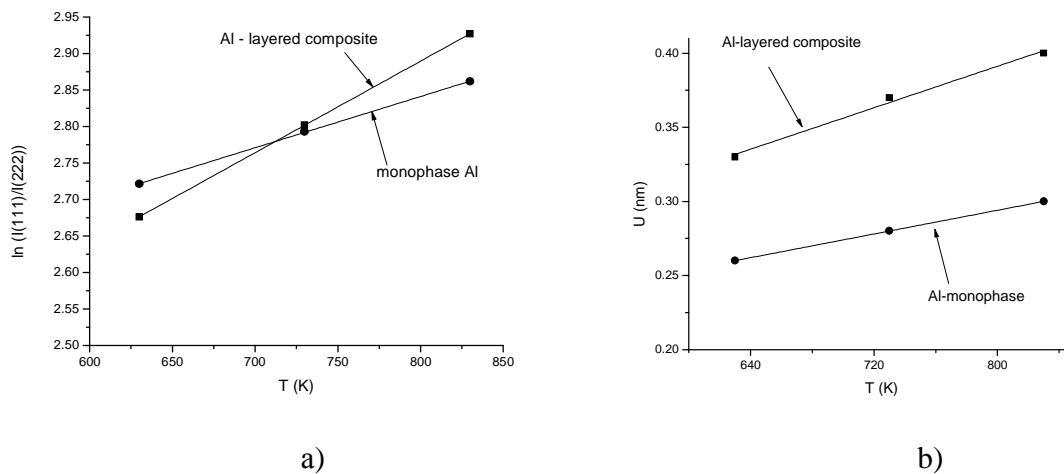
Fig. 2.5 Dependence ln γ(T) for Al in a composition of layered sample and single phase etalon (a) and average thermal displacements of Al atoms in single phase and layered sample Al-Si (b).

The obtained data are referred to average by volume values of dynamic displacement. As dynamic displacements are characterized by distribution functions with parameters depending on distance to interfaces it is possible to assume that near these interfaces the amplitudes of oscillation attain still big values.

2.4. Conclusions

It is shown that the thermal characteristics of crystals (Debay temperature and value of dynamic thermal displacement of atoms) significantly depend on a structural state of a material. At high temperatures in eutectic systems, at least in diffusion zones near to interfaces, the above-stated thermal characteristics of components appear essentially distinct from those in a monophase condition and there essential weakening of interatomic bonds and increase of amplitude of thermal oscillations of atoms occur. This phenomenon can be a principal reason for elevation of diffusion activity in grain boundary volumes of phases in eutectic systems and to stimulate the elevation of speeds of some high-temperature processes (sintering of powders, creep, etc.).

3. Computer modeling for direct investigations of interatomic interactions and dynamics of atomic-structural transformations at sintering at heat treatment and deformation of investigated ceramic materials (molecular dynamic modeling of temperature influence on stress-strain curves of alloys TiC-ZrC and investigation of processes of contact melting in system Cu-Si.)

Super refractory materials namely first of all carbides of transitive metals of IV-VI groups ($T_{melting}$ up to 4000ºC), possess a number of high physico-mechanical properties, that is governed their wide technical employment, in particular as components for UHTCs. A number of peculiarities of behavior of these materials, namely superplasticity of eutectic alloys TiC-ZrC was found at hot pressing of powder mixtures and while investigating bending strength of samples heated up to high temperatures [28-31]. However up to now the mechanism of this phenomenon has yet to be find out.

The aim of this effort is to investigate the processes developed in model systems at high temperatures:

3.1. Atomic mechanisms of deformation and fracture of nanocrystals of titanium and zirconium carbides and their alloys in a broad temperature interval by the MD method.

3.2. Diffusion and melting processes at formation of eutectic structures and to carry out MD for the system Si – Cu, in which this phenomenon was observed experimentally.

3.1.1. Molecular dynamic modeling of deformation processes of tension of TiC nanorods

For investigation of processes of deformation of tension and fracture of TiC nanorods the author's software package of molecular dynamics which employs pair potential model of interatomic interactions was applied [32].

Rod size was 7x3x3nm, the total number of atoms in rod -3993, from which Ti atoms - 1996 and C atoms - 1997. The rod was oriented along crystallographic direction [100]. The influence of temperature and strain rate on a character of atomic-structural re-arrangements and an appearance of dependencies energy-deformation and stress-deformation was investigated. Elongation was made in isothermal mode. Number of atoms and pressure were constant and a pressure was supposed as 0 that approx. corresponds to atmospheric pressure.

Two sets of experiments with various iteration steps were carried out: a) elongation $dL = 0.001$ nm per iteration with time step $dt = 0.05$ fsec and b) $dL = 0,00002$ nm, $dt = 0.001$ fsec. This experiment was required to define the influence of parameters dL and dt at equal ratio dL/dt on a character of deformation. Elongation was performed at temperatures 300, 1000, 2000, 3000 and 3530 K, embracing the interval from a room temperature to melting one.

Figs. 3.1-3.3 illustrate the first set of experiments with parameters $dL = 0.001$ nm, $dt = 0.05$ fsec. Projections on these figs. correspond to the appearance on plane (110), which is convenient as atoms of metal and carbon in ideal structure are not imposed on each other. Elongation at room temperature (300 K) occurs under conditions of low thermal mobility of atoms (fig. 3.1*a*). While elongating (fig. 3.1*b*), atoms activity

increases. It is more noticeable in the mid part of sample that is associated with their position on projection (110). The next stage (fig. 3.1*c*) is characterized by a formation of big hearts failure, which further causes a break of sample (fig. 3.1*d*). The appearance of appearing cracks with sharp edges and abrupt transition from ideal structure to a damaged one witnesses a rather brittle character of fracture that is in a good agreement with natural brittleness of carbide at low temperatures.
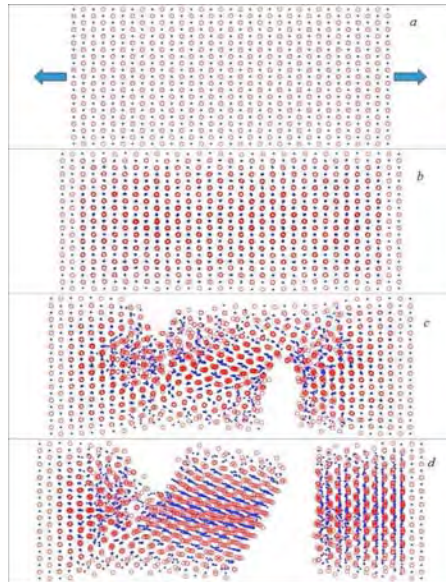
Number of iterations: a) 0*;* b) 500; c) 1000; d) 1500

Fig. 3.1 Tension of TiC nanocrystal at temperature 300K (*dt*=0,05 фc; *dL*=0,001nm). Rows point tension direction

Fig. 3.2 illustrates atomic re-arrangements in elongated samples at temperatures 2000 K. Unlike the previous case, there are no strongly expressed atomic trajectories along the axis of elongation.
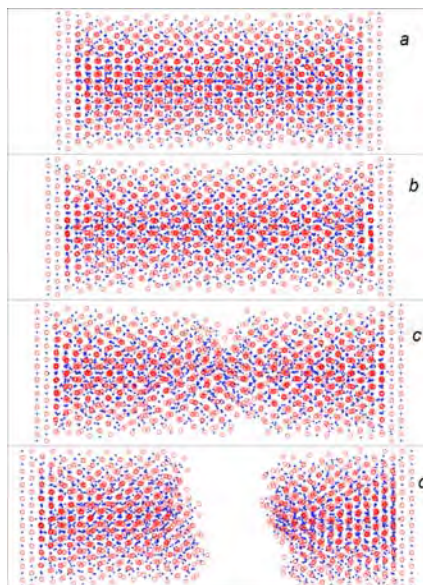
Number of iterations: a) 500*;* b) 1000; c) 1500; d) 2000

Fig. 3.2 Tension of TiC nanocrystal at temperature 2000K (*dt*=0,05 фc; *dL*=0,001nm)

This can be associated with, that at relatively low temperature shear mechanisms of deformation along atomic planes dominate, at the same time when at 2000 K another mechanism is valid, namely the mechanism of volumetric shifts of atoms on the background of intensive thermal movements.. Typical round areas of thermal movements of metal atoms surrounded by carbon atoms filling in gaps are observed (fig. 3.2*a*, *b*). In projections carbon atoms look like chain structures though in volume they are mainly disunited. Fracturing crack appears in central part of sample due to volumetric shifts of atoms where a break occurs (fig. 3.2*c*, *d*).

Elongation at melting temperature (3530 K) is showed on fig. 3.3. Initially sample's elongation due to a small narrowing and volumetric mass transfer occurs (fig. 3.3*a*, *b*). Further there occur the accumulation of stress and a break of interatomic bonds in a zone of transition from cold ends to warm average zone which behaviors itself like liquid accepting a ball-like form (fig. 3.3*c*, *d*). Due to high thermal activity atoms of a mid part easily travel in a zone of stress concentration, facilitating bonds break. In the second part of experiments with parameters of calculation dL = 0,00002 nm, dt = 0,001 fsec rather similar results were obtained but fracture character has both similar and distinctive features. Similarity is that at room temperature, hearths failure appear due to shear deformation after arrival of critical stress and critical value of elongation (~ 1 nm). As a distinction one should note more brittle character of fracture in their first set of experiments i.e. in case of parameters of calculation.
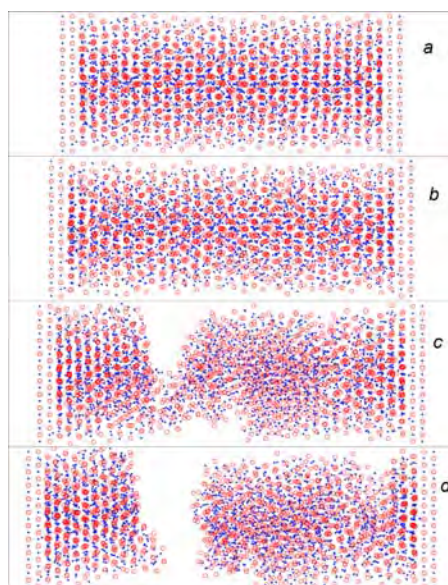
Number of iterations: a) 500*;* b) 1000; c) 1500; d) 2000

Fig. 3.3 Tension of TiC nanocrystal at temperature 3530K (*dt*=0,05 фc; *dL*=0,001nm).

Changes of energy of interatomic bonds in a course of elongation were also investigated. Fig. 3.4 shows a change of bonds energy (system's potential energy) in the first set of experiments with calculation parameters dt=0,05 fsec; dL=0,001nm.

Curves on fig. 3.4a show energy with account for heating up to the temperature of experiment, and on fig. 3.4b - the same energy but minus heating. The last is in proportion to stress thus the curves on fig. 3.4b are analogous to stress-strain curves. The show that TiC nanorods possess the lowest strength at room temperature, and the highest one – at 1000 K. At temperatures above 2000 K the strength changes only weakly.
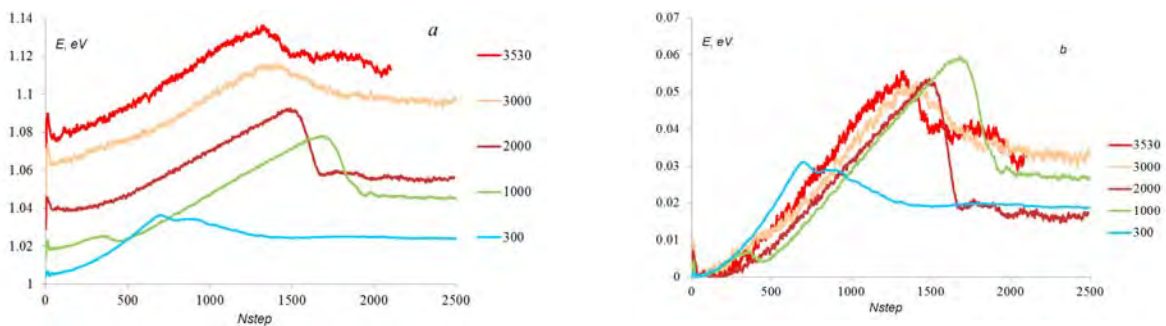
Fig.3.4 Change of energy of interatomic bonds in the process of tension of TiC nanorod at various temperature with parameters of fast calculation dt=0,05 fsec; dL=0,001nm: a – total energy, including heating from 0 K; b – energy minus heating one. Temperature showed in Kelvin.

Thus, the developed model of interatomic interactions in refractory carbides of d-transitive metals [32] allows effectively using the method of molecular dynamics to carry out virtual strength tests of nanocrystals at various types of loading in a broad temperature interval.

3.1.2. MD modeling of mechanical properties of nanowires of titanium and zirconium carbides

Unlike nanorods which possess final length, nanowires in model representation possess unlimited length due to the application of periodic boundary conditions, which are superposed along wire axis. Interaction forces were described by the potentials of embedded atom with account for second neighbors [33,34]. Modeling was carried out by Lammps codes [35]. Similar to modeling of nanorods a pressure was supposed as 0. Investigations of the influence of strain rate and temperature on stress-strain curves, value of Young's modulus were carried out. Melting processes were considered as well.

The samples were modeled as follows. From TiC and ZrC crystals (structure B1) the sample with cross section $6a_0$x$6a_0$ and length $60a_0$, where a_0 – carbide lattice parameter was cut off. The sample was oriented along crystallographic direction [001], which was combined with axis z. Axes x and y were combined with crystallographic directions [100] and [010] respectively. Periodic boundary conditions were superposed only along axis z. Samples elongation along the axis z was carried out with constant relative strain rate. At

temperature T=300 К the samples were subjected to elongation with strain rates $\dot{\varepsilon}$ =0.02, 0.01, 0.005, 0.002 and 0.001 pico sec $^{-1}$. For $\dot{\varepsilon}$ =0.01 pico sec^{-1} the investigations were done in temperature interval 50 – 3000 K.

To begin with let's consider the influence of strain rate on appearance of stress-strain curves at constant temperature T=300 К (fig. 3.5).
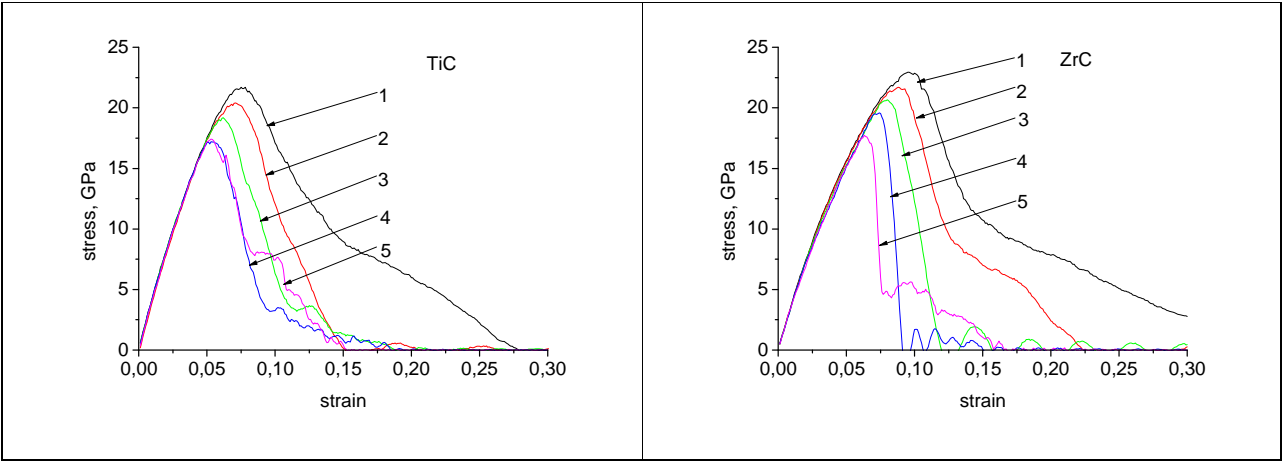
Relative strain rate $\dot{\varepsilon}$: 1 - 0.02; 2 - 0.01; 3 - 0.005; 4 - 0.002; 5 - 0.001 1/пс

Fig. 3.5 Stress-strain curves for T = 300 K and various relative strain rates

It should be noted that all stress-strain curves on fig. 3.5 possess a rather abrupt break. Maximums of curves are systematically shifted towards the area of small deformations, and fracture stress decreases when relative strain rate decreases as well. Maximum Young's modulus is observed at minimum relative strain rate.

The next fig. 3.6 represents stress-strain curves at various temperatures. Fracture stress monotonously decreases as temperature elevates. At temperature 3200 K (TiC) and 3400 K (ZrC) there occurs an elongation of liquid sample and stress does not depend on strain rate.
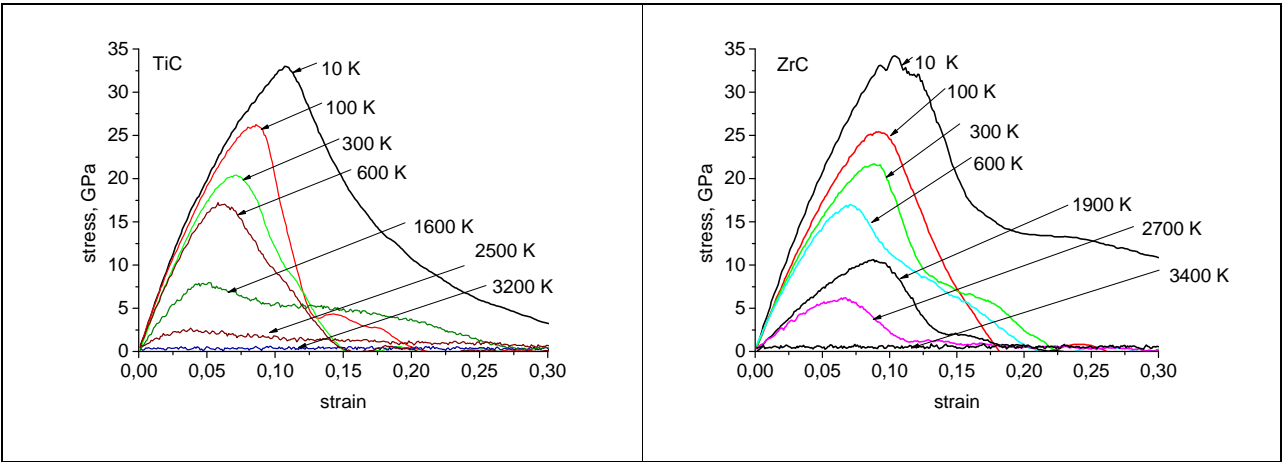
Fig. 3.6 - Stress-strain curves at relative strain rate 0.01 1/pico sec and various temperatures

For TiC and ZrC the calculated Young's modules show linear dependence vs. temperature (see fig. 3.7).
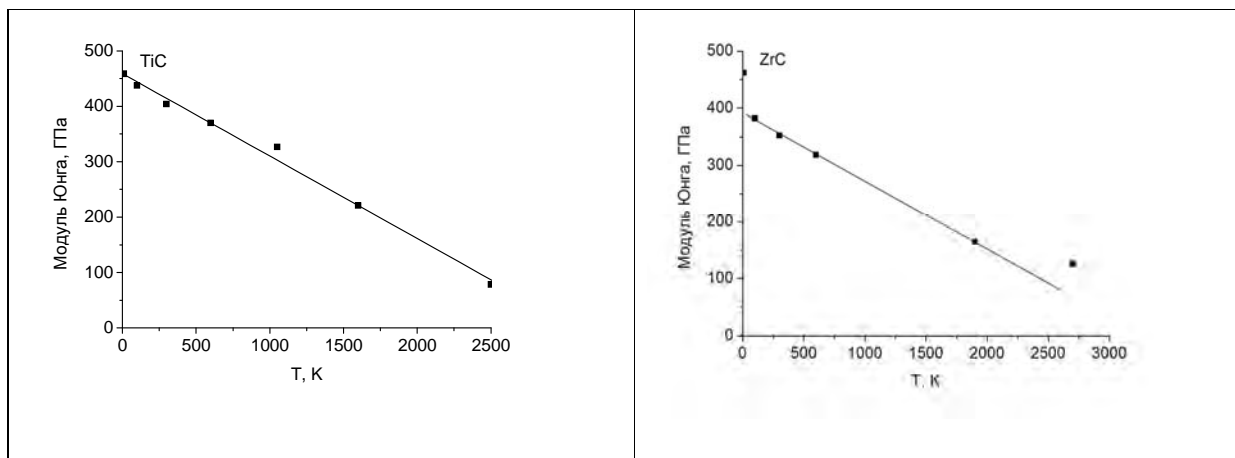
Fig. 3.7 – Dependence of Young's modulus vs. temperature at relative strain rate 0,01 1/ pico sec

3.1.2 TiC-ZrC alloys

The system TiC-ZrC is characterized by a continuous number of solid solutions at high temperatures and their disintegration at lowered temperatures. Liquidus curve has a minimum as in eutectic systems (see fig. 3.8).
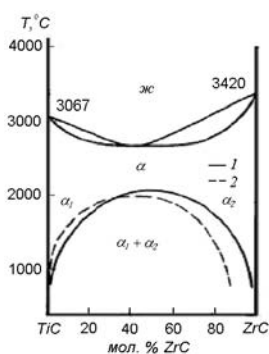
Fig. 3.8 - Equilibrium diagrams of pseudo-binary carbide system TiC –ZrC. Solid curves – calculation in approx. of regular solutions [36], dash line – experiment

Sample type 1

	Sample type 2
	Sample type 3

Ti   Zr   c
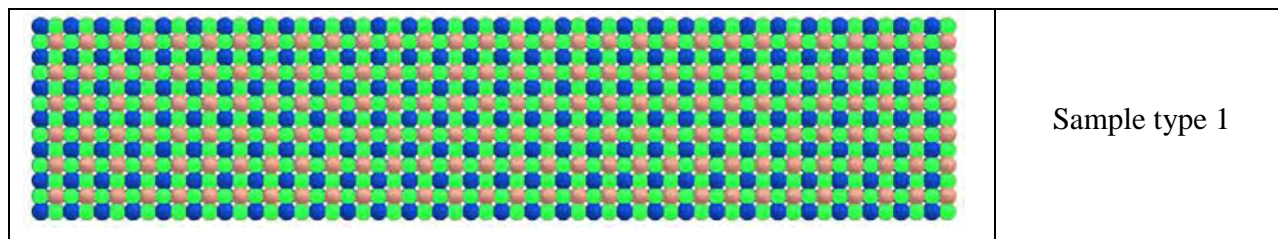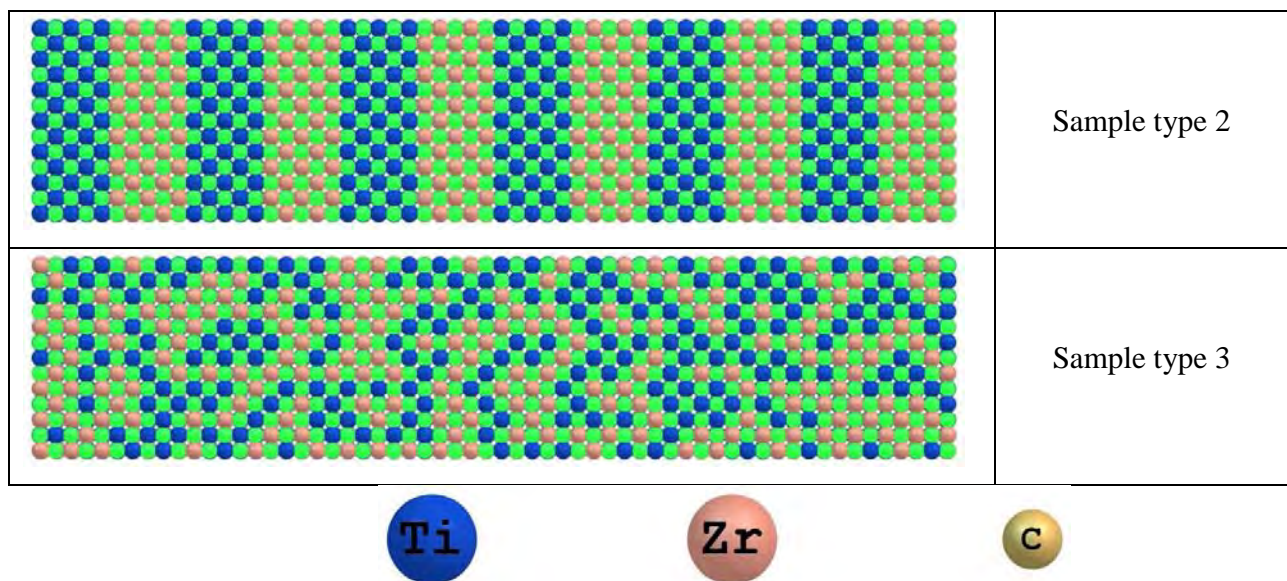
Fig. 3.9 – Samples of alloys TiC-ZrC – initial configuration

Structures of disintegration possess plate-like structure with a crystal lattice like NaCl. For modeling a composition $Ti_{0.5}Zr_{0.5}C$ was chosen. To express a variety of possible structures the samples of 3 types were modeled (fig. 3.9). The sample of first type (type 1) was obtained from TiC crystal, in which the planes [001] were alternatively filled with Ti and Zr atoms. Thus, the sample type 1 was ordered alloy. Sample type 2 was built by alternating layers TiC and ZrC (similar to plate-like eutectic or eutectoid). Layer's width – two elementary cells. In sample type 3 Zr and Ti atoms are distributed randomly (disordered alloy).

MD modeling of samples elongation was carried out in a broad temperature interval from room temperature up to 2400 K, at which a continuous row of solid solutions is observed.

Fig. 3.10 illustrates the obtained stress-strain curves at relative strain rate 0.01 1/pico sec. First of all a qualitative distinction of behavior of stress-stain curves for the sample type 1 and samples 2,3 should be noted. For the sample type 1 for all temperatures the area of yielding is absent and the whole appearance of curves is similar to that one observed for pure titanium carbide and zirconium carbide. An abrupt break for the samples type 2 and 3 is observed only at room temperature (300 K) and at significant deformation. For the rest temperatures (except 600 K, the sample type 3) weak oscillations of stress are observed with a growth of deformation (600, 1150, 2000 K – the sample type 2; 1150, 2000 K – the sample type 3), or yielding area (2400 K).
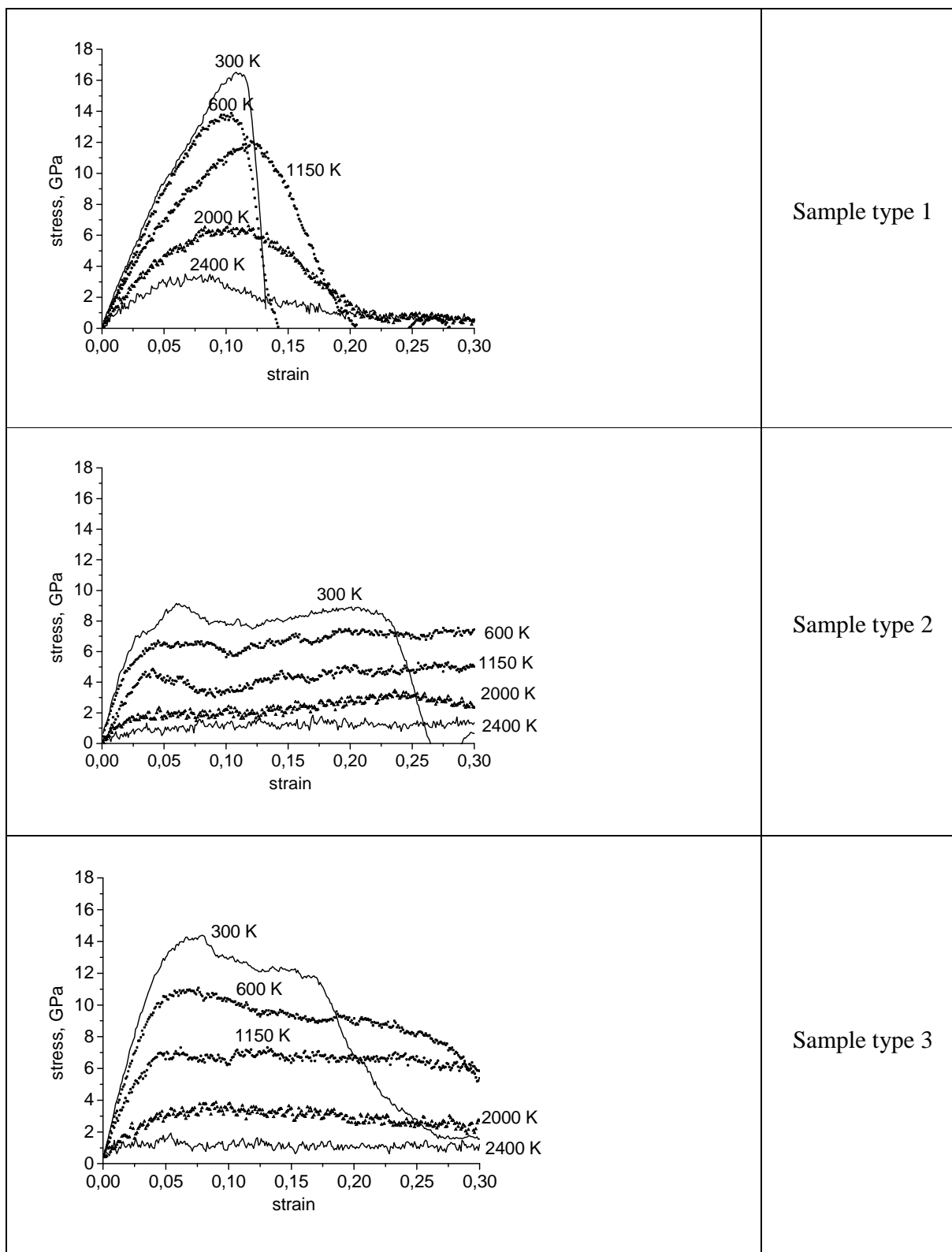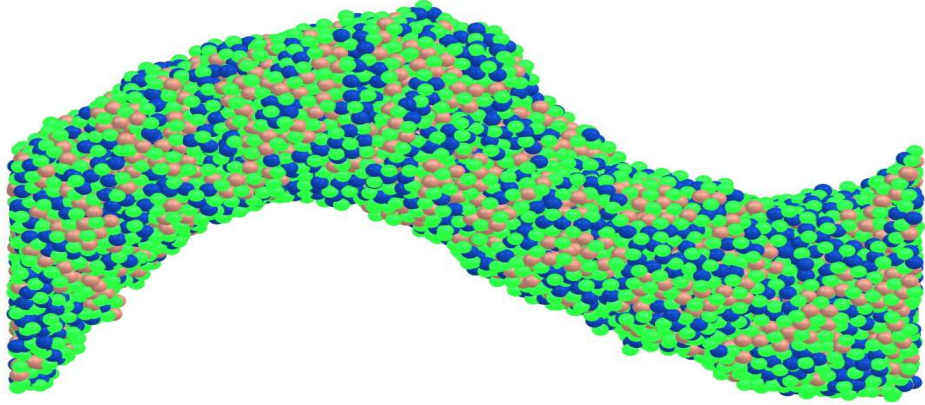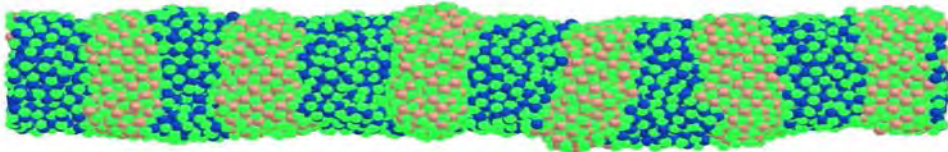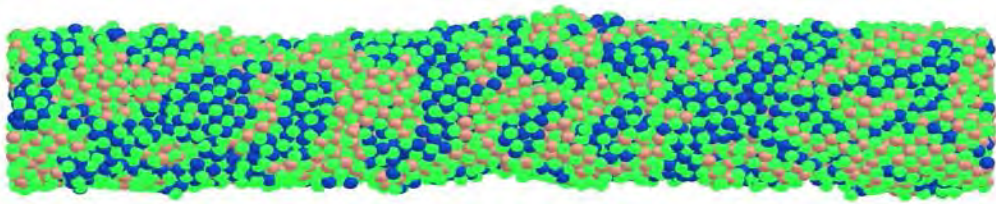
Fig. 3.10 - Stress-strain curves for samples of type 1, 2, 3

Fig. 3.11 – Samples of alloys TiC-ZrC at 2400 K and relative strain rate $\varepsilon = 0.25$

Fig. 3.11 shows samples forms which they are obtained after elongation up to a relative deformation 25% and temperature 2400 K. Strong distortion of form of sample type 1 is obviously associated with high micro-stresses appearing as a result of disordering of initial structure.

3.2. Investigation of diffusion and melting processes in system Si - Cu

Section 1 and 2 showed that high temperature behavior of eutectic systems (sintering, creep, phenomena of contact melting) on the base of refractory compounds is defined by formation of powerful diffusion zones, in which elevated amplitude of atoms oscillations are observed.

This section reports the results of investigation of diffusion and contact melting processes in system Si - Cu. This system is of interest as it is eutectic and the work [21] revealed so called diffusion zones in it at heating. Fig. 30 illustrates the phase state diagram Si – Cu.
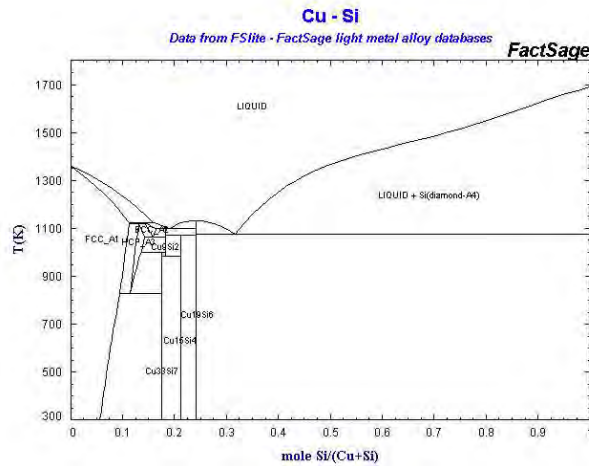
Fig. 30 – Phase state diagram Si – Cu

In accordance with this diagram T_m(Cu)=1337 K, T_m(Si)=1677 K, and eutectic point has the coordinates T_e =1060 K, c_e=32% Cu.

To model the process, which occur in the contact area of Cu and Si at heating, the potentials of interatomic interactions developed in [29] were used. Values of equilibrium lattice parameters obtained in [29] are: $a0$(Cu)=3.620 Å, $a0$(Si)=5.431 Å. Initial scheme is available in fig. 31.

Cu   Si
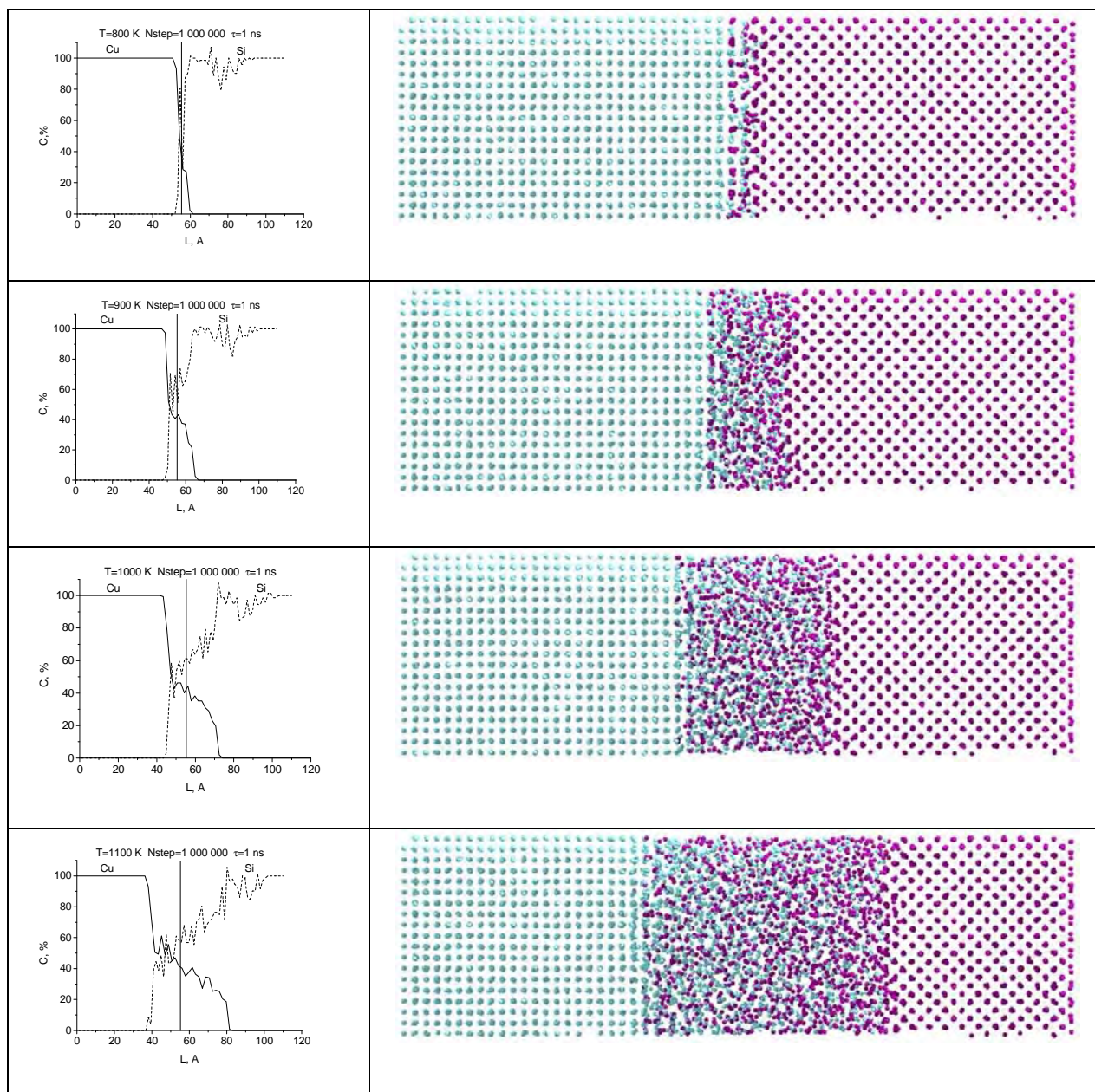
Fig. 31 Cu -Si sample – initial configuration

Fig. 32 – Distribution of Si and Cu concentrations along the sample after holding during 1 nsec at given temperature

Si and Cu samples have a quadratic section with size: for Cu – 9*a0*(Cu)=32.580 Å, for Si - 6*a0*(Si)=32.586 Å. Initial distance between samples Cu- Si was 2 Å.
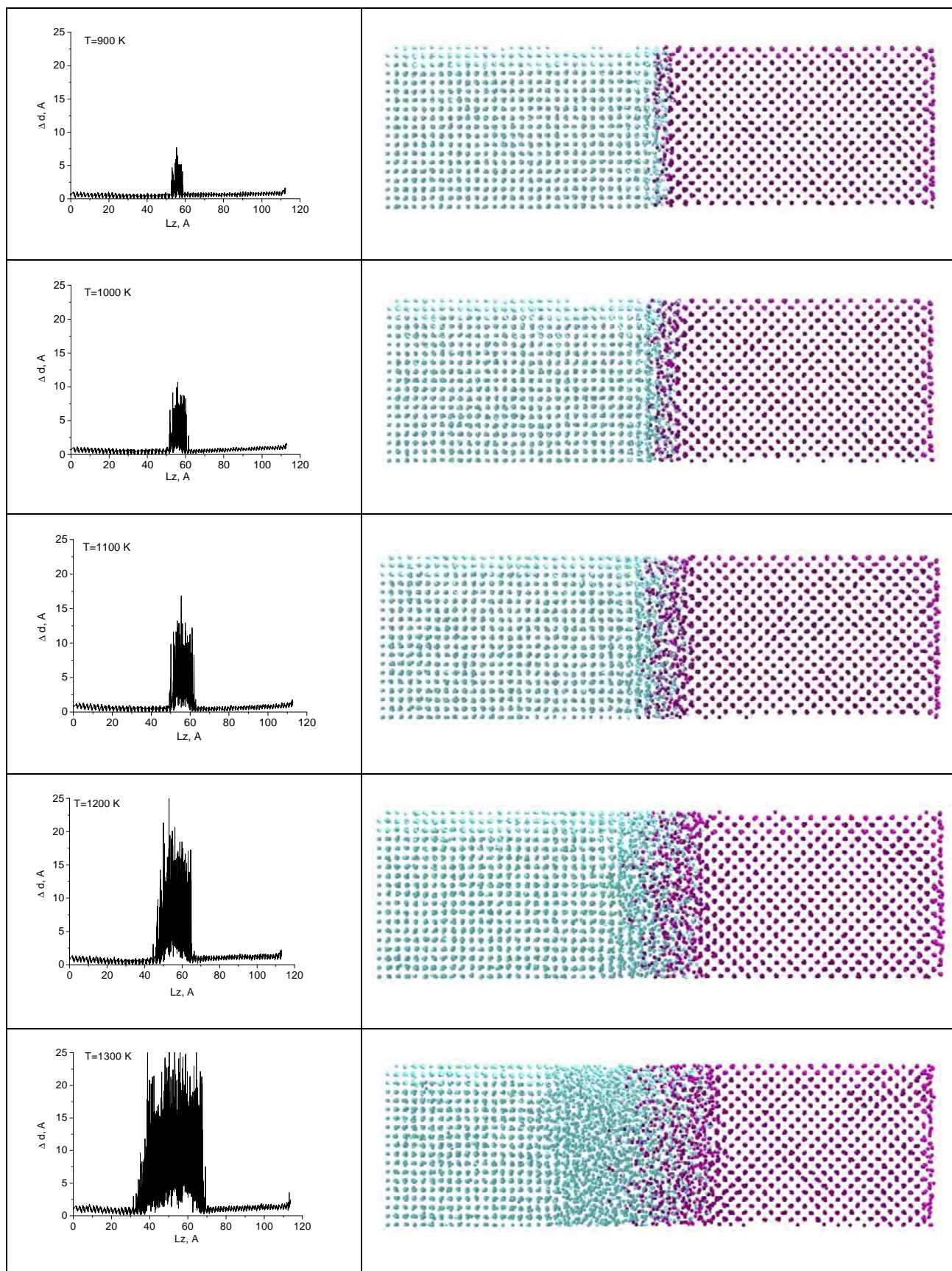
Fig. 33 – Distribution of offset value of atoms from initial positions along the sample

Periodic boundary conditions are imposed only towards directions *x* and *y*. Samples were hold at given temperature (T=500, 800, 900, 1000, 1100 K) during a time correspondent to one billion time steps. At time step 1 fsec (10^{-15} sec) this time period is 1 nsec (10^{-9} sec). The next image (fig. 32) in the left part shows the graphs of distribution of Si and Cu concentrations along the sample and the right part – sample image after holding during 1 nsec. Vertical line on graphs means the initial boundary between Si and Cu.

Appreciable diffusion is observed starting with 900K. At all temperatures a diffusion rate of Cu in Si is about twice bigger than *visa versa*. This result is in a good agreement with those facts that, atomic radius of Cu is a few less than Si and coefficient of compactness of face-centered structure is bigger than diamond like structure. At temperatures close to eutectic ones (1000, 1100 K) diffusion proceeds rather intensively.

To investigate melting process the sample was subjected to gradual heating with a step 100 K. At each temperature the sample was hold during 50000 time steps (50 pico sec). The results of modeling are available in fig. 33. The left part presents the dependencies of value of atoms offset from initial positions from coordinate *z*. Offset value in diffusion zone quickly grows while temperature rises and in the field of eutectic one (1000, 1100 K) is twice or in 3 times bigger than at 900 K. While arriving to melting temperature of Cu a growth of disordered area from Cu part goes more intensively than from Si part (T=1300 K). Despite that the obtained results do not allow to define a phase state in diffusion zone – solid or liquid, one may assert that melting process starts namely in a diffusion zone.
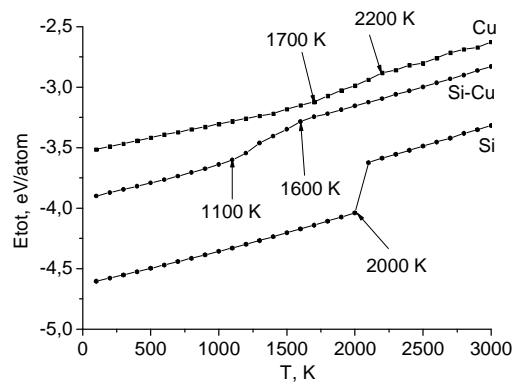

Fig. 34 – Dependence of potential energy *vs.* temperature for Si and Cu for the system Cu - Si

Qualitatively melting temperature can be defined from the dependence of potential energy and temperature [30]. These kinds of dependencies for Cu, Si and the system Cu-Si are available on fig. 34. Temperature was raised gradually with a step 100 K starting from 100 K. As melting temperature the average one between the temperatures at which an abrupt jump on the dependence potential energy - temperature exists was taken. In our case the abrupt jump exists only for Si, thus melting temperature of Si $T_m^{'}$ (Si)≈2050 K. For Cu

and the system Cu-Si the abrupt jumps (sudden change) are absent, and possess long temperature intervals, in which a deviation from linear growth of potential energy are observed. The beginning and the end of these intervals are illustrated on figs. 34. Accepting the average values of melting temperature we obtain: T_m'(Cu)≈1950 K, T_m'(Cu-Si)≈1350 K. Mismatch of the obtained melting temperatures with table values can be explained as in [29] the potentials were not calibrated to obtain right values of melting temperature. For the obtained melting temperatures the following ratios are valid: T_m'(Cu-Si) $< T_m'$(Cu) $< T_m'$(Si).

Thus the carried out molecular dynamic modeling qualitatively confirmed a formation of diffusion zone at heating in the contact area Cu-Si and showed that melting process starts slowly and in namely in diffusion zone.

This section reports the results of investigation of diffusion and contact melting processes in system Si - Cu. This system is of interest as it is eutectic and the work [21] revealed so called diffusion zones in it at heating. Fig. 30 illustrates the phase state diagram Si – Cu.
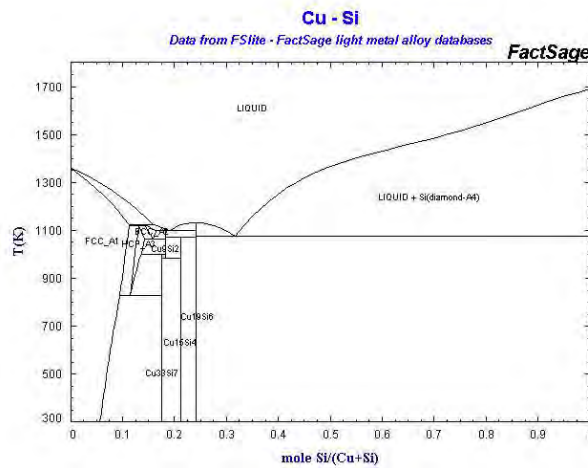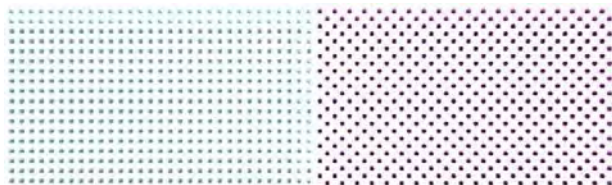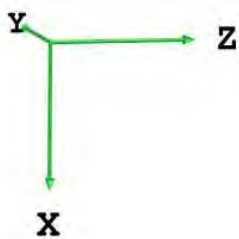

Fig. 30 – Phase state diagram Si – Cu

In accordance with this diagram T_m(Cu)=1337 K, T_m(Si)=1677 K, and eutectic point has the coordinates T_e =1060 K, c_e=32% Cu.
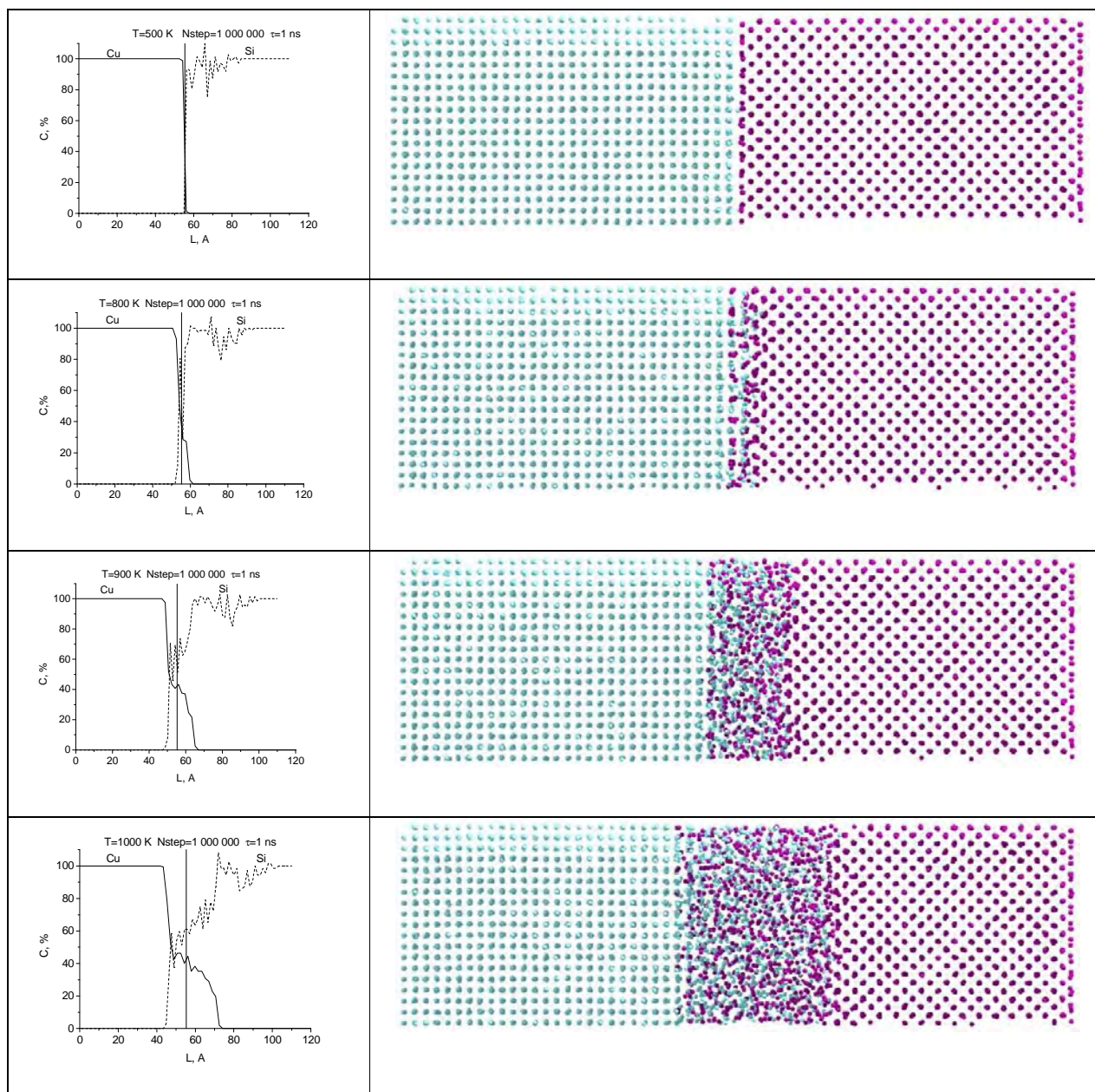
To model the process, which occur in the contact area of Cu and Si at heating, the potentials of interatomic interactions developed in [29] were used. Values of equilibrium lattice parameters obtained in [29] are: $a0$(Cu)=3.620 Å, $a0$(Si)=5.431 Å. Initial scheme is available in fig. 31.

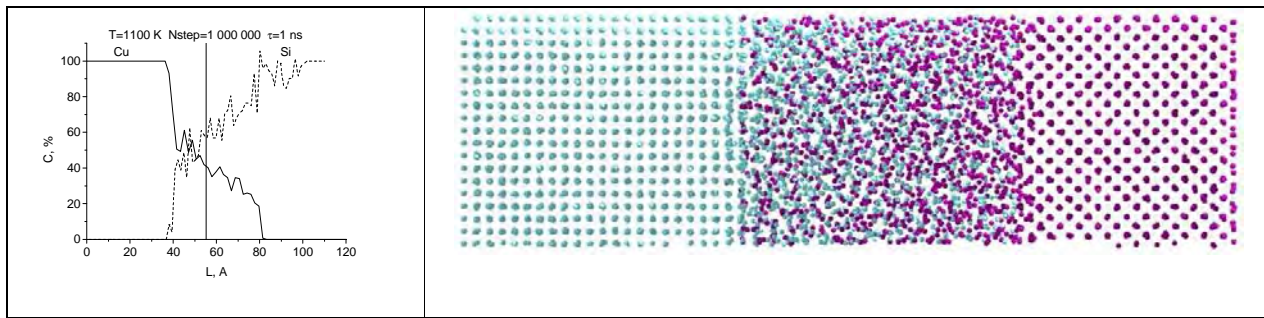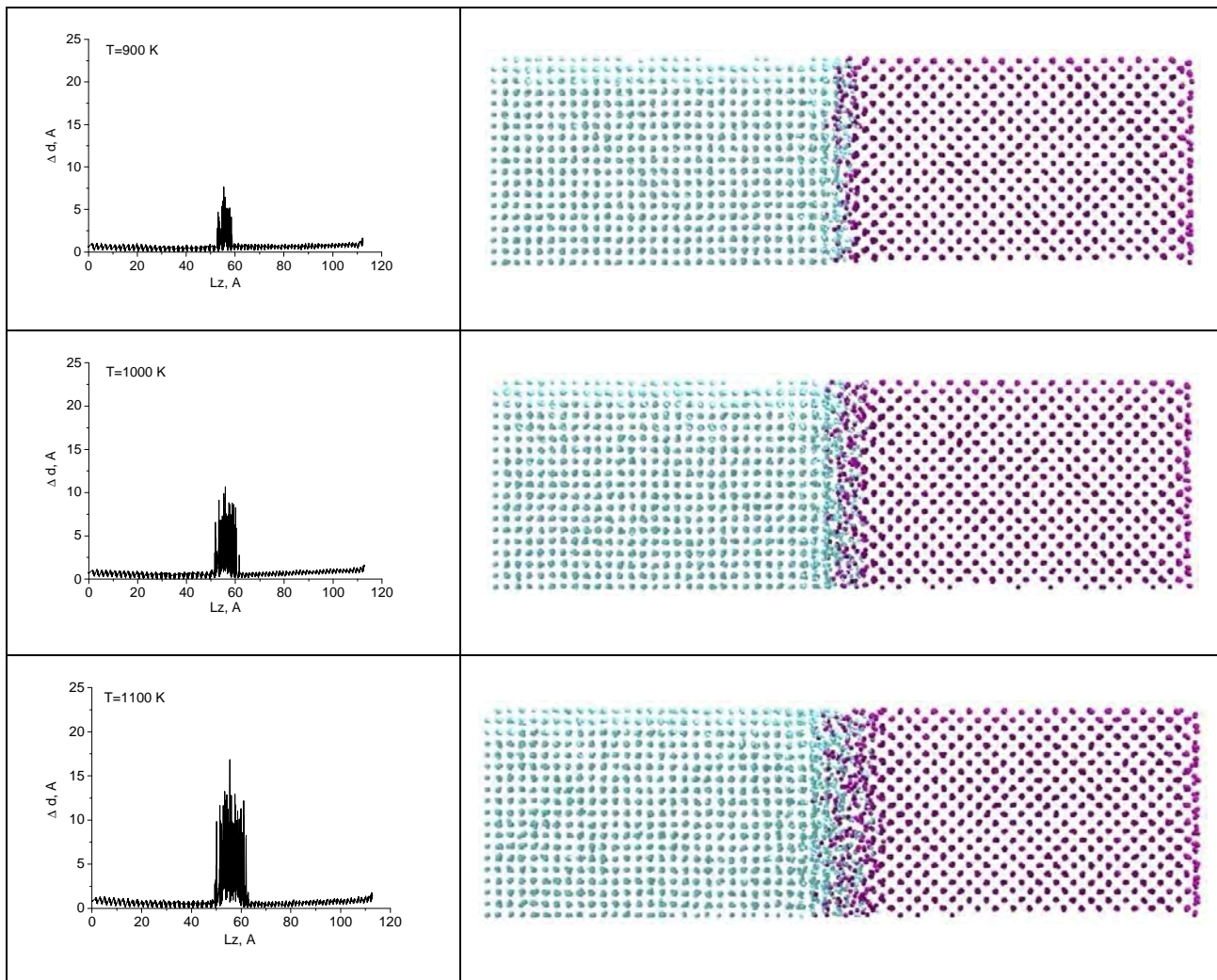Fig. 31 Cu -Si sample – initial configuration

Fig. 32 – Distribution of Si and Cu concentrations along the sample after holding during 1 nsec at given temperature

Si and Cu samples have a quadratic section with size: for Cu – $9a0$(Cu)=32.580 Å, for Si - $6a0$(Si)=32.586 Å. Initial distance between samples Cu- Si was 2 Å.
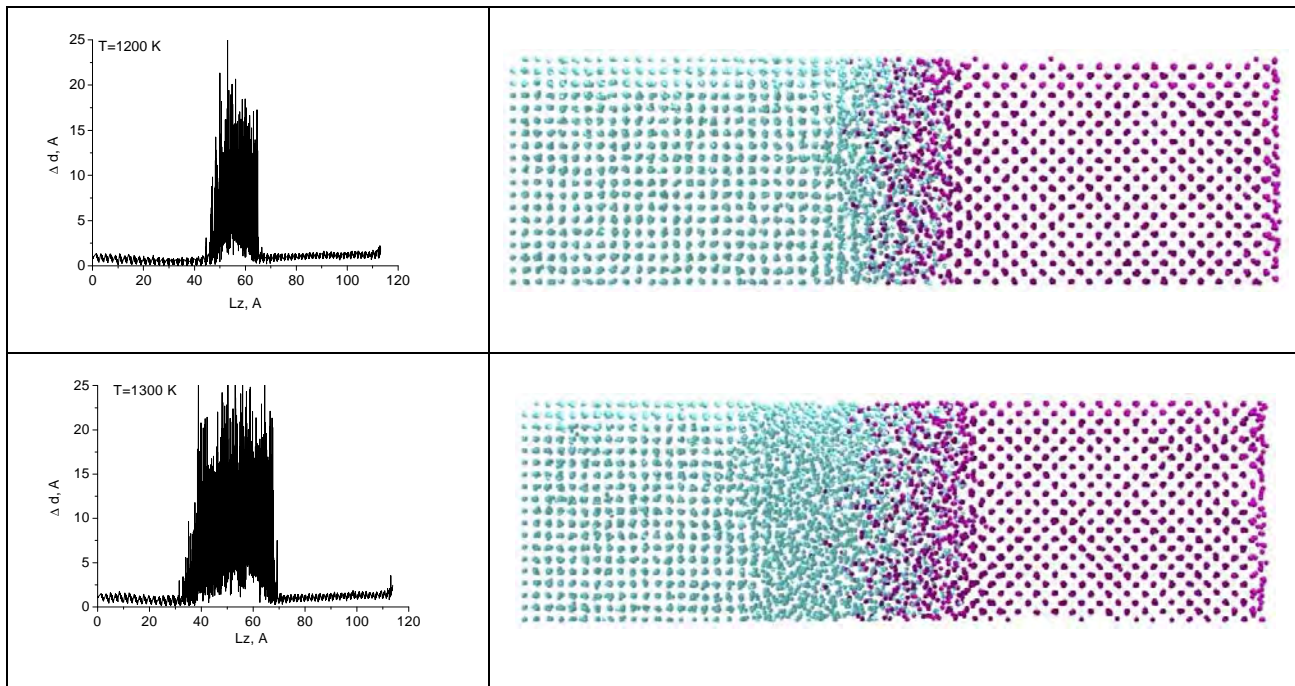
Fig. 33 – Distribution of offset value of atoms from initial positions along the sample

Periodic boundary conditions are imposed only towards directions *x* and *y*. Samples were hold at given temperature (T=500, 800, 900, 1000, 1100 K) during a time correspondent to one billion time steps. At time step 1 fsec (10^{-15} sec) this time period is 1 nsec (10^{-9} sec). The next image (fig. 32) in the left part shows the graphs of distribution of Si and Cu concentrations along the sample and the right part – sample image after holding during 1 nsec. Vertical line on graphs means the initial boundary between Si and Cu.

Appreciable diffusion is observed starting with 900K. At all temperatures a diffusion rate of Cu in Si is about twice bigger than *visa versa*. This result is in a good agreement with those facts that, atomic radius of Cu is a few less than Si and coefficient of compactness of face-centered structure is bigger than diamond like structure. At temperatures close to eutectic ones (1000, 1100 K) diffusion proceeds rather intensively.

To investigate melting process the sample was subjected to gradual heating with a step 100 K. At each temperature the sample was hold during 50000 time steps (50 pico sec). The results of modeling are available in fig. 33. The left part presents the dependencies of value of atoms offset from initial positions from coordinate *z*. Offset value in diffusion zone quickly grows while temperature rises and in the field of eutectic one (1000, 1100 K) is twice or in 3 times bigger than at 900 K. While arriving to melting temperature of Cu a growth of disordered area from Cu part goes more intensively than from Si part (T=1300 K). Despite that the obtained results do not allow to define a phase state in diffusion zone – solid or liquid, one may assert that melting process starts namely in a diffusion zone.
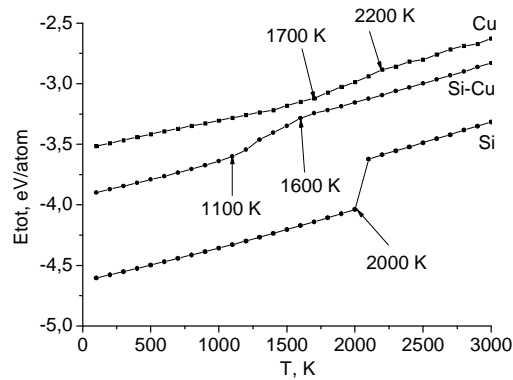
Fig. 34 – Dependence of potential energy *vs.* temperature for Si and Cu for the system Cu - Si

Qualitatively melting temperature can be defined from the dependence of potential energy and temperature [30]. These kinds of dependencies for Cu, Si and the system Cu-Si are available on fig. 34. Temperature was raised gradually with a step 100 K starting from 100 K. As melting temperature the average one between the temperatures at which an abrupt jump on the dependence potential energy - temperature exists was taken. In our case the abrupt jump exists only for Si, thus melting temperature of Si T_m'(Si)≈2050 K. For Cu and the system Cu-Si the abrupt jumps (sudden change) are absent, and possess long temperature intervals, in which a deviation from linear growth of potential energy are observed. The beginning and the end of these intervals are illustrated on figs. 34. Accepting the average values of melting temperature we obtain: T_m'(Cu)≈1950 K, T_m'(Cu-Si)≈1350 K. Mismatch of the obtained melting temperatures with table values can be explained as in [29] the potentials were not calibrated to obtain right values of melting temperature. For the obtained melting temperatures the following ratios are valid: T_m'(Cu-Si) < T_m'(Cu) < T_m'(Si).

Thus the carried out molecular dynamic modeling qualitatively confirmed a formation of diffusion zone at heating in the contact area Cu-Si and showed that melting process starts slowly and in namely in diffusion zone.

General conclusions

1. The investigation of interaction of components of ceramic ZrB_2-SiC with metals Cr, Ni and alloy NiCr showed the following:

*   The interaction of zirconium boride with chromium within quasi-binary state diagram Cr–ZrB_2 with variation of concentration of zirconium boride from 4 to 77% was investigated. It's shown that the process goes under the mechanism of contact melting that is typical for eutectic systems. Eutectic melting temperature is near 1800^0C at concentration of ZrB_2 in alloy is near 16% by mass.

- Eutectic wets boride surface with wetting angle close to 40^0 and, while interacting with a formation of more refractory compounds disappears.

- Phase composition of products of interaction depends on components ratio in alloy and temperature, representing bi- and ternary compounds built mainly on the base of crystal lattices of zirconium and chromium borides.

- Eutectic character of quasi-binary diagram Cr–ZrB$_2$, small wetting angle between eutectic and boride surface, phase interactions in products of interaction, located in intergrain layers, and an opportunity of uniform distribution through the whole volume of charge via steam phase make chromium rather promising material for its use as activating agent for sintering.

- Being based on the results obtained at previous stages devoted to the investigation of hafnium and zirconium borides with nickel and chromium and their alloys, for sintering of the above said borides and ceramics ZrB$_2$-20 mass. % SiC as sintering activator the alloy Cr-20 mass. % Ni was taken. Approbation of sintering activator was carried out at sintering of the above said ceramic with addition of 5 vol. % of chosen alloy. As a result it was found out that optimum sintering mode for this composition is temperature 1600 - 1850°C at isothermal holding 1 hour. Thus the porosity is found within up to 5 % , ceramics grain size is of 10-15 mkm, ceramic bending strength up to 400MPa and hardness - 88-89 HRA. Interaction of ceramics components brings to the presence of chromium boride based secondary phases apart from ZrB$_2$ и SiC.

2. Результаты, касающиеся формирования структуры керамики системы ZrB$_2$-SiC-Cr$_3$C$_2$ и кинетики ее уплотнения при горячем прессовании приводят к возможности развития технологии получения ультравысокотемпературной керамики с учетом следующих факторов:

- It is found out that the use of Cr$_3$C$_2$ as the activator of ZrB$_2$ reduces temperature of hot pressing from 2170°C to 1520 … 1740°C depending on Cr$_3$C$_2$ content.

- It is found out that in the system [ZrB$_2$+Cr$_3$C$_2$] an intensive contact interaction with formation of diffusion zones which begins at temperature 1310°C, takes place.

- Within the diffusion zone, the processes of phase formation with formation of new high-temperature refractory compounds in a form of zirconium carboborides, borides and chromium carboborides, zirconium – chromium carboborides intensively develop. Intensive diffusion of chromium and carbon in zirconium diboride, accompanied by formation of porous free states in zirconium diboride (on depth up to 50-100 mkm at temperature 1360°C) near diffusion zone is observed.

- As a whole, the observed activation of sintering of zirconium diboride up to porous free state in the investigated system containing eutectic components, is explained by an intensive diffusion of atoms of chromium and carbon in ZrB$_2$ through a zone of contact interaction and development of phase transformations in diffusion zone itself. The results of investigation do not contradict the assumption that the process of sintering in the conditions of contact interaction and formation of diffusion zone occurs with

a formation of disappearing eutectic liquid phase spent on formation of new high-temperature refractory compounds (the phases on the basis of zirconium carbide and chromium borides).

- An introduction of active agent in a form of chromium carbide in ceramic ZrB_2-SiC allows in the mode of vacuum sintering to obtain dense ceramic at sintering temperatures 1800-1900° C. Sintering occurs in condition of eutectic interactions with disappearing liquid phase and formation of secondary borides of chromium-zirconium and zirconium carbide; mechanical properties of ceramic increases with increase of the amount of chromium carbide up to 10-15 mass.%.

- The ceramic ZrB2-SiC-Cr3C2 at temperature about 1700°C can be deformed by 50 % and higher without essential degradation of mechanical properties. Creep process is developed almost in the mode of superplasticity under the slip mechanism of zirconium boride and silica carbide grains on grain boundary interlayers with nanocrystalline grains of carbon-boride of zirconium and diborides (carbo-boride) of zirconium –chromium.

3. It is shown that the thermal characteristics of crystals (Debay temperature and value of dynamic thermal displacement of atoms) significantly depend on a structural state of a material. At high temperatures in eutectic systems, at least in diffusion zones near to interfaces, the above-stated thermal characteristics of components appear essentially distinct from those in a monophase condition and there essential weakening of interatomic bonds and increase of amplitude of thermal oscillations of atoms occur. This phenomenon can be a principal reason for elevation of diffusion activity in grain boundary volumes of phases in eutectic systems and to stimulate the elevation of speeds of some high-temperature processes (sintering of powders, creep, etc.).

4. Computer programs for MD modeling and testing of the developed potentials including calculations of thermodynamic state of nanocrystals of carbides and relaxation changes in their structure associated with surface influence were developed. The potentials and programs are convenient for their use as virtual "trying stand" at various mechanical tests of nanocrystals (tension, compression, bending, nanoindentation, etc). It is found out that as temperature increases Young's modulus of the considered objects decreases under a linear law. Fracture stress and deformation increase at elevation of relative strain rate and fall when temperature increases. MD modeling of contact melting in eutectic system Cu-Si qualitatively confirmed the formation of diffusion zone at heating in the area of contact Cu-Si and showed that melting process starts namely in diffusion zone.

References

1. A. Belossi, S. Guicciardi V. Medri, F. Monteverde, D. Scuti, L. Silvestroni, Processing and properties of ultra-refractory composites based on ZR - and Hf-borides: state of the art and perspectives, in Boron rich solids, edited by N. Orlovskaya and M. Lugovy, Springer Publ., Dordrecht, Netherland, pp. 147-160.

2. Samsonov G.V. Refractory compounds / Samsonov G.V, I.M.Vinnitskiy.– M.: Metallurgy, 1976.– pp.558.

3. 2. Samsonov G.V Boron and its compounds and alloys / Samsonov G.V, L.Ya. Markovsky, A.F. Zhygach, M.G. Valiashko –K.: AN USSR, 1960.– pp.590.

4. Sciti D. /Microstructure and mechanical properties of ZrB_2 –$MoSi_2$ ceramic composites produced by different sintering techniques / D. Sciti, F. Monteverde, S. Guicciardi, G. Pezzotti, A. Bellosi// Materials Science and Engineering.–2006.–A434.–p 303–309.

5. Rezaie A. Evolution of structure during the oxidation of zirconium diboride– silicon carbide in air up tu 1500^0C./ A. Rezaie, W.G. Fahrenholtz, G.E. Hilmas// J. of the European Ceramic Societi.–2007.–Vol 27.–p.2495–2501.

6. Wang X.G. Pressureless sinteren mechanism and microstructure of ZrB_2–SiC ceramics doped with boron./ X.G. Wang, W.M.Guo, G.J. Zhang.// Scripta Materialia,–2009.–Vol.61,–p.177–180.

7. Kiparisov S.S. About sintering mechanism at production of low porous articles from titanium diboride / Kiparisov S.S., G.A. Libenson, A.P. Pankevich. // News of high schools. Non ferrous metallurgy.– 1974.– №5.– pp. 145–149.

8. Kiparisov S.S. About production of sintered low porous articles from titanium diboride / Kiparisov S.S., G.A. Libenson, A.P. Pankevich // Non-ferrous metallurgy.–1975.– №1.– pp. 66–67.

9. Zhang S.C. Pressureless Densification of Zirconium Diboride with Boron Carbide Additions./ S.C. Zhang, G.E. Hilmans, W.G. Fahrenholtz.// J. Am. Ceram. Soc.–2006.– Vol.89, №5.–P.1544–1550.

10. Zhynkovsky G.L. Activation of sintering of refractory borides. / Zhynkovsky G.L., Evtushok, O. N. Grigoriev et al. // Powder metallurgy.– 2011.–№3/4.–pp. 109–116.

11. Fedorchenko I.M. Bases of powder metallurgy. /I.M. Fedorchenko, R.A. Andrievsky.–K.: AN USSR, 1961– pp.420.

12. Shurin A.K. State diagram and structure of alloys of quasi-binary systems Cr–ZrB_2, Cr–HfB_2. / Shurin A.K, V.E. Panarin // Reports of AN USSR. Seria A.–1975.–№1.–pp.86–90.

13. Zalkin V.M. Nature of eutectics and the effect of contact melting. – M: Metallurgy, 1987. – p. 152.

14. Physico-chemical properties of elements / edited by G.V. Samsonov –Kiev: Naukova dumka,1965.– p. 808.

15. Investigation of kinetics of densification of materials on the basis of ZrB2-Cr3C2 at hot pressing.// Bega N.D., Vinokurov V.D., Grigoriev O. N, et al.// III international Samsonov conference, Kiev, Ukraine, May 2012.

16. V.G.Kajuk, V.A.Masljuk Structure formation of alloys of system Cr3C2-TiN and property of materials on their basis, Powder metallurgy, 2004, №1/2, p. 47-52

17. Grigoriev O.N., Galanov B.A., Kotenko V.A. et. al. Mechanical properties of ZrB2-SiC (ZrSi2) ceramics//J. Europ. Ceram. Soc. — 2010. — Vol. 30. — P. 2173—2181.

18. Grigoriev O.N. Structure and Properties of SiC-TiB$_2$ Ceramics / Y.G. Gogotsi, V.I. Subbotin, V.V. Kovalchuk // J. Mater. Processing and Manufacturing Science.-1998.-Vol.7.-№ 1. – P.99-110.

19. Zalkin V.M., On the theory of eutectic alloys and presentation of the theory in textbooks on physical metallurgy, Metal Science and Heat Treatment, 2009,-V.51, -3-4, - pp. 153-160/

20. B. Bokhonov , M. Korchagin, In situ investigation of stage of the formation of eutectic alloys in Si–Au and Si–Al systems, Journal of Alloys and Compounds, -2000. -312, -pp. 238–250

21. B. Bokhonov , M. Korchagin, In-situ investigation of the formation of eutectic alloys in the systems silicon–silver and silicon–copper, Journal of Alloys and Compounds. -2002. – 335. – pp.-149–156.

22. Bystrenko A.V. Kartuzov V.V, Contact melting and the structure of binary eutectics near eutectic point, Journal of Alloys and Compounds. -2014. – 617. – pp.-124–128.

23. A.Ustinov, L. Olikhovska, T. Melnichenko, A.Shishkin. Effect of overall composition on thermally induced solid-state transformation in thick EBPVD Al/Ni multilayers, Surf. and Coat. Technologies. – 2008, - 202.- pp. 3832 - 3838.

24. Rusakov A.A. X-ray metallography. – M., Atomizdat, 1977, - p.480.

25. Umanskiy Ya.S. X-ray metallography.- M., Metallurgy, 1967, -p.235.

26. X-ray and electron-optical analysis. Gorelik S.S., Rastorguev L.N., Skakov Yu.A., - M., Metallurgy, 1970, - p.366.

27. Dollase W.A. Correction of intensities for preferred orientation of the March model // J. Appl. Cryst. – 1986. – V. 19, – P. 267–272.

28. Sugiyama Kazumasa, Kaji Nobutaka, Hiraga Kenji, "Re-Refinement of a-(AlMnSi)", Acta Crystallographica. Section C, - 1998.- 54(4), pp. 445-447

29. Ogorodnikov V.V., Sverdlik N. N. Theoretical analysis of homogenization process of disperse mixtures of pseudo binary system TiC – ZrC at sintering and hot pressing // High temperature carbides. Kiev, "Naukova dumka". – 1975.

30. Ogorodnikov V.V., Sverdlik N. N. Experimental investigation of densification and homogenization process of disperse mixtures of pseudo binary system TiC – ZrC at sintering and hot pressing // High temperature carbides. Kiev, " Naukova dumka ". – 1975.

31. Andrievskiy R.A., Spivak I.I., Klimenko I.I. // Academy of Science USSR. – 1972. – **203**, №6 - pp. 1279 – 1281.

32. V.V. Ogorodnikov, O.N. Grigoriev, V.L. Bekenev, V.V. Kartuzov, Interatomic potentials of interactions for especially refractory compounds, Mathematical models and numerical experiment in materials science, Kiev, IPMS Publishing house, 2013. pp. 86-97.

33. Kim Young-Min, Lee Byeong-Joo. Modified embedded-atom method interatomic potentials for the Ti–C and Ti–N binary systems // Acta Materialia. – 2008.- **56**, N 14 – P. 3481–3489.

34. Kim Young-Min, Lee Byeong-Joo, Baskes M.I. Modified Embedded Atom Method Interatomic Potentials for Ti and Zr // Phys. Rev. – 2006. - **B74**, N 1. - 014101.

35. Plimpton S. Fast Parallel Algorithms for Short-Range Molecular Dynamics // J. Comp. Phys. – 1995. - **117**, N 1. – P. 1-19.

36. Ogorodnikov V.V., Ogorodnikova A.A. Calculation of state diagrams of pseudo binary systems formed by carbides Ti, Zr and Hf // Inorganic materials. – 1977. **- 13**, № 4.

37. Jelinek B., Groh S., Horstemeyer M. F. et al. Modified embedded atom method potential for Al, Si, Mg, Cu, and Fe alloy // Phys. Rev. – 2012. – **B85**, N 24. – 245102 (18 p.).

38. Li X., Huang J. Molecular dynamics studies of the kinetics of phase changes in clusters // J. Sol. Sta. Chem. – 2003. – **176**, N 1. – P. 234-242.

PUBLICATIONS OR PRESENTATIONS TO DATE:

1. Bega N.D., Vinokurov V.B., Grigoriev O.N., et. al., «HOT PRESSING SHRINKAGE KINETICS OF THE ZrB_2 - Cr_3C_2 CERAMICS», The III-rd International Samsonov's Conference "MATERIAL SCIENCE OF REFRACTORY COMPOUNDS", Kiev, Ukraine, 23-25 May, 2012

2. O.N. Grigoriev, L.M. Melakh, V.A. Kotenko et. al., "Ultra-High temperature ceramics for aerospace technics " on the XII International Congress on Engine Building, Crimea, Ukraine, 17-19 September, 2012

3. O.N. Grigoriev, L.M. Melakh, V.A. Kotenko et. al., Ultra-High temperature ceramics for aerospace techniques, Journal of Aerospace Engineering and Technology, 2012.-#8/95.- P. 119-128 (in Russian).

4. O.N. Grigoriev, Ceramics and cermets on the base of oxygen free refractory compounds, Powder metallurgy – 2012.-№1/2.- pp. 100-116.

5. V.V. Ogorodnikov, O.N. Grigoriev, V.L. Bekenev, V.V. Kartuzov, Interatomic potentials of interactions for especially refractory compounds, Mathematical models and numerical experiment in materials science, Kiev, IPMS Publishing house, 2013. pp. 86-97.

6. V.V. Ogorodnikov, O.N. Grigoriev, V.L. Bekenev, V.V. Kartuzov, Molecular dynamic modeling of physico-mechanical properties of nanocrystalline titanium carbide, Mathematical models and numerical experiment in materials science, Kiev, IPMS Publishing house, 2014, vol.16. p. 103-119

7. V.V. Ogorodnikov. Computer modeling of atomic mechanisms of deformation and fracture of refractory carbides by MD methods // News of Altay State University, 2014. – № 1\1. pp. 99-102.

8. O.N. Grigoriev, M.V. Karpets, A.I. Ustinov, X-ray definition of dynamic displacements of Al atoms in one phase condition and in eutectic alloy Al-Si, in Electron microscopy and strength of materials, Kiev, IPMS Publishing house, 2014, vol.24.

9. Presented report Grigoriev O.N., Vinokurov V.B., Danilenko N.I., Klimenko L.I., Contact interaction in ZrB_2-SiC-Cr_3C_2 system on IV-[th] Samsonov's conference"Material Science of Refractory Compounds", May 2014:

High temperature hardness and creep at indentation

We investigated the influence of additions of silicide $MoSi_2$ and silicon carbide SiC on hardness of boride ZrB_2 at high temperatures. To resolve this problem we used the methodology of creep and high temperature hardness by means of one axis compression by samples edges in a form of prisms of squire section, which axis are located perpendicular to each other. Tests were carried out in vacuum at temperatures $1200 - 1400\ ^{o}C$ with variation of loading from 5 to 89 kg. Change of penetration depth of samples in each other was controlled by optical method by means of cathetometer. Measurements accuracy was ±10 mkm.

Meyer's hardness was calculated as a ratio of loading value (P) to print's projection area (S). Projection area from mutual penetration of two equal-strength prisms, compressed by edges, was calculated as $S = (2^{0.5} \cdot H)^2$, where H – depth of mutual penetration of prisms. Definition of hardness at various loads shows, that its' value does not almost depend on loading value up to some its value (fig. 1.39). Above this value, obviously there occurs cracking and the depth of samples mutual penetration is defined by other processes. As temperature and materials resistance to cracking grow an interval of loading where hardness stays constant, expands (fig. 1.40).

Temperature dependence of hardness value for ZrB_2 , doped with $MoSi_2$ and SiC, is illustrated on fig. 1.41. Hardness was defined in interval of loadings at which its value remains constant. Elevation of the amount of $MoSi_2$ in ZrB_2 brings to decrease of hardness at low temperatures, however increases it at higher temperatures. Optimum strengthening at high temperatures is arrived in alloy ZrB_2-20% $MoSi_2$ (MS3). Addition of 20% SiC does not elevate hardness ZrB_2 at elevated temperatures.
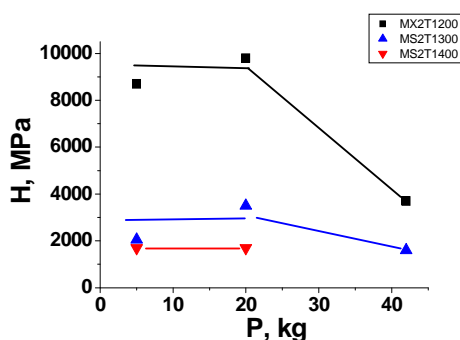
Fig. 1.39 – Dependence of hardness value of composite ZrB_2 – 10% $MoSi_2$ (MS-2) vs. applied load and a temperature of experiment
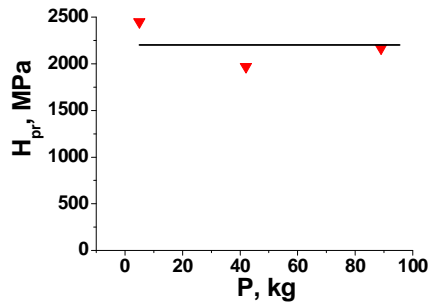
Fig. 1.40 – Dependence of hardness value for the composite ZrB$_2$-20% SiC at 1400 ^{o}C vs. applied loading
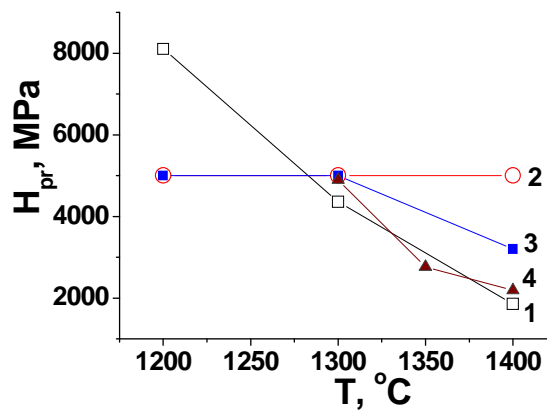

Fig. 1.41 – Dependence of hardness ZrB$_2$, alloyed with MoSi$_2$ and SiC, vs. temperature of experiment: 1 – 10mass.% MoSi$_2$; 2 – 20mass.% MoSi$_2$; 3 – 30mass.% MoSi$_2$; 4 – 20mass.% SiC;

A review of known methods of high temperature measurements of hardness and investigation of creep of high temperature materials has been carried out. Development of a methodology of definition of high temperature hardness and investigation of creep by means of compression (edge in edge) of orthogonal right-angled prisms of cross-sections has been initiated. For further analysis of a dependence of high temperature hardness *vs.* time of isothermal holding (creep) the well-known D. Tabor (1970) ratio is used:

$$p^{-m/3} - p_o^{-m/3} = A\exp\left[\frac{-Q}{3RT}\right]\left(t^{1/3} - t_o^{1/3}\right),$$

where p – average contact pressure at indentation in a moment of time t, p$_o$ – average contact pressure at indentation in a moment of time t$_o$, m – constant, associated with strain rate at high temperature creep testing, A – constant, Q – activation energy, t – time from the beginning of application of loading, t$_o$ – time when loading is fully applied.

The creep resistance of model ZrB$_2$-SiC (20%) and ZrB$_2$-MoSi$_2$ (10, 20 and 30%) ceramics was investigated. The tests were performed in vacuum at temperatures of 1200 - 1400°C with a load from 6.4 to

89kg. Changing of penetration depth of samples in each other was controlled by the optical method using a cathetometer. A distance change between the holders of upper and lower samples has been measured (measurement accuracy $\pm$ 10µm). The results of tests in coordinates of rapprochement of samples (ΔH) –time (τ) are illustrated on figs. 1.42-1.43
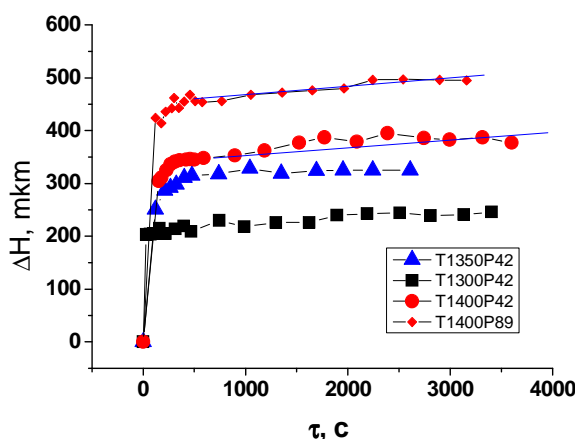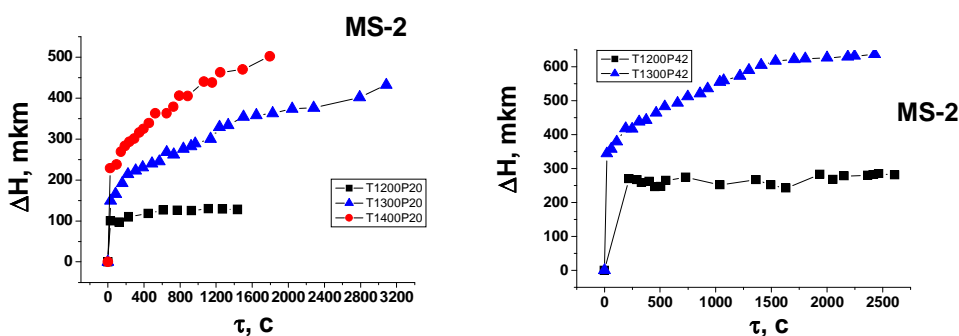

Fig 1.42 Indentation creep curves for ZrB_2-20% SiC ceramics (T1400P42 means that testing was performed at 1400°C and loading - 42 kg)

Studies showed that hot hardness and creep are very tightly interrelated. As hardness increases, the tendency to creep decreases. For ZrB_2-10$MoSi_2$ ceramics with temperature increase in the range of 1200-1400°C hardness decreases and creep increases. At an increase of $MoSi_2$ content in ceramics up to 20% a dependence of hardness and creep *vs.* temperature in the range of 1200 - 1400 ^{o}C is not observed. Further growth of $MoSi_2$ content up to 30% does not influence on hardness, but brings to the appearance of creep at 1400°C. ZrB_2-SiC (20%) ceramics has in 1.8 time higher hardness than ZrB_2-$MoSi_2$ (20%) ceramics at 1300°C. It stays harder at 1400°C if compare with ZrB_2-$MoSi_2$ (20%) ceramics at 1300°C. However, for both ZrB_2-$MoSi_2$ (20%) and ZrB_2-SiC (20%) ceramics hardness decrease with temperature increase in temperature range 1300-1400°C is observed. It can be concluded that the optimum heat resistance in ZrB_2-$MoSi_2$ system is attained at 20% $MoSi_2$. In ZrB_2-SiC system more heat-resistant composites can be developed.
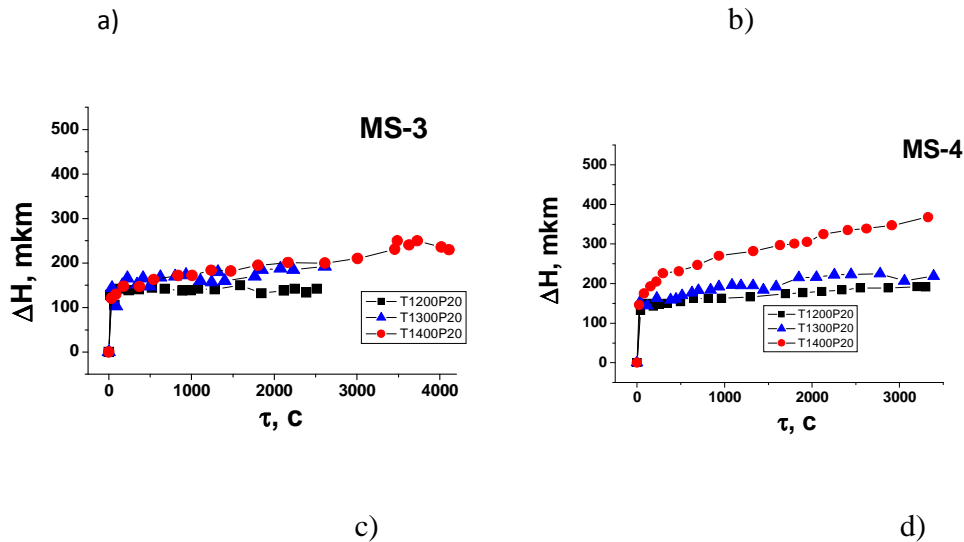
c)   d)

Fig 1.43. Indentation creep curves for ZrB_2-$MoSi_2$ ceramics (T1400P42 means that testing was carried out at $1400^{o}C$ and loading – 42kg; MS-2 (10% $MoSi_2$); MS-3 (20% $MoSi_2$); MS-4 ($MoSi_2$))

Creep was evaluated by a decrease of defined value of hardness as a result of growth of print value, which occurred at elevation of time of holding at temperature under loading. At absence of cracking at holding a some simulation of loading was preserved while changing a value of loading. Flow of material characterized by fall of hardness and defined at compression by edges of prismatic samples within an error of the experiment did not depend on loading (fig. 1.44).
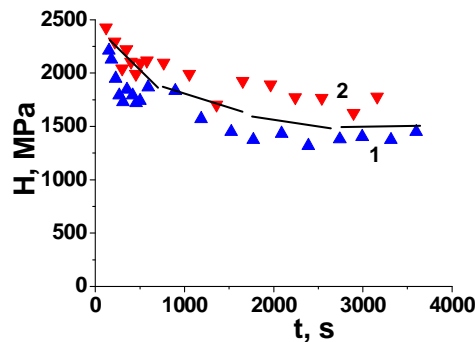

Fig. 1.44 – Dependence of a character of hardness change ZrB_2-20% SiC, defined at compression of prismatic samples under 90°, with increasing time of holding at 1400 ^{o}C vs. applied loading: 1- 42 kg; 2 – 86 kg

Dependence of creep vs. temperature of experiment for the composites of different composition is presented on fig. 1.45.
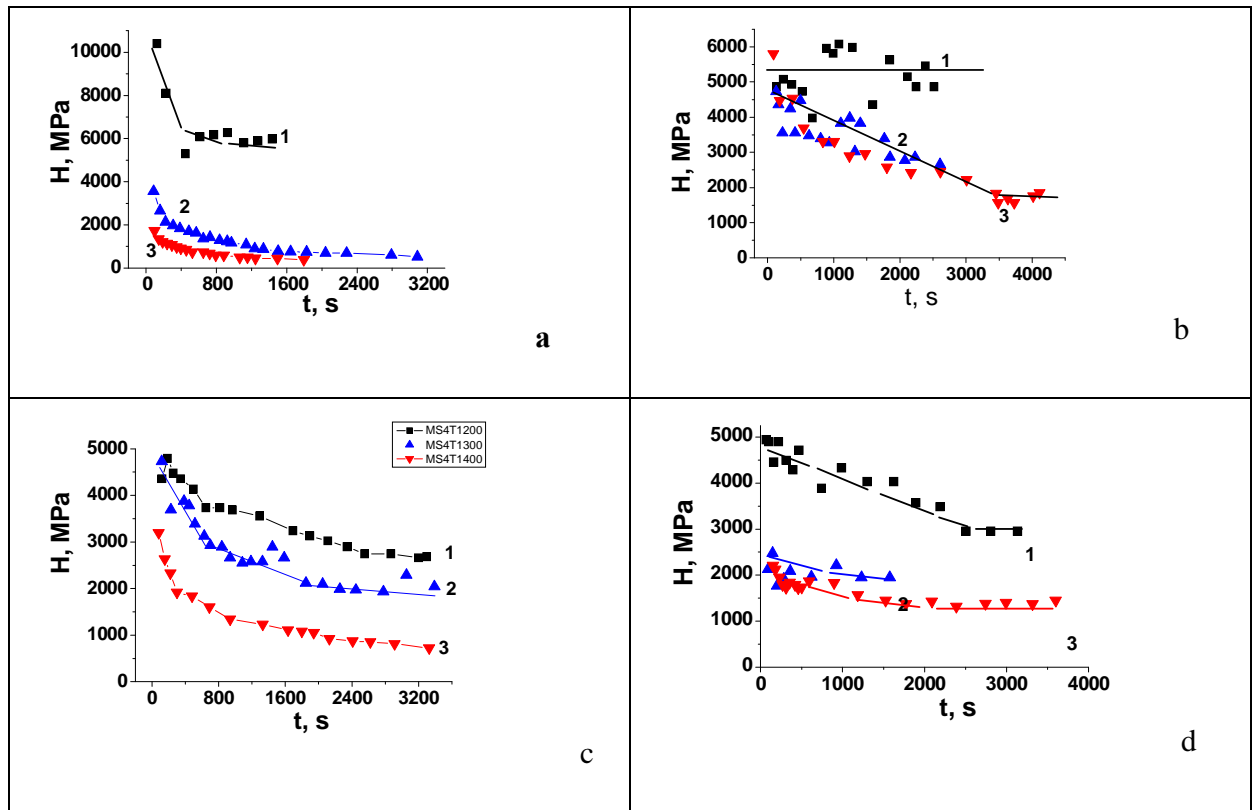
Fig. 1.45 – Fall of hardness ZrB_2, associated with material's flow under loading, defined at compression of prismatic samples under 90°, vs. temperature and material's composition: 1 – 1200^oC; 2 – 1300^oC; 3 – 1400^oC; a - ZrB_2-10% $MoSi_2$; b - ZrB_2-20% $MoSi_2$; c - ZrB_2-30% $MoSi_2$; d - ZrB_2-20% SiC

The obtained data show that at this loading the alloy ZrB_2-20% $MoSi_2$ preserves maximum strength at holding at high temperatures. At 1200^oC a residual strength of alloy ZrB_2-20% $MoSi_2$ is comparable with a strength of alloy ZrB_2-10% $MoSi_2$, and at higher temperature it is in 2 times more than for other composites with $MoSi_2$, and in 1,5 times than for composite ZrB_2-20% SiC.

As a whole creep processes of ultrahigh temperature ceramic in temperature interval 1200-1900° C in conditions of measurement indentation creep and in experiments on material's creep at uniaxial compression are investigated. For both methods the curves deformation-time at chosen levels of loading were recorded. Maximum strength in the process of holding at high temperatures is preserved by the alloy ZrB2 - 20 % $MoSi_2$. Residual strength is 2 times higher than for other composites with $MoSi_2$ (5-15%), and in 1,5 times than for the composite ZrB_2 - 20 vol.% SiC.